Freie Universität Berlin

Fachbereich Biologie, Chemie, Pharmazie

Institut für Chemie und Biochemie

Dendritic Nanocarriers for the Transport of Copper Ions across Biological Barriers and their Cellular Release

DISSERTATION

zur Erlangung des akademischen Grades des

Doktors der Naturwissenschaften (Dr. rer. nat.)

vorgelegt von

M.Sc. Sabrina Nowag

aus Berlin

März 2014

Diese Arbeit wurde in der Arbeitsgruppe von Prof. Dr. Rainer Haag im Zeitraum von Dezember 2009 bis März 2014 am Institut für Chemie und Biochemie der Freien Universität Berlin angefertigt.

1. Gutachter: Prof. Dr. Rainer Haag

2. Gutachter: Prof. Dr. Beate Koksch

Disputation am 6. Mai 2014

Für meine Familie

Danksagung

Zuerst möchte ich Prof. Dr. Rainer Haag danken, dass er mir die Möglichkeit gegeben hat meine Doktorarbeit in seiner Arbeitsgruppe anzufertigen und für die Unterstützung in jeglicher Hinsicht während der letzten vier Jahre.

Ich danke Prof. Dr. Beate Koksch für die Übernahme des Zweitgutachtens.

Meinen Kooperationspartnern möchte ich für die tolle Zusammenarbeit und ausgiebige Diskussionen danken, besonders Prof. Dr. Gerd Multhaup und Susanne Fehse vom Institut für Biochemie der FUB, Prof. Dr. Christophe Mingotaud, Prof. Dr. Jean-Daniel Marty und Camille Frangville vom CNRS in Toulouse, Frankreich, Prof. Dr. Pietzsch, Prof. Dr. Jörg Steinbach, Dr. Holger Stephan, Dr. Ralf Bergmann und Kritee Pant vom Helmholtz-Zentrum Dresden-Rossendorf.

Ich danke Frank Kuppler für die ICP-MS Messungen, Christina Kühl für die Assistenz bei biologischen Untersuchungen sowie Katharina Achazi und Jens Dernedde für die Hilfe bei der Konzeption biologischer Experimente. Der Firma Mivenion danke ich für die Synthese von Farbstoffen, die ich für die Markierung meiner Verbindungen benutzte.

Ich möchte den Mitarbeitern der AG Multhaup danken, die mich sofort aufgenommen und unterstützt haben, als ich mich an der Biochemie probiert habe. Insbesondere danke ich Susanne Fehse, Clara Schäfer, Andrea Senge, Vivienne Engelschalt und Linda Schauenburg für wertvolle Ratschläge.

Meinem Forschungspraktikanten Christoph Schlaich danke ich für seine Hilfe im Labor. Bei Florian Paulus möchte ich mich für die Synthese von Polyglycerin bedanken, das die Basis für die Nanotransporter in dieser Arbeit war. Dr. Pamela Winchester danke ich für die sorgfältigen Korrekturen der Manuskripte und dieser Arbeit.

Der gesamten AG Haag danke ich für das gute Arbeitsklima und die Unterstützung bei jeglichen Fragestellungen.

Meinen Subgroupleadern Dr. Paul Servin, Dr. Rahul Tyagi und Dr. Balu Thota sowie den ehemaligen und jetzigen Mitgliedern der Subgroup „Supramolecular Architectures“ danke

ich für ergiebige Diskussionen sowie Hilfestellungen und die Weitergabe ihres Wissens und ihrer Erfahrungen.

Meinen Laborkollegen von Nanopartica danke ich, dass sie mich mit viel Herz bei sich aufgenommen haben. Philipp Hultsch und Stefano Stefani danke ich für die tolle Arbeitsatmosphäre. Paul Servin danke ich für die vielen Ratschläge, die Motivation, die Unterstützung während der gesamten Zeit, das Korrigieren dieser Arbeit und für seine Freundschaft.

Dr. Juliane Keilitz möchte ich besonders danken für ihre Betreuung zu Beginn und Ende der Doktorarbeit sowie für ihre Sorgfalt bei der Korrektur dieser Arbeit. Ich habe dir auch sonst viel zu verdanken.

Maja Kandziora, Daniel Gladow, Ralf Albrecht, Cathleen Schlesener und Maike Lukowiak danke ich für ausführliche Gespräche chemischer und nicht-chemischer Natur und eure Freundschaft. Danke, dass ihr immer da ward, Freud‘ und Leid mit mir geteilt habt und mir so manchen Arbeitstag versüßt habt.

Bei Blondie, Melli, Melanie, Tiffy, Lau und Jan bedanke ich mich für die jahrelange Freundschaft. Es ist viel wert Freunde zu haben, mit denen alles ist, wie es früher war, obwohl sich alles geändert hat.

Besonderer Dank gilt meinem Freund Martin für seine Unterstützung, Ruhe und Geduld. Ich freue mich auf ein Leben mit dir in der Schweiz.

Der größte Dank gilt meiner geliebten Familie, die mir alles ermöglicht hat und immer für mich da ist. Insbesondere meinen Eltern verdanke ich alles. Ihr seid meine Vorbilder und meine Motivation.

Table of Contents

1 Introduction 1

1.1 The Role of Copper in Neurodegenerative Diseases 1

1.1.1 The Blood-Brain Barrier 2

1.1.2 Neurodegenerative Diseases 3

1.2 Drug Delivery Systems 12

1.2.1 Dendritic Nanocarriers 13

1.2.2 Stimuli-Responsive Nanocarriers 23

1.3 Cu Binding Ligands 31

2 Scientific Goals 34

3 Publications and Manuscripts 36

3.1 Copper Transport Mediated by Nanocarrier Systems in a Blood-Brain Barrier In Vitro Model 36

3.2 Biocompatible, Hyperbranched Nanocarriers for the Transport and Release of Copper Ions 74

4 Summary 91

5 Outlook 93

6 Zusammenfassung 94

7 References 97

8 Curriculum Vitae 103

Abbreviations

AD	Alzheimer's disease
APP	amyloid precursor protein
Atox1	antioxidant protein-1
ATP	adenosine triphosphate
ATP7A/B	Cu transport ATPasen
Aβ	β-amyloid peptide
BACE1	β-site precursor protein cleaving enzyme-1
BBB	blood-brain barrier
BSA	bovine serum albumin
BTZ	bortezomib
CAC	critical aggregation concentration
CCS	Cu chaperone of SOD1
CLSM	confocal laser-scanning microscopy
CMS	core multishell
CNS	central nervous system
Cox-17	Cyto oxidase complex
CP	coordination polymers
CQ	clioquinol
CRS	core-random shell
CS	core shell
CSF	cerebrospinal fluid
Ctr1	copper transporter protein-1
Cytox	cytochrome C oxidase
DDS	drug delivery system
DLS	dynamic light scattering
DMEDA	dimethylethylene diamine
DNA	deoxyribonucleic acid
DOX	doxorubicin
dPGS	sulfated dendritic PG
EDTA	ethylenediamineacetic acid
EPR	enhanced permeation and retention
FDA	US Food and Drug Administration
gtsm	glyoxalbis(N(4)-methylthiosemicarbazonate)
HBP	hyperbranched polymers

HD	Huntington disease
hPG	hyperbranched polyglycerol
Htt	Huntingtin portein
L-DOPA	L-dopamine
MD	Menkes disease
mPEG	monomethoxy poly(ethylene glycol)
MRI	magnetic resonance imaging
MTX	methotrexate
MX	mitoxantrone
ND	neurodegenerative disease
NP	nanoparticle
PAMAM	poly(amidoamine)
PD	Parkinson's disease
PDI	polydispersity index
PE	polyethylene
PEG	poly(ethylene glycol)
PEI	poly(ethylene imine)
PG	polyglycerol
PG-AD	adamantyl-functionalized hPG
PGSA	poly(glycerol-*co*-succinic acid)
PLA	polylactide
PPI	poly(propylene imine)
PrP	prion protein
PrP^{Sc}	posttranscriptionally modified PrP
PTX	paclitaxel
RES	reticuloendothelial system
SOD1	superoxide dismutase-1
TA	tannic acid
TMEDA	trimethylethylene diamine
Trientine	Triethylene tetraamine
WD	Wilson disease

1 Introduction

1.1 The Role of Copper in Neurodegenerative Diseases

The essential trace metal copper (Cu) is needed for various biological functions whereby its levels are tightly regulated in systemic environments. Cu is also a cofactor of many metalloenzymes which are critical for transcription and post-transcriptional modification of various metabolically active proteins. The Cu uptake into eukaryotic cells is mediated by a channel-like, high-affinity copper transport protein-1 (Ctr1, Figure 1) and is partially mediated by low-affinity transport mechanisms.[1] After Ctr1 transports external Cu(I), three different chaperones bind and distribute Cu intracellularly: (i) The Cu chaperone of Cu/Zn superoxide dismutase-1 (CCS) delivers Cu to Cu/Zn superoxide dismutase-1 (SOD1) which enters mitochondria and is an important antioxidant defense, (ii) Cyto oxidase complex (Cox-17) transports up to four Cu(I) ions to cytochrome c oxidase (Cytox), which also delivers Cu to mitochondria. (iii) Antioxidant protein-1 (Atox1) binds Cu(I) on its surface in the trans-Golgi network and delivers Cu to ceruloplasmin and the metal binding domain in the N-terminus of ATPases ATP7A and ATP7B, which excrete Cu from cells.[2] A disturbed Cu transport can cause a Cu imbalance in the central nervous system (CNS) and has been reported to be associated with several human neurodegenerative diseases (ND). Their treatment is very challenging, because the brain has to be addressed and active agents must be transported across the blood-brain barrier.

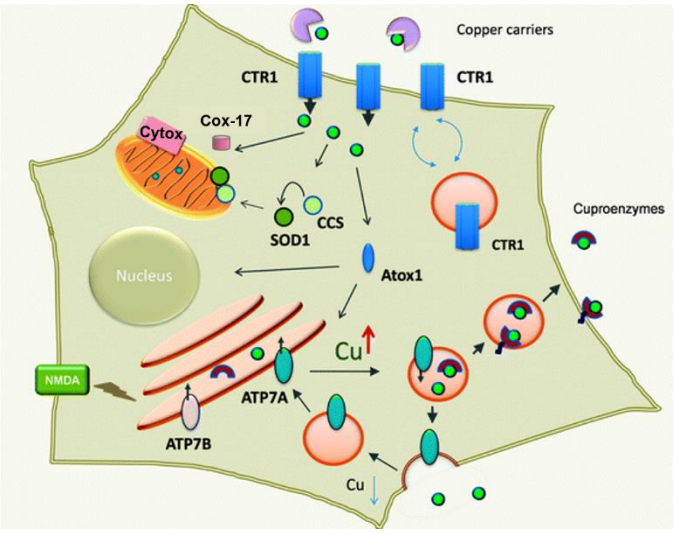

Figure 1. Cu distribution in a cell in the central nervous system. Cu (green balls) enters cells via Cu transport protein-1 (CTR1) and is then distributed by Cu chaperones. Cu efflux is mediated by ATP7A. Figure adapted from literature.[3]

1.1.1 The Blood-Brain Barrier

The blood-brain barrier (BBB) is a physical barrier between blood and brain or CNS, respectively, which protects of the brain by inhibiting the uptake of dangerous agents. Endothelial cells, which are connected via tight junctions and line capillary blood vessels to the blood side, largely constitute the BBB. The barrier is a highly selective filter that still allows nutrients to enter and metabolic products to exit. The transport occurs in most cases not paracellularly through the tight junctions, but rather via a transcellular route (Figure 2). The transport of small hydrophilic compounds including polar drugs is regulated by specific transport systems on the luminal (blood) or abluminal (brain) membranes and is usually restricted by tight junctions.[4] Lipophilic compounds, on the other hand, can diffuse through the endothelium due to the large surface area of the lipid membrane. Transport proteins within the endothelium deliver glucose, amino acids, and other substances across the BBB. Proteins, peptides, and other large hydrophilic molecules can only pass the BBB by specific receptor-mediated transcytosis or less specific adsorptive transcytosis. Poor transport of native plasma proteins like albumin has been observed, but a cationic surface facilitates the uptake via adsorptive transcytosis. For the development of drugs that need to pass the BBB

to enter the brain, pathways b-e in Figure 2 are suitable, but most drugs currently being used for CNS delivery enter via route b.

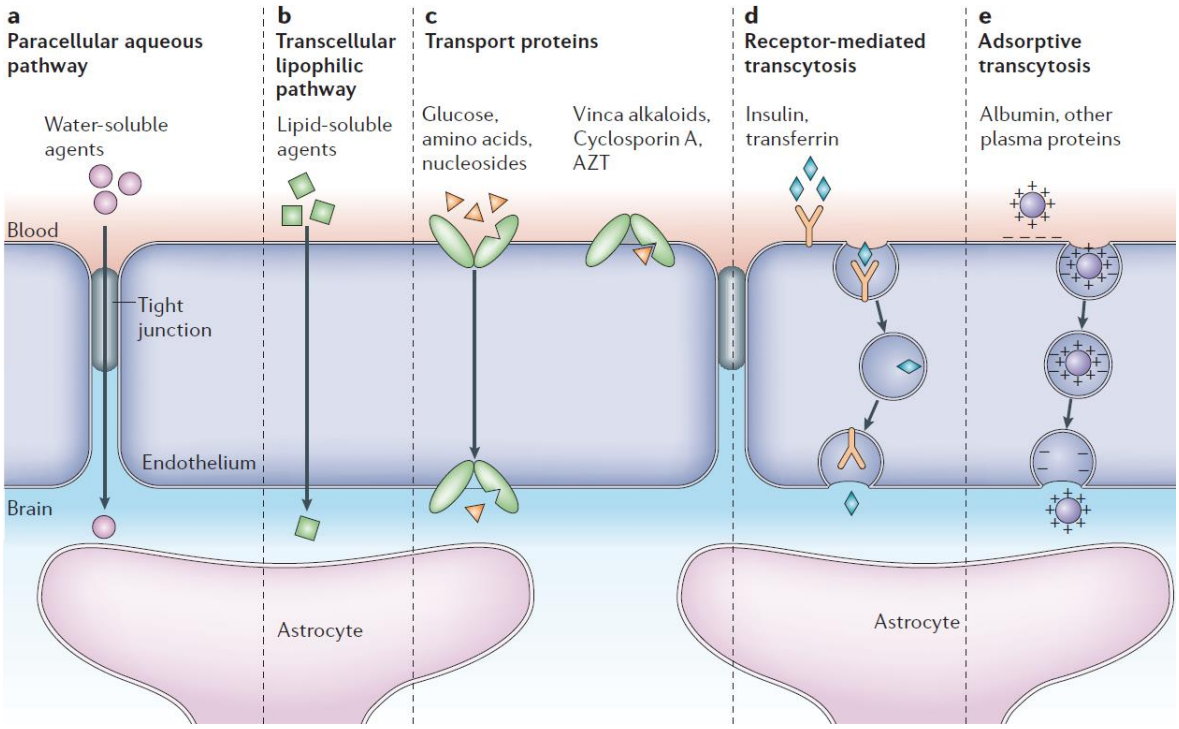

Figure 2. Schematic diagram of the endothelial cells that form the blood-brain barrier (BBB) and their association with the perivascular endfeet of astrocytes. (a)-(e) are pathways for molecular traffic across the BBB. Figure reprinted from literature.[4]

1.1.2 Neurodegenerative Diseases

Neurodegenerative diseases (ND) are a class of disorders that share a progressive loss of neural structure and function and are characterized by a slowly occurring, genetic, or sporadic effect upon the CNS. The loss of neurons causes severe neurological symptoms like dementia and movement disorders. Similarities between different ND pathologies are protein misfolding followed by aggregation and accumulation as deposits in the brain, which causes neurodegeneration.[5]

As mentioned above, Cu plays a role in the development of ND and a disturbed Cu homeostasis was observed in each case. Several proteins, which are involved in

neurodegenerative processes, have been identified as Cu binding proteins, i.e., the Cu-ATPases ATP7A and ATP7B, and play a role in CNS physiology. The genetic mutation of Cu-ATPases can cause severe neuronal damage as in cases of Menkes disease and Wilson disease. Cu can also interact with the amyloid precursor protein (APP) and β-amyloid peptide (Aβ), whereby complexation with the latter leads to aggregates that can deposit and form amyloid plaque in Alzheimer's disease. Cu also plays a role in prion diseases, where it induces misfolding of the prion protein. In Parkinson disease, the protein α-synuclein binds Cu, which leads to deposition of the protein. The Cu complex of the Huntingtin protein is involved in the pathogenesis of Huntington disease.

The involvement of Cu in ND has led to the development of therapies that regulate the Cu homeostasis in ND patients. As a results, various Cu chelators have been developed to increase or reduce the Cu amount in the CNS. Other interesting therapies have been investigated as well.

Wilson Disease

The Wilson disease (WD) is a rare, autosomal recessive disorder of Cu transport.[6] WD patients exhibit a genetic defect of the Cu-transporting P-type transmembrane ATPase ATP7B, which encodes a Cu transport protein. The reduced ATP7B activity disturbs biliary Cu excretion and leads to pronounced accumulation of Cu in the liver followed by the death of liver cells (hepatocytes), cirrhosis, or acute episodes of hemolysis.[7] Damaged hepatocytes may release Cu, which causes Cu accumulation in the CNS, brain, kidney, or even in the cornea of the eyes (Kayser-Fleischer rings).[8] The accumulation of Cu in the brain causes neurological symptoms. The disturbed Cu homeostasis in the liver of WD patients is also associated with a reduced Cu transport in the blood due to altered transport behavior of plasma ceruloplasmin.[9] Besides ATP7B, several other genes seem to be involved in WD.[10]

Symptoms of WD mostly appear in the early life as tremor, parkinsonism, choreoathetosis, ataxia, and impaired cognition.[11] However, some therapeutic approaches have been developed over the last decades, which effectively treat WD and reduce the amount of toxic free Cu. Patients with acute liver failure receive liver transplants to restore Cu excretion capacity.[10] When only neurologic symptoms are present, a lifelong medical

therapy is suggested. The general therapy includes D-penicillamine or Triethylene tetraamine (Trientine) as Cu chelators (Figure 3a-b) and/or Zn salts. The chelators bind to Cu and facilitate its excretion, while Zn disturbs the uptake of Cu into the intestines and induces the endogenous chelator metallothionein.[12] D-penicillamine as well as trientine are an effective initial therapy for hepatic patients[13-14] but show no real improvement in neurological diseases. Some studies even described a neurological deterioration after chelating therapy.[15] The ammonium tetrathiomolybdate (TM, Figure 3c) was discussed as an alternative chelating agent but clinical trials are still pending.[16] Since treatment with Zn salts caused less Cu excretion than with chelators, there were also less side effects.[17-18] However, some cases of neurologic worsening after Zn therapy have also been described.[19] In conclusion, the presently available therapies seem to have more or less severe side effects.

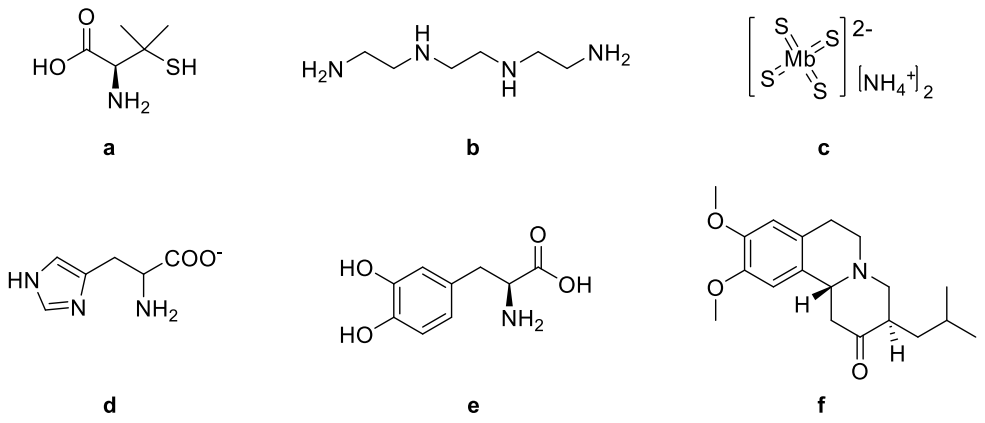

Figure 3. Chemical structures of Cu chelators used for the treatment of neurodegenerative diseases. (a) D-penicillamine, (b) triethylene tetramine (Trientine), (c) ammonium tetrathiomolybdate (TM), (d) histidine, (e) dopamine (L-DOPA), and (f) tetrabenazine.

Menkes Disease

Menkes disease (MD) is a rare, X-linked recessive, neurodegenerative disorder of the Cu metabolism.[7] The disease is triggered by a gene defect, which encodes the Cu transporting protein ATP7A.[20] The impaired ATP7A causes a failure of Cu transport into intestines, placenta, or BBB. The resulting deficiency of Cu in vital organs including the brain leads to reduced activity of essential cuproenzymes like dopamine β-hydroxylase, SOD, and Cytox.[21-23] The Cu deficiency in the brain results in severe neurologic abnormalities

including mental retardation, seizures, hypothermia, and feeding difficulties. Other features of MD are hair, skin, and bone abnormalities and failure to thrive.[24] Most patients die by the early age of 3 years.[25-26]

In general, MD patients are treated with Cu histidine (Figure 3d), which can be efficiently taken up by the brain.[27] However, this treatment showed variable outcomes.[28-29] Cu histidine was effective when residual ATP7A activity was present, but ineffective in severe cases with insufficient transport of the protein into the brain.[30] Furthermore, it was suggested that a combination of both Cu(I) and Cu(II) complexes could be beneficial as treatment.[31] In conclusion, treatment options remain limited and other treatments need to be developed.

Parkinson's Disease

Parkinson's disease (PD) is a severe, progressive neurodegenerative disorder with an unknown cause of disease.[32] PD is linked to degeneration of dompaminergic neurons of substancia nigra in the brain. The deficiency of dopamine results in an excess of acetylcholine and causes motor disturbance, tremor, rigidity, and cognitive as well as behavioral alterations.[33] A gene mutation may be responsible for the development of PD. The gene codes for the protein α-synuclein, which can be found in aggregated form constitutes most of the abnormal deposits (Lewy bodies) in neurons of PD brains.[34-35] Transition metals are associated with the deposition of α-synuclein, because Cu, Zn, and Fe bind to α-synuclein.[36] Zn and Fe are elevated in substantia nigra, while Cu is decreased in this region, but increased in the cerebrospinal fluid (CSF).[37-39] The accumulation of transition metals in the brain may have variable reasons. On the one hand, industrial exposure of heavy metals was linked to the development of PD,[40] but on the other, an altered metal homeostasis may be responsible.[41] Elevated iron level may cause oxidative stress and is included in the deposition of Lewy bodies.[37-38] However, the role of Cu in PD is so far not well understood.

Since neurodegeneration cannot be treated yet, only the treatment of the symptoms of PD is possible. The main approach is to increase the dopamine level by applying L-dopamine (L-DOPA, Figure 3e) or dopamine agonists or to decrease dopamine degradation by applying the corresponding inhibitors. It is also possible to apply anticholinergic agents

to decrease the excess of acetylcholine.[42] In severe cases, surgeries were performed, e.g., a deep brain stimulation, and promising results were obtained.[43] In conclusion, until the cause of PD is not fully understood, future approaches will further focus on symptomatic treatments.

Prion diseases

Human prion diseases are a group of fatal neurodegenerative disorders exhibiting the same symptoms, which are progressive dementia and cerebellar ataxia. The group consists of five diseases: Creutzfeld-Jakob disease, Gerstmann-Straussler-Scheinker syndrome, kuru, new variant Creutzfeld-Jakob disease, and fatal familial insomnia.[5] These transmissible diseases are characterized by neuronal spongiform degeneration as well as deposition of β-amyloid peptide (Aβ). Prion diseases have the prion protein (PrP) in common, which is involved in the development of the disease.[44] As PrP is known to be a Cu binding protein, it has been suggested that Cu plays a role in the pathophysiology of prion disease.[45-46] The Cu complex of PrP acts as a neuroprotective agent and is therefore involved in antioxidant protection of cells. The posttranslationally modified form of PrP is termed PrP^{Sc} and its toxic aggregates have been claimed to be the cause of prion diseases, although the mechanism of its involvement is still elusive.[47-48] Furthermore, PrP^{Sc} does not show neuroprotective function.[49-50]

Due to insufficient understanding of the main agents involved in the development of prion diseases, therapies are difficult. To date, no prescribed treatment is available.[51] However, some approaches have been developed for a potential therapy.[52-54] An antibody therapy seems to be the most promising approach, where an amino acid sequence present in the abnormally folded PrP^{Sc} could be specifically coded by an antibody, which stimulates the immune response to PrP^{Sc}.[55] Recently, anti-prion antibodies were also developed that were able to cross the BBB and target cytosolic PrP^{Sc}.[56] Besides the antibody therapy, also dendritic polyamines like poly(propylene imine), and poly(amidoamine) were able to destabilize PrP^{Sc} aggregates[57] and eliminate from cells,[58] and to eradicate prion infectivity in a mouse model.[57]

Huntington's Disease

Huntington's disease (HD) is an autosomal dominant disease. Neurodegeneration in HD leads to progressive motor, cognitive and psychiatric deterioration.[59] The cause of HD is the expansion of a CAG trinucleotide repeat within the Huntingtin gene, which encodes the Huntingtin (Htt) protein.[60-61] The gene defect causes the mutant Htt protein that is responsible for neuronal cell death.[62] The altered Htt is distributed in most brain regions and possesses an unusual conformation, which is thought to be toxic.[63] HD is also suggested to be involved in iron and Cu homeostasis[60] and Cu mediates the aggregation of Htt which may be relevant in HD pathogenesis.[60]

Current medical treatments are based on symptom management.[64] Tetrabenazine (Figure 3f), the only FDA-approved drug for HD, targets the suppression of involuntary movements, but it does not inhibit the further development of the disease.[65] Present therapies in clinical or pre-trials focus on neuroprotective strategies.[66]

Alzheimer's Disease

Alzheimer's disease (AD) is a progressive neurodegenerative disorder and the most frequently occurring form of dementia. It is characterized by the deposition of amyloid plaque, neurofibrillary tangles, and neuronal cell loss or dysfunction.[7] Amyloid plaque is located extracellularly and mainly consists of aggregated amyloid-β peptide (Aβ). Intracellularly, an hyperphosphorylated species of the tau protein forms neurofibrillary tangles.[67-68] The development of AD is not yet fully understood, but the amyloid hypothesis is the most accepted described cause of the disease. The hypothesis indicates that the accumulation of insoluble Aβ aggregates in the CNS initiates a pathogenic cascade, which results in the manifestation of AD.[69-70] Aβ is formed during enzymatic cleavage of the membrane protein APP, the amyloid precursor protein.[71] APP possesses three domains, the major part is the extracellular domain followed by the transmembrane domain and the cytoplasmic domain.[72] APP is cleaved by three protein-processing complexes, namely α-, β-, and γ-secretases.[70] β-secretase (BACE1) cleaves APP in the extracellular region, whereafter γ-secretase cleaves within the transmembrane domain to form Aβ (Figure 4).[73-74] Thereby different lengths of Aβ are formed, Aβ40 and Aβ42. While Aβ40 is harmless, Aβ42

tends to aggregate and easily forms oligomers and fibrils, which cause the amyloid plaque.[75-76] Aβ aggregates were found to be toxic under in vivo and in vitro conditions and to affect learning behavior in rats.[77] In addition to Aβ, high amounts of Cu have also been observed in amyloid plaques[78] leading to the suggestion that Cu may be involved in AD pathogenesis.[79]

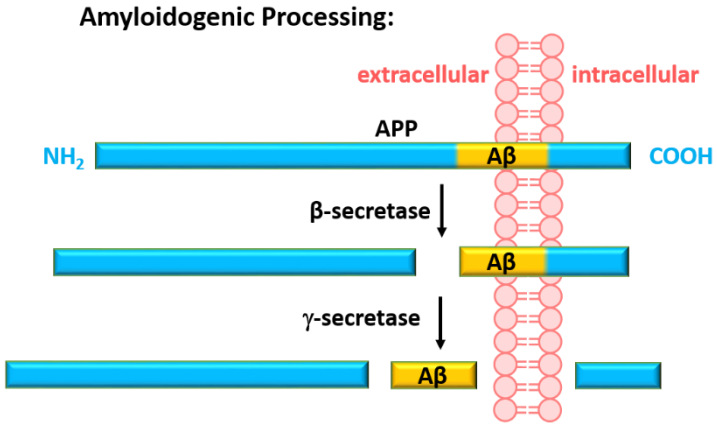

Figure 4. Amyloidogenic processing of the amyloid precursor protein (APP) to β-amyloid peptide (Aβ). Figure adapted from literature.[80]

To date no effective treatment of AD exists.[41] The current substances in clinical trials mainly focus on preventing Aβ aggregation or inhibition of secretase.[72] Recently, it was found that Cu can also induce BACE1 oligomerization, which might influence substrate recognition and activity[81] and be a suitable approach to decrease the formation of Aβ. Immunotherapies or metal-related therapies are also under investigation.[82-83]

Regarding the amyloid hypothesis many reports dealt with the involvement of Cu in AD. It was hypothesized that Cu-complexation with Aβ leads to insoluble aggregates followed by the main pathological findings, the amyloid plaque. The complex formation was observed to be reversible. Thus, different groups have worked on chelators that were able to compete with Aβ for the metal ions and thereby disassemble aggregates and resolubilize Aβ.[51] Clinical trials with AD patients showed that the chelator clioquinol (CQ) resolubilized Aβ aggregates but also caused side-effects,[84] which led to the development of the analog compound PBT2 (Figure 5).[85] A clinical trial phase II showed that PBT2 reduced toxic concentrations of Aβ, however, PTB2 had no significant effect on serum metal

concentrations. This indicated, that PTB2 is not a potent metal chelator but rather restores the homeostatic balance, however the mechanism remains unclear.[86]

Another approach focuses on the import of Cu into cells, because it was found that Aβ production was reduced, when CHO-APP cells were treated with Cu.[87] Furthermore, Crouch et al. reported on bis(thiosemicarbazone) (Cu(II):gtsm) complexes (Figure 5), which increased bioavailable Cu and were able to inhibit Aβ oligomerization.[88] Another well investigated chelator is clioquinol (CQ, Figure 5), which also found application in the treatment for HD.[89] In an AD mouse model, CQ facilitated the transport of extracellular Cu into cells to increase soluble Aβ and Cu levels in the brain.[90]

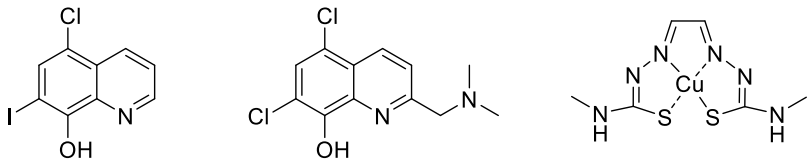

Clioquinol (CQ) **PBT2** **Cu(II):gtsm**

Figure 5. Clioquinol (CQ), PBT2, and Cu-bis(thiosemicarbazone) (gtsm) complex as treatment for AD.

A reduced number of Aβ plaques and decreased plasma Aβ levels were found when Cu levels were elevated above normal by dietary administration of Cu in AD mouse models.[91] This treatment with Cu sulfate restored the Cu level in the CNS and SOD1 activity, which was decreased in transgenic mice brains. AD patients orally treated with Cu-orotate in a clinical phase II trial exhibited stabilized Aβ levels in the CSF, but neither a beneficial nor a detrimental effect on AD development could be observed. It might be that the Cu-salt was not transported across the BBB to neuronal cells in a sufficient amount. However, the observation of stabilized Aβ levels due to Cu treatment is in agreement with the results from an AD mouse model with genetically increased Cu level in brain due to co-expression of ATP7B. These mice showed lower Aβ levels and less Aβ-associated plaques.[92]

Alternative Cu Therapy of Neurodegenerative Diseases

As discussed in the previous sections, Cu plays a key role in neurodegenerative diseases. While WD exhibits a Cu overload, AD and MD are defined as Cu deficiency diseases and PD as well as HD are described as disorders with disturbed Cu homeostasis. In order to regulate the Cu homeostasis in ND, chelator therapies seem to be a promising approach. However, high amounts of the chelator are necessary to achieve a high local concentration of Cu in order to change the Cu level to a therapeutically relevant amount. The required high concentration of chelator can cause severe side effects due to toxicity of the chelator or Cu ions and targeting of the brain might also be a problem for some of the smaller molecules. Therefore, biocompatible polymeric nanocarriers, which are able to transport high amounts of Cu across biological barriers, especially the BBB, are interesting candidates to address the disturbed Cu homeostasis of ND. They can be tailored to required properties for fewer side effects and to shield the Cu ions from the environment.

One example for polymeric Cu-nanocarriers was described by Treiber et al. and increased Cu levels in cells. The authors reported polymer-based core-shell (CS-NP) and core-multishell nanoparticles (CMS-NP), which were used to transport Cu into yeast cells and were able to increase the intracellular Cu level.[93] Imported Cu was released into cytosol and was accessible for SOD1. Aβ levels could be efficiently reduced by CS-NP. Although the transport across the BBB of such polymeric delivery systems has not yet been investigated, the use of polymeric drug delivery systems is a promising approach to increase cellular Cu level in the brain.

1.2 Drug Delivery Systems

In the last decade, the development of "smart" drug delivery systems (DDS) has increased enormously.[94] In the broader sense, DDS are engineered matter, which are able to transport and release biologic active compounds or drugs for therapeutic applications. DDS for therapeutic applications can be tailored to the corresponding disease. Drugs or other matter can be delivered by DDS, e.g., to tumors, brain, inflamed tissue, or specific organs.[95]

In treatment with conventional drugs is often unfavorable, because of drugs' limited characteristics. DDS can indeed improve these properties, for example, by shielding the toxicity of drugs to improve solubility of lipophilic substances or the biocompatibility, whereby the concentration of the drug in the body can be increased. Furthermore, the bioavailability and blood retention time of drugs can be enhanced by DDS.[96] In the ideal case, DDS are able to carry the cargo to the targeted tissues instead completely distributing them all over the body. For a blood transport, the DDS must embed its cargo deeply enough to reach the targeted tissue, but must also release the substance in the demanded region in such a way that the drug is still active. To this end, the DDS must not modify or harm the load. Furthermore, DDSs should be able to cross biological barriers to reach the demanded site of action.[97]

One major challenge is the biodegradation of the DDS. On the one hand, DDS must be stable until the targeted area is reached and the drug is released. On the other hand, the DDS should somehow be removed from the body after liberation of the cargo, e.g., by blood clearance or by biodegradation of the DDS scaffold, and the undesired accumulation in organs should be avoided.

Also the particle size of a DDS can be adjusted to the demanded requirements because size is a main factor in terms of blood clearance. Particles with sizes below 200 nm can avoid recognition from the reticuloendothelial system and therefore remain longer in the blood.[98] Particles with sizes below 6 nm, however, are known to be excreted renally (Figure 6).[99] Therefore, DDSs on a nanometer-scale should be advantageous for achieving a long blood half-life time. These so-called nano-DDS are nanoparticles (NPs) which can encapsulate, transport, and deliver bioactive matter or therapeutic drugs. Another name for nano-DDS is the term "nanocarrier," which will be used throughout this thesis.

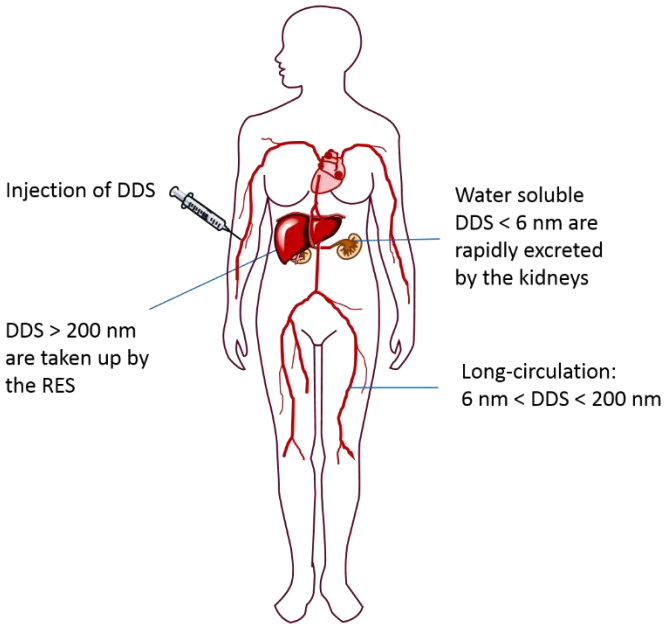

Figure 6. Schematic illustration of biodistribution of intravenously injected nanoparticles showing drug delivery systems (DDS) uptake by the reticuloendothelial system (RES), and nanoparticles excretion by the kidney. Figure adapted from literature.[100]

1.2.1 Dendritic Nanocarriers

Nanocarriers have gained significant attention in recent years, because they are typically 3 to 200 nm in size and therefore ideal for achieving long blood circulation times as well as having high drug delivery potential. The nancarriers can be composed of diverse types of polymers, e.g., dendrons, dendrimers, hyperbranched polymers (Figure 7), block-co-polymers, micelles, hydrogels, or core-shell-type architectures. In this chapter, some examples of nanocarriers based on different polymer architectures will be introduced.

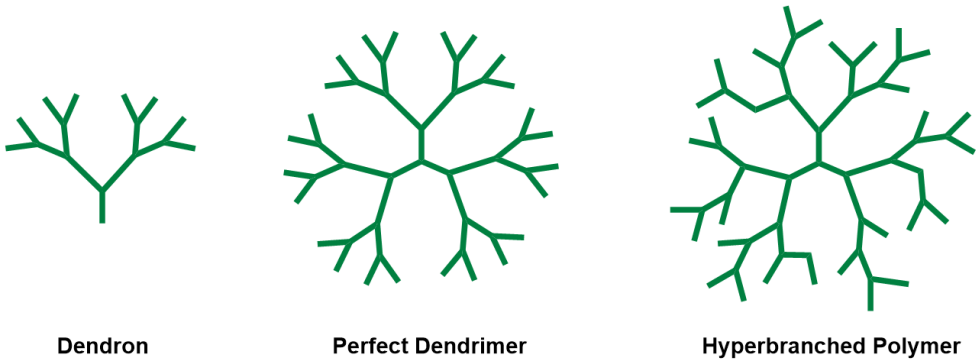

Figure 7. Schematic illustration of different macromolecular structures: dendrons, perfect dendrimers, and hyperbranched polymers.

Dendrimers

The term "dendrimer" is composed of the words dendrite and polymer. Dendrite (from the greek word "dendron" for tree) describes a branched structure of a molecule. A polymer is a large molecule, which consists of many (greek: poly) repetitive units (greek: méros). The dendrimer structure can be divided into three parts: the core, the branched repeating units and the terminal end groups (molecular surface). Dendrimers can be synthesized by the divergent and the convergent method (Figure 8).[101-104] In the divergent method, the monomers associate around the initiator core in tree-like layers. These repeating layers are also called generations, which is generally the classification of dendrimers. Per definition, the first layer relates to the first generation and so forth. With the divergent method, the exact size and number of terminal groups can be set, although reactions with high conversions are required to avoid defective areas.[101] The convergent method starts with the formation of so-called "dendrons," which are the tree-like, perfectly branched arms of a dendrimer. In the last step the dendrons are attached to the core. Some advantages of the convergent method are the easy separation of perfect and blemished macromolecules because of their size differences.[103] The synthetic routes result in a well-defined and regularly branched structure and globular shape of the dendrimer as well as a monodisperse size distribution with a polydispersity index (PDI) ≈ 1.0.

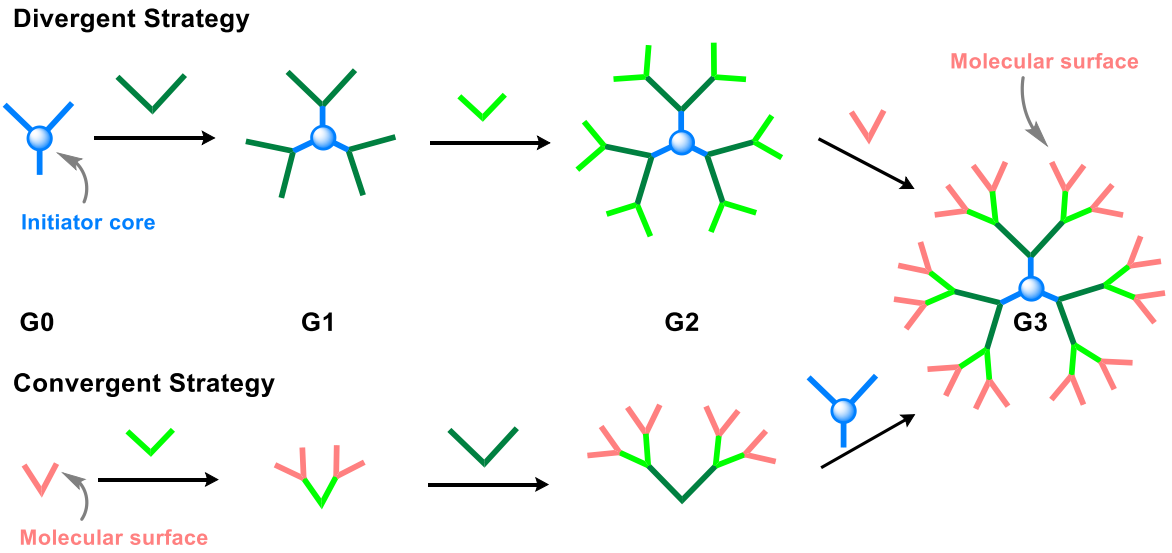

Figure 8. Two principle synthetic methods for constructing dendrimers: (a) the divergent method, in which the synthesis begins from a polyfunctional core and continues radially outwards, (b) the convergent method in which the synthesis begins in the periphery of the final macromolecule and proceeds inwards.

Due to the large number of terminal groups, dendrimers can create multivalent interactions, which can be stronger and more specific than the corresponding total number of monovalent interactions.[105] This property was named the "dendritic effect"[106] and has opened a lot of possible applications.[97] Other studies showed that dendrimers have further interesting properties which differ from linear polymers with similar molecular weight.[107-111]

After pioneering works in the field of dendrimers,[112] a lot of efforts has been made to utilize macromolecular chemistry for medical applications. New biomedical techniques and tools have thus evolved and found application in gene therapy, neutron capture therapy, drug delivery, photodynamic therapy, magnetic resonance imaging, solubility enhancement, and as nanocomposites.[113] Dendrimers have also been used in material science, e.g., in homogeneous catalysis.[114]

The probably most prominent dendrimer is poly(amidoamine) (PAMAM, Figure 9). It has been modified frequently for the use in biomedical applications. Other well investigated dendrimers are: poly(propylene imine) (PPI), melamine-based dendrimer, and poly(glycerol-*co*-succinic acid) (PGSA) (Figure 9).

Drug delivery with dendrimers is either based on a non-covalent encapsulation of a drug inside the cavities of the dendrimer, or on the covalent conjugation of the drug onto the dendrimer. PAMAM has often been used as scaffold for the covalent DDS approach.[115-117] The dendrimer not only enabled the solubilization of drugs in aqueous medium but also transported the drugs into cancer cells, where they were distributed and the free drug accumulated in specific cell compartments.[116] PGSA was investigated as non-covalent DDS for the encapsulation of camptothecines, which are naturally-derived hydrophobic anti-cancer drugs. To this end, PGSA was functionalized with terminal hydroxyl groups or with carboxylates. Both types delivered camptothecin to cancer cells.[118] The hydrophobic anti-cancer drug PTX could moreover be stabilized by a hydrophilic polyglycerol (PG) dendrimer.[119] Both examples show that no hydrophobic core is necessary for the encapsulation and solubilization of hydrophobic drugs.

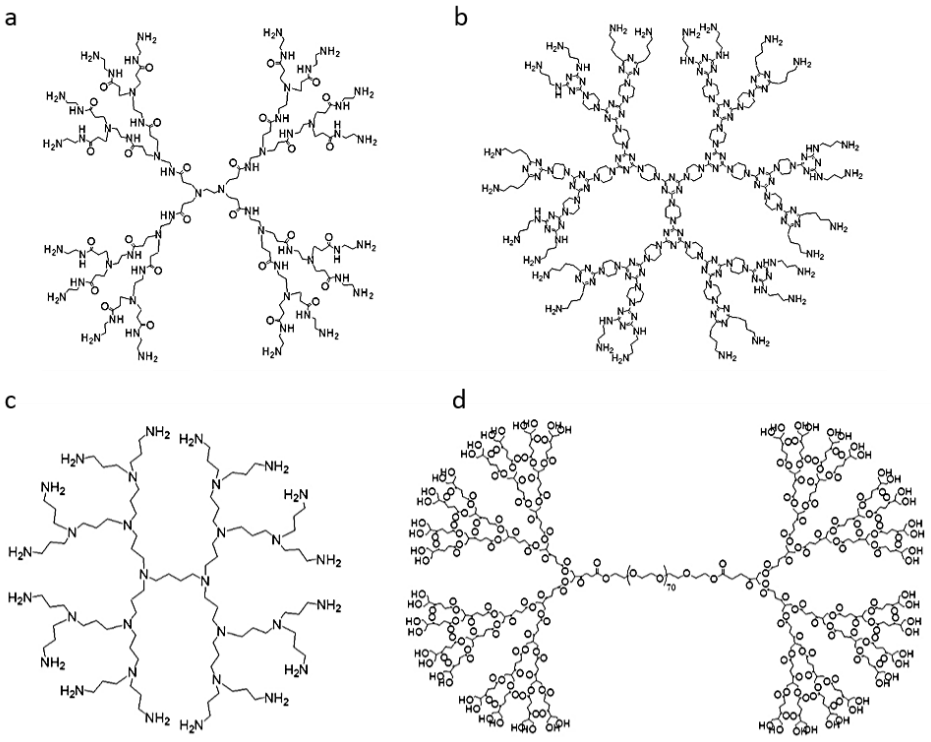

Figure 9. Structures of dendrimers used for delivery in cancer therapies. (1) poly(amidoamine), (2) melamine-based dendrimer, (3) poly(propylene imine), and (4) dendrimer based on glycerol and succinic acid with a poly(ethylene glycol) (PEG) core. Figure adapted from literature.[120]

Melamin-based dendrimers have been shown to encapsulate the drugs MTX and 6-mercaptopurine that result in a reduced drug toxicity. This demonstrates the shielding of the drug from its environment.[121] Non-covalent transport can also be induced by electrostatic interactions, as in the case of PAMAM which was able to form complexes with DNA due to an ionic attraction between DNA and PAMAM.[122-123] These DNA/dendrimer complexes could enter cells via endocytosis and improved transfection, which enables their application in gene delivery. Further studies have been confirmed that PAMAM and PPI were able to encapsulate hydrophilic and hydrophobic drugs or other active substances.[97,124] The dendrimers enhanced the drug's stability and thus their bioavailability. With thier apolar core and polar periphery, PAMAM dendrimers can be compared to unimolecular micelles.[97] The advantage of dendrimers over micelles is their stability and resultant independence from the dendrimer concentration[125] However, only a few examples have been reported that allow the drug to release in a controlled fashion.[126] In some cases, the encapsulation and release of the cargo is the result of an equilibrium.[125] Leaching of the active agent could make such systems useless for therapeutic application. Furthermore, due to the multiple synthetic steps, the preparation of dendrimers is difficult and expensive.

Hyperbranched Polymers

In the previous chapter, we looked at the advantages of dendrimers as DDS. Due to high costs and tedious synthesis upscaling such dendrimers is difficult. Hyperbranched polymers (HBP, Figure 7) provide an alternative scaffold with similar properties but with a much easier synthesis.[127]

HBP are globular macromolecules with a highly branched scaffold and large number of functional groups. In contrast to dendrimers, HBP are irregular in terms of branching and structure and are therefore polydisperse (PDI ≥ 1.1). Naturally occurring HBPs are polysaccharides like glycogen, dextran, and amylopectin which have already been known since the 1930s.[128] Kim and Webster were the first to use the term "hyperbranched polymers" in their report on the synthesis of soluble hyperbranched polyphenylene.[129-130]

Four synthetic strategies can be used to obtain HBP: (i) the step-growth polycondensation of AB_x ($x \geq 2$) or $AB_2 + B_3$ monomers,[129,131-133] (ii) the self-condensing vinyl polymerization of AB* monomers,[134] (iii) the multi-branching ring-opening polymerization of latent AB_x monomers,[135] and (iv) the polyaddition of monomers with initiating function and a propagating function in the same molecule.[136]

Several HBP have been produced to study their properties and potential applications, e.g., polyphenylenes, polyesters, polyamides, polyurethanes, polyethers, polystyrene, poly(acrylate)s, and polyamines.[137] HBP have found multiple applications as membranes, sensors, soluble functional supports, liquid crystals, blend components, additives, coatings, nanofoams, and delivery devices.[137]

Hyperbranched poly(ethylene imine) (PEI) (Figure 10) which can be synthesized by ring-opening polymerization was the first commercially available HBP. It possesses tertiary, secondary, and primary amines and can be easily modified due to its large number of functional groups. However, PEI is not biocompatible and leads to long-term problems in in vivo experiments.[138] An alternative, very interesting framework is the non-toxic, biocompatible, and protein-resistant polyglycerol (PG, Figure 10).[138-141] PG possesses a hyperbranched, globular polyether scaffold and can be synthesized in a one-pot reaction.[135] Numerous terminal hydroxyl groups enable the easy modification of PG, which turn it to an attractive and versatile matrix for many biomedical applications, e.g., diverse guests can be encapsulated in the cavities of the scaffold.[142] Sulfated dPG (dPGS) was found to have anti-

inflammatory features.[143] Recently reported fluorescently labelled or radiolabeled dPGS can be used for inflammation specific, imaging purposes.[144-145]

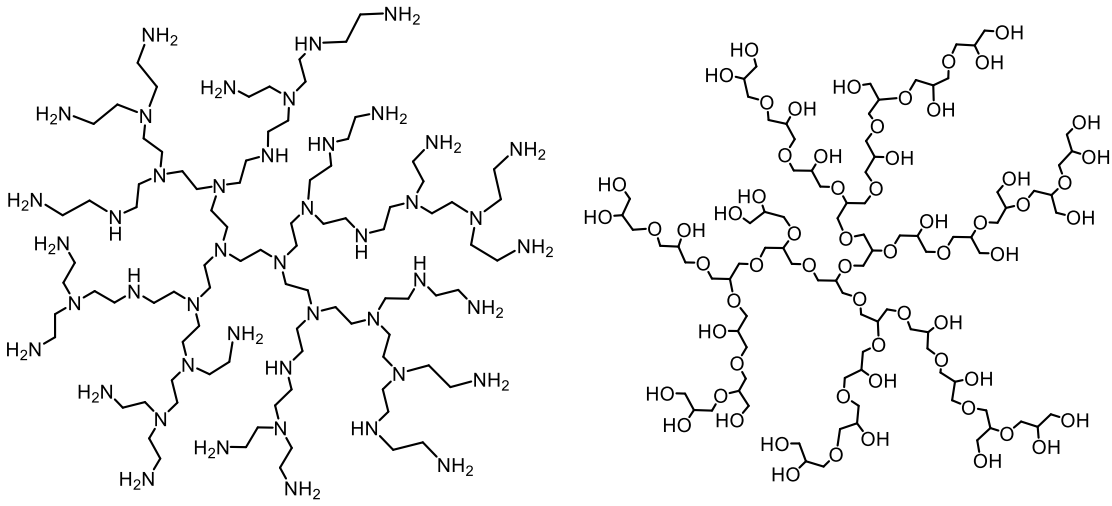

Hyperbranched Poly(ethylene imine) Hyperbranched Polyglycerol

Figure 10. Chemical structures of hyperbranched poly(ethylene imine) (PEI) and hyperbranchend polyglycerol (hPG).

Hyperbranched Polymers as Nanocarriers

In order to transport guest molecules, HBP can either be used as they are, or as a core with one or more shells attached to obtain so-called core-shell (CS) or core-multishell (CMS) architectures (Figure 11). The properties of the resulting CMS architectures will therefore tremendously differ from those of the pure HBP.

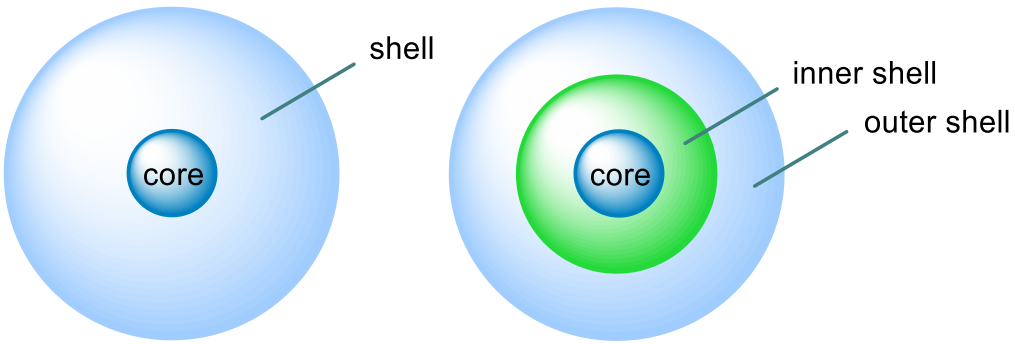

Figure 11. General structures of a core-shell (left) and a core-multishell architecture (right).

For the transport of drugs, CS architectures can be designed by attaching a drug either covalently or non-covalently. A few recent examples of supramolecular complexes will be introduced here including the physical interaction of a polymer with the guest molecule, e.g., hydrogen bonding, van-der-Waals interactions, and electrostatic interactions.

The Paleos group investigated functionalized HBP as potential contrast agents. They prepared multifunctional gadolinium complexes by using commercially available hyperbranched aliphatic polyesters. Protective PEG groups and folate as targeting ligand, as well as Gd-chelating moieties were coupled to the scaffold. The resulting HBP was biodegradable, non-toxic, and showed folate receptor specificity and was therefore proposed for MRI applications.[146] The dendritic polyester Boltorn, either unmodified or modified with lipophilic fatty acids, or amphiphilically modified with lipophilic and hydrophilic chains, has been investigated in regard to loading with the anti-cancer drug PTX. All types showed high drug loading efficiencies, low toxicity, and drug release, which makes them potential PTX carriers.[147]

PEI can be functionalized with a shell of, e.g. fatty acids, for the stabilization of guest molecules. When palmitic and stearic acid were coupled as a shell to PEI, more than 100 molecules of Congo Red could be transported by one polymer molecule (MW ~ 10 kDa).[148] As mentioned above, PEI is not suitable for biomedical applications, due to its non-biocompatibility, and can be replaced by PG. In order to compare nanocarriers with PEI or PG core, both scaffolds were equipped with a polylactide (PLA) shell. Both nanocarriers encapsulated Rose Bengal and Congo Red and the obtained transport capacities were dependent on the core size.[149] The same authors showed that the shell influenced also the loading capacity. The poly(L-lactide) led to higher loadings than PLA when used as shell on a PG core.[150]

Evolution of PEI and hPG Nanocarriers

In order to stabilize polar and non-polar substances, various approaches have been developed. For example, stable micelles formed by surfactants, were able to encapsulate hydrophobic guest molecules.[151] However, imperfect micelles could be formed resulting in undesired leakage of the guest molecule. Furthermore, the micellization strongly depends on the critical micelle concentration, which is risky for in vivo applications, because the

aggregates would disassemble due to the drastic concentration changes after injection leading to uncontrolled release of the drug.

The demand for concentration-independent, unimolecular micelles for the transport of guest molecules has thus risen. Core-shell architectures have been designed to address this issue. In a tandem coordination, ring-opening, hyperbranching polymerization process, a core shell structure was synthesized consisting of a hydrophobic dendritic PE core and a hyperbranched polyglycerol (hPG)-shell, which was grafted from the core. The PE-PG copolymer exhibited a high internal polarity gradient which allowed the stabilization of poorly water soluble molecules like pyrene and Nile red with a unimolecular transport mechanism. In contrast to small amphiphiles, the carrier was able to transport the load into cells under extremely high dilution conditions (Figure 12).[152]

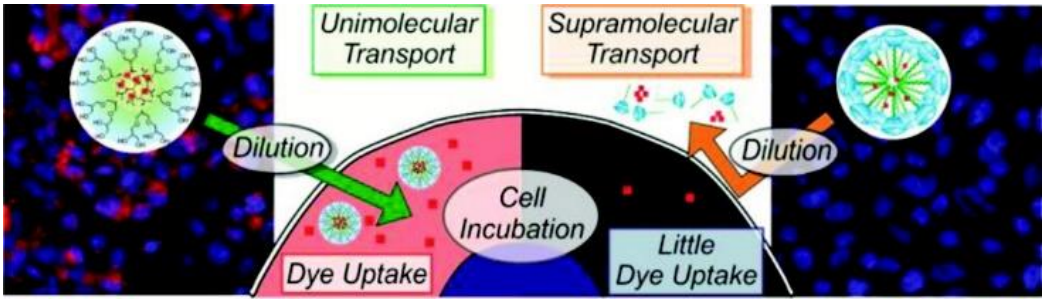

Figure 12. Comparison of unimolecular, concentration-independent transport into cells by core-shell architecture (left) and supramolecular transport of self-assembled amphiphiles, which breaks down after dilution. Reprinted with permission from [152]. Copyright 2012 American Chemical Society.

Inspired by nature, core-multishell (CMS) architectures with a hydrophobic core, lipophilic inner shell and hydrophilic outer shell were established to mimic the polarity gradient of liposomes on a unimolecular level (Figure 13). Especially hyperbranched PEI and hPG have been intensively explored as cores for CMS nanocarriers.

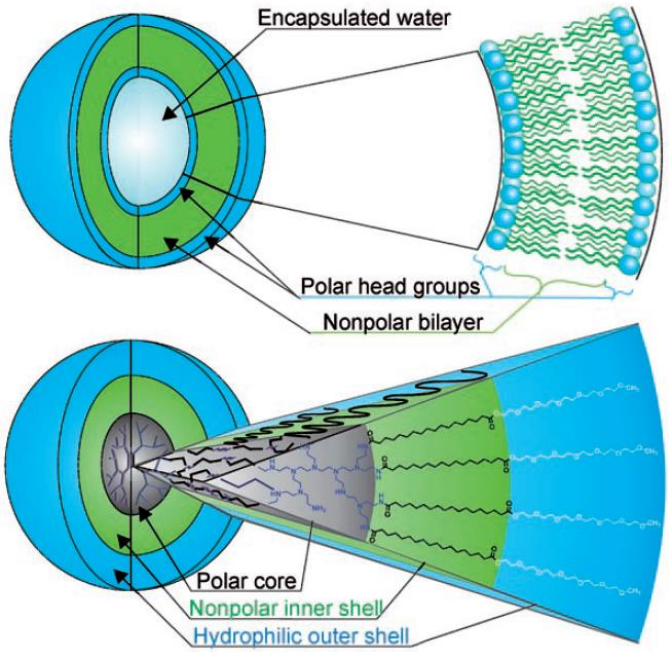

Figure 13. Comparison of liposomal structure (above) and core-multishell architecture (below). Both with polar core, nonpolar inner shell and hydrophilic periphery. Figure reprinted from literature.[153]

CMS architectures based on a PEI core and a double layer of hydrophobic alkyl chain and hydrophilic PEG chain are very interesting (Figure 14). In contrast to the previous assumption that these nanocarriers would operate in a unimolecular fashion, the authors reported that aggregates formed above a certain concentration (CAC) of CMS nanocarriers. The stabilization of polar and nonpolar guest molecules was only possible by the self-assembled aggregates, but not by the unimolecular CMS polymer. However, a CMS architecture can adapt to various environmental polarity conditions ranging from toluene to water and has been termed a "chemical chameleon" due to its versatility.[153] The same CMS nanocarrier could autoreduce gold ions to gold nanoparticles (Au NPs) within the PEI core. Furthermore, the resulting Au NPs-polymer system was stable in water and organic solvents.[154] Later studies showed that CMS architecture was able to stabilize Cu ions and transported it across cell membranes, which increased the cellular Cu level in yeast cells.[93]

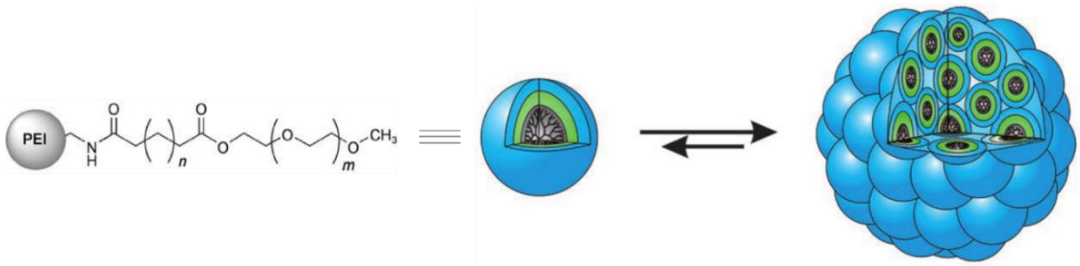

Figure 14. Structure of the core-multishell (CMS) nanocarrier PEI-alkyl-PEG (left). Above the critical aggregate concentration, CMS nanocarrier forms aggregates (right), which can transport polar and nonpolar guest molecules. Figure reprinted from literature.[153]

CMS polymer can also encapsulate anti-tumor drugs and dyes in aqueous and organic solvents. As a test-substance the dye indotricarbocyanine tetrasulfonate was stabilized and applied in vivo, where an accumulation in the tumor tissue was monitored. Hence, CMS nanocarriers are potential candidates for use as diagnostic and therapeutic agent due to their tumor targeting feature.[155]

CMS seem to be a very versatile tool for the stabilization of various guest molecules. However, the adaptability of PEI in biomedical applications is questionable due to its toxicity.[138] As mentioned above, PG is an excellent alternative to replace PEI because of its advantageous biological and chemical behavior. PG has also been studied as a building block for CMS nanocarrier and was functionalized with a double shell of alkyl and PEG. Furthermore, this arrangement allowed the homogeneous stabilization of metal ions, which found application as catalysts, after their reduction to metal nanoparticles.[156-157] Internalization of Coumarin and Nile Red was also possible with CMS architectures. Interestingly, the guest and its concentration influenced the aggregation of host and guest. Nile Red-loaded CMS nanoparticles showed dye aggregates at high dye concentrations, but not at low dye concentration. Furthermore, both dyes were located in the outer shell of 8 nm sized CMS polymers and led to aggregations of CMS particles with 100-120 nm diameters.[158]

Another CMS-architecture is composed of a PG-core with either a double shell of biphenyl and PEG or a random attachment of both shells to the core. The encapsulation capability was tested by using various dyes. It was observed that the loading capacity is strongly dependent on the shell arrangement.[159] The same building blocks where used to synthesize core-functionalized CMS which co-stabilized two hydrophobic drugs simultaneously. Pyrene was stabilized in a unimolecular fashion and was released in the

presence of enzymes. The encapsulation of Nile Red resulted in the formation of CMS-aggregates and release occurred after changing the pH.[160]

1.2.2 Stimuli-Responsive Nanocarriers

One of the major challenges in drug delivery is the targeted release of a cargo which can be triggered by an internal or external stimulus, e.g., reductive or oxidative conditions, temperature, light, pH, or the presence of an enzyme. The release can either occur by cleaving the linker between carrier and bioactive material or by structural change of the carrier, i.e., degradation, disassembly, which liberates the encapsulated guest molecule (Figure 15). Encapsulation systems for biological matter or drugs are especially interesting in biomedicine for the encapsulation and transport of environmental-sensitive matter. Since the damage and deactivation of sensitive compounds like cells, bacteria, proteins, drugs, and dyes must be prevented, the release needs to take place under mild conditions. It is beneficial to utilize appropriate disease (side-)characteristics for the design of new stimuli-responsive nanocarriers, e.g., specific protein overexpression and pH change. This would reduce side effects, because the release would only occur in spatially defined tissues. The following chapter will only concentrate on recently reported pH-responsive nanocarriers.

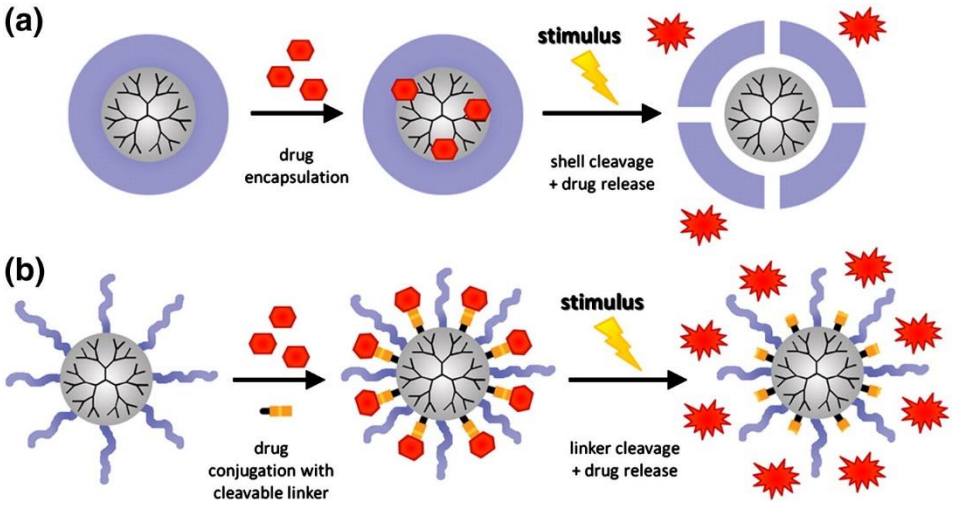

Figure 15. Different mechanisms for stimuli-responsive release of active agents from nanocarriers: (a) supramolecular complexes and (b) scaffolds with cleavable linkers for the drug conjugation. Figure reprinted from literature.[161]

pH-Responsive Nanocarriers

Parts of this chapter are published in the following highlight article:

S. Nowag and R. Haag, *Angew. Chem. Int. Ed.* **2014**, *53*, 49-51; *Angew. Chem.* **2014**, *126*, 51-53.

An often used release stimulus is the pH gradient between extra- and intracellular regions and between healthy and diseased tissue.[162] The late endosomal and lysosomal compartments of mammalian cells exhibit pH-values of ~5, while the extracellular region is known to be at pH 7.4.[162] Thus, a pH-sensitive transporter can selectively deliver its cargo into cells or into inflamed tissue. For that reason, pH 5 seems to be the best choice for a pH-cleavable group. The release at low pH also favorable because of the high diffusion rates of protons[162] and their resulting high accessibility at the cleavage site.

Carriers based on macromolecules or stable self-assemblies can be equipped with pH-cleavable bonds, e.g., hydrazones, imines, acetals as well as coordinative bonds, which is advantageous for a release of the payload at low pH (Figure 16).

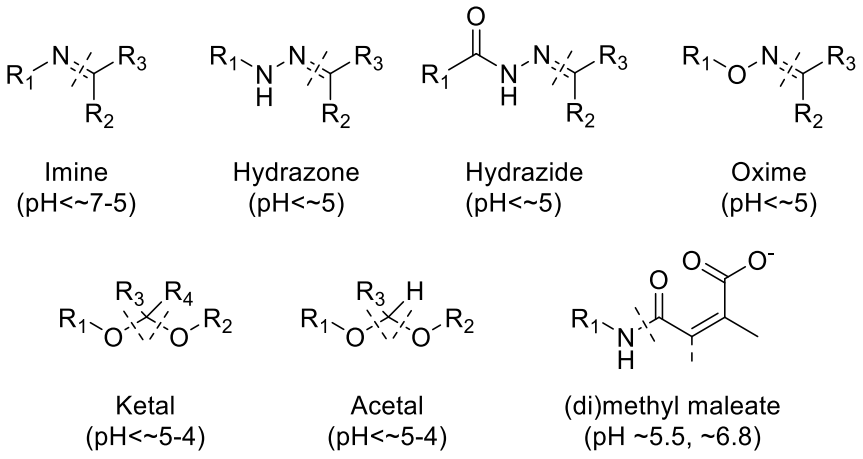

Figure 16. Examples for pH-responsive bonds. Figure adapted from literature.[161]

The transport of drugs, especially anti-tumor drugs, is critical because the entrapped cargo must remain harmless during transport and regain its cytotoxic activity after liberation in the targeted tissue. For this purpose, nanocarriers must fulfill the above-mentioned criteria and target tumor tissue based on enhanced permeation and retention (EPR).[163]

A polymeric carrier which also contains catechol moieties was established by Su et al. and was investigated for the selective delivery of the anticancer drug bortezomib (BTZ) into cancer cells.[164] They reported that the catechol units could covalently bind to BTZ, biotin moieties were responsible for the targeted uptake into cancer cells, and PEG was used as a building block to reduce nonspecific interactions with proteins and cells. The bond between catechol and the boronic acid moiety of BTZ was pH-dependent. Under mild acidic conditions, as in tumor tissue, the drug was released and showed enhanced cytotoxicity towards cancer cells.

The transport of DOX was also performed in dendritic PG-PEG core-shell type systems. PEG was linked via pH-labile imine bonds to aromatic linkers with PEG units attached. High loading of DOX and indocarbocyanine was observed. DOX-loaded carriers showed sufficient in vitro cytotoxicity, while dye-loaded carriers accumulated in vivo in the targeted tumor tissue.[165] Furthermore DOX-PG-PEG conjugates have been used as multifunctional prodrugs. Therefore, DOX was coupled via an acid-labile hydrazone linker to PG and, subsequently, a PEG shell was attached. The resulting drug-loaded polymers had a suitable size for passive tumor targeting and could enhance the antitumor efficacy in vivo.[166]

Another recent example for nanometer-sized carriers are the core-crosslinked polymeric micelles described by Zhong et al.[167] These micelles consisted of biodegradable diblock copolymers containing acid-labile acetal and photo-crosslinkable acryloyl groups in the hydrophobic polycarbonate block and could encapsulate PTX with high loading efficiencies of up to 15 wt %. After crosslinking of the core, the PTX-loaded nanocarriers remained stable at physiological pH and the release of the drug was inhibited. At a mildly acidic pH of 5, however, the acetal groups were hydrolyzed and PTX was released from the now polar interior (Figure 17). Empty micelles showed negligible cytotoxicity in a control experiment, while PTX-loaded nanocarriers retained high anti-tumor activities which proved the efficient drug release into tumor cells. However, the cytotoxicity of the encapsulated drug was lower than that of free PTX, since the cellular uptake was slower and the acetal hydrolysis had to be activated in the endosomal compartment. A drawback of this system is the limited degradability of the polyacrylate core after crosslinking.

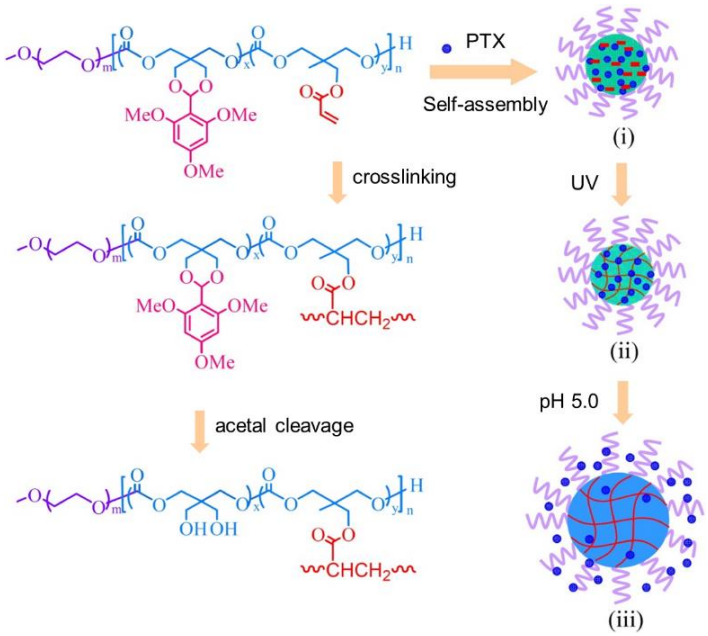

Figure 17. Photo-crosslinkable pH-responsive degradable block copolymer micelles. (i) Paclitaxel (PTX)-laden micelles (ii) were crosslinked by UV irradiation. (iii) Crosslinked PTX-laden nanoparticles showed extracellular stability and release of the drug under mild acidic conditions. Figure reprinted from literature.[167]

Degradation of acid-labile acetals is one of the benefits of the bioinert nanogels recently described by Steinhilber et al.[168] Nanogels with tunable sizes between 100 and 1000 nm were prepared by crosslinking hyperbranched polyglycerol (hPG) building blocks with Cu mediated click chemistry. Numerous hydroxy groups and a highly branched polymeric scaffold offer good water solubility, high biocompatibility, and protein resistance of hPG.

Although unspecific protein interaction is prevented with hPG, the enzyme asparaginase could be encapsulated by hPG nanogels under mild conditions. hPG nanogels were synthesized by surfactant-free and inverse nanoprecipitation. Acid-labile, cyclic benzacetal bonds permit the degradation of the nanogel into small fragments in a mild acidic environment (pH 5). This allows release of the protein in a cell compartment with mild acidic pH without loss of activity (Figure 18).

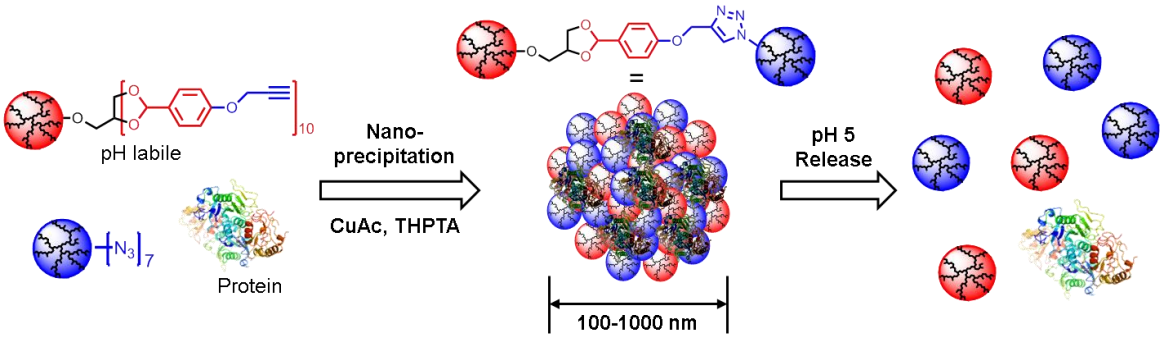

Figure 18. Protein encapsulation by nanoprecipitation by bioorthogonal crosslinking of hyperbranched polyglycerols (hPG) and a pH-dependent degradation of the hPG nanogel with release of the protein. Figure adapted from literature.[168]

In many cases, the efficacy in the control of drug delivery is influenced by the fixed pH-responsive phase behavior of nanogels. Thus, on-site modulation of the pH-response has to be possible as well for enhanced drug delivery. To address this issue, Zhou et al. recently reported pH-responsive nanogels (< 200 nm) based on a non-linear PEG network with interpenetrated chitosan chains.[169] The PEG network combined the advantages of linear PEG (biocompatibility) and thermo-responsive polymers in one scaffold. Nanogels responded to pH-changes from pH 5.0-7.4 and could be further remotely modulated by external thermic changes. The anticancer drug 5-fluorouracil was loaded into the nanogels. Both loaded and unloaded nanogels could vary their surface charge from neutral to positive around tumor extracellular pH (6.0-6.2) to facilitate uptake into cells. The acidic pH in tumor cells released the drug from the nanogel as a result of nanogel swelling. The drug-loaded gel only showed low toxicity in chemo-thermo studies but had a high therapeutic efficacy in chemo-cryo treatments. Thus, these nanogels have great potential for more efficient and safer anticancer therapeutics.

Although nano- and micrometer-scaled carrier systems for biomedical applications have many advantages, not only biological matter and drugs must be transported and released. In some neurodegenerative diseases, there are metal ion imbalances as illustrated above. Therefore, the transport of metal ions and their controlled pH-triggered intracellular release is an important challenge, whereby only a few examples have been reported so far.[93,170]

Coordination Bonding in pH-Responsive Carriers

As mentioned above, the delivery of metal ions is necessary for the treatment of some ND. A very prominent natural metal delivery system is transferrin. It transports iron ions into cells and releases iron pH-dependently due to coordination binding.[171] However, metals can also be used as a linker between hosts and guests, which can be relevant, e.g., for cancer therapeutics. The ligand-functionalized host binds to the metal, which in turn binds to the coordination sites of the guest. Coordination bonds between metals and ligands respond to pH-changes because metals and protons are Lewis acids and compete in binding the ligand, which is a Lewis base.[94] This kind of metal linker was frequently applied in various mesoporous materials, which have been used as carriers for drugs into cells.[94] Due to their nontoxicity, non-immunogenicity, and biodegradability, biomacromolecules like albumins are excellent candidates for the delivery of drugs into cells.[172] Albumin-metal complexes have been designed to bind anticancer drugs. The resulting complexes consisted of BSA with coordinated Zn^{2+} ions. Mitoxantrone (MX) was loaded on the complex surface to form BSA-Zn-MX architectures at physiological pH. Decrease in pH led to a release of MX due to breakage of the coordination bonds (Figure 19). Pure BSA-Zn complexes showed low cytotoxicity, while MX-loaded architectures exhibited an enhanced inhibitory capacity.[173]

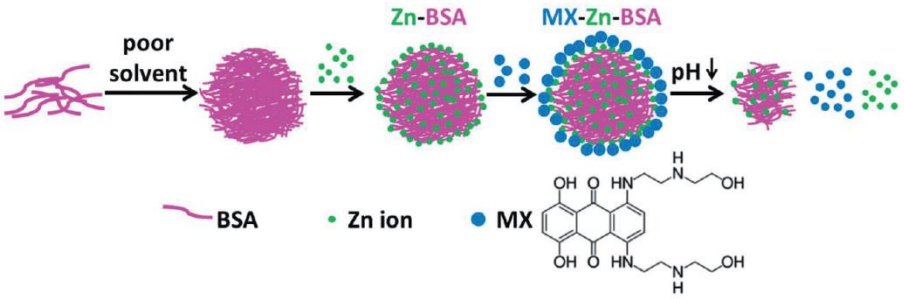

Figure 19. Bovine serum albumin (BSA) forms complexes with Zn ions whereupon mitoxantrone (MX) can coordinate to Zn. The resulting BSA-Zn-MX aggregate disassembles at low pH. Figure reprinted from literature.[173]

MX is also able to bind to Cu ions and form strong complexes. Due to its strong coordination bond, the resulting MX-Cu NPs are stable at highly acidic pH. However, when PEG was added with ethylene oxide moieties as weak coordination binding side, PEG competed with MX as host to bind Cu. Therefore, the coordination bond was weakened and pH-sensitivity was observed.[174]

Xing et al. reported core-shell coordination polymers (CPs), in which the core consisted of CPs based on Zn or Fe ions and different anticancer drugs and was instable at physiological pH. The shell consisted of a CP of the ligand 1,4-bis(imidazol-1-ylmethyl)benzene (BIX) and metal ions. The core-shell CPs were responsive to acidic pH present in tumors and released the drugs efficiently.[175] These polymeric complexes seem to be a versatile tool for drug delivery by using different drugs, metals, or ligands.

An example for a dendrimer, which is able to complex Cu(II), Zn(II), and Ni(II) ions was reported by Bosman et al.[176] The authors presented different generations of PPI dendrimers as multi(tridentate) ligands with defined size and structure, which were able to stabilize up to 32 metal ions.

Caruso et al. have described a novel micro-encapsulation system for various substrates based on a one-step assembly of coordination complexes between metal ions and tannins, which are naturally occurring polyphenols in plants.[177] Tannic acid (TA) is based on polyphenols coupled to glucose through ester bonds (Figure 20). The molecule is highly water soluble due to its high number of hydroxy groups. The spontaneous complexation of Fe^{III} ions with the TA catecholic unit and the adhesion of TA on diverse surfaces were utilized in a simple approach to form films on a multiplicity of substrates, for example, organic and inorganic templates, and even bacteria.

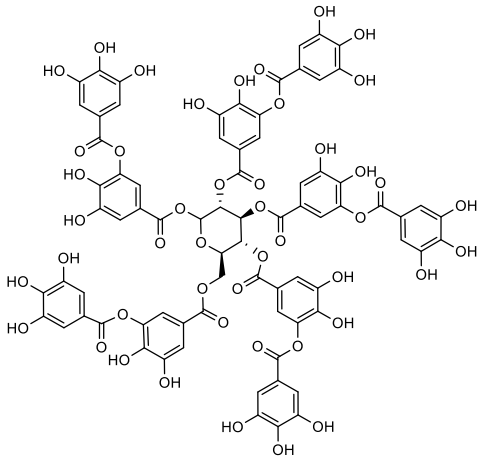

Figure 20. Chemical structure of tannic acid as building block for micro- and nanocarriers.

The self-assembly of TA is a pH-dependent process (Figure 21). At pH < 7 the metal ion forms mono- and bis-complexes with TA, while at pH > 7 one metal ion coordinates to three TA molecules and forms stable films regardless of the size and shape of the template.

Due to these properties, the assemblies are stable at physiological pH and disassemble under mild acidic conditions, thereby releasing encapsulated guests. This makes them interesting candidates for biomedical applications. The possibility of using different metal ions and polyphenols makes this approach highly versatile. The high biocompatibility and low costs of the materials are further essential benefits for the encapsulation and release of other important payloads such as drugs. Since the metal-ion release is also a feature of the above-mentioned TA-metal ion complex,[177] this universal carrier system has great potential for different kinds of transport applications.

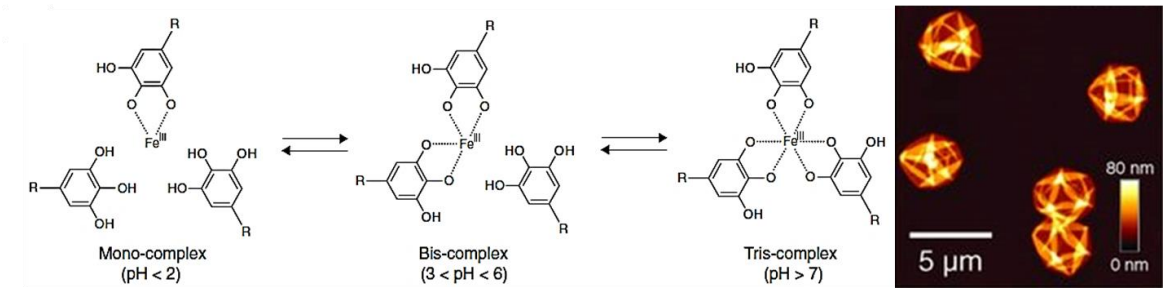

Figure 21. pH-Dependent coordination of catecholic moieties to iron(III) (left) to form films and capsules (right) on different substrates, for example, polystyrene. Figure reprinted from literature.[177]

In conclusion, nanocarriers find versatile application because of the feasibility of their production according to the requirements of the corresponding disease, e.g., biocompatibility, tissue targeting and controlled release. Especially the last section illustrated that polymers can form coordination bonds with metal ions, which makes them interesting candidates to address diseases with disturbed metal homeostasis. However, considering the criteria for metal ion delivery and metal binding properties, the combination of metal binding ligands with polymeric scaffolds seems to be a promising approach as treatment of neurodegenerative disorders. The next chapter will therefore focus on Cu binding ligands and their coordination to Cu.

1.3 Cu Binding Ligands

Chapter 1.1.2 illustrated that Cu interacts with proteins which are involved in ND. In some cases, chelators, e.g., clioquinol, are used as therapeutic agents to modify or reverse the disturbed Cu level of such disorders. Since the chelator has the leading role in the complex formation and stability, this chapter will discuss different kinds of Cu ligands and their coordination and structural arrangement to Cu.

The most frequently occurring Cu complexes include Cu(I) or Cu(II), although few examples of Cu(III) complexes are known too.[178] According to the concept of hard and soft acids and bases, Cu(I) and Cu(II) ions form complexes with different ligand donor atoms. While Cu(I) prefers ligands with soft atoms like P, C, thioether S, and aromatic amines with mostly tetracoordinated tetrahedral arrangements, Cu(II) binds to ligands with N, O, S, and halides with coordination numbers from four to six.[178] Complexes of Cu(II) exhibit tetracoordinated square-planar, pentacoordinated trigonal bipyramidal, and hexacoordinated octahedral geometries (Figure 22).

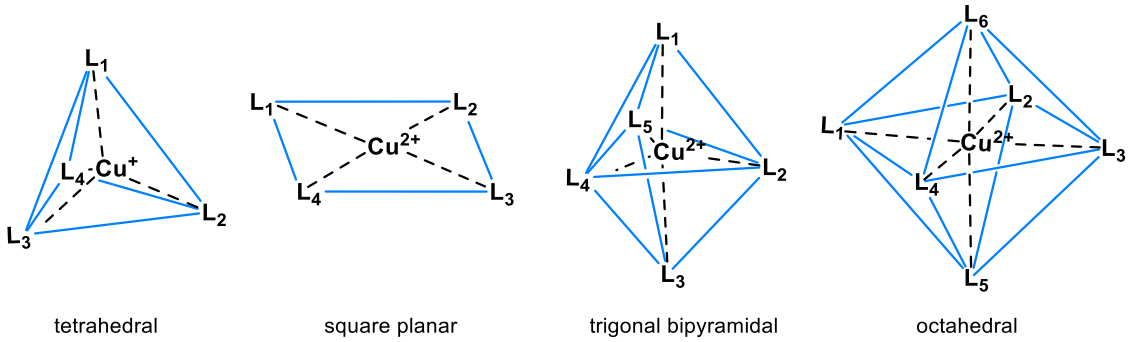

Figure 22. Structural arrangement of Cu complexes. Cu(I) complexes with four ligands possess a tetrahedral geometry, while Cu(II) complexes with four to six ligands have square planar, trigonal bipyramidal, and octahedral geometries.

One of the most prominent Cu chelators is ethylenediaminetetraacetate (EDTA), a hexadentate ligand with a very strong coordination to Cu(II), which is useful for transmetallation in Cu excess disorders. However, EDTA coordinates indiscriminately to other ions like Zn(II), Ca(II), and Mg(II), which prohibits the in vivo application of EDTA.[51]

For Cu deficiency diseases, Cu should be complexed strong enough for a transport through blood and yet be releasable in a controlled fashion. Due to the fact that complexes of Cu with amino ligands are reversible via exchange of the metal by a proton, amino ligands are suitable candidates to release Cu pH-dependently into cells, e.g., by utilizing the decreased pH in the inflamed tissue of the AD-brain. Furthermore, it has been observed that positively charged particles have a greater chance to pass the BBB,[179-181] which also underlines the applicability of amino ligands as part of AD-therapeutic agents, because amines can be protonated in aqueous medium.

Amino ligands can be of bi-, tri-, tetradentate, or macrocyclic nature and differ in their complex stability. Tetramethylethylene diamine is a bidentate ligand (Figure 23a), and other ligands are required in order to achieve an appropriate coordination number. As a chelating moiety on polymeric nanocarriers, methyl-substituted diamino ligands are preferred because of their lipophilicity and resulting potential ability to cross the BBB.[4]

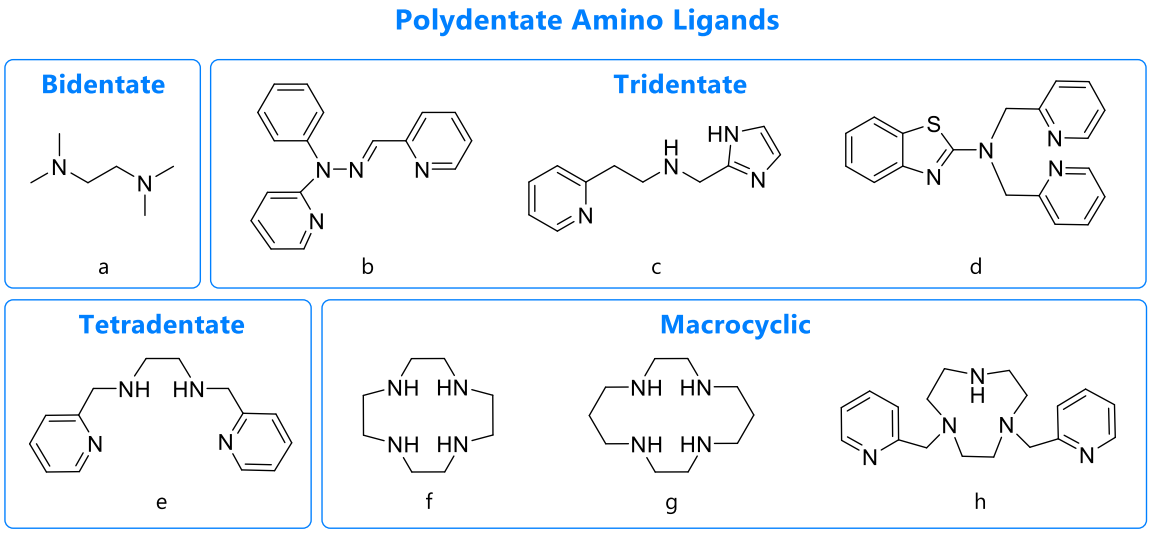

Figure 23. Some examples for polydentate amino ligands. (a) Tetramethylethylene diamine as bidentate ligand, (b) 2-((2-phenyl-2-(pyridin-2-yl)hydrazono)-methyl)pyridine, (c) N-((1H-imidazole-2-yl)methyl)-2-(pyridin-2-yl)ethanamine and (d) N,N-bis(pyridin-2-ylmethyl)benzothiazol-2-amine as tridentate ligands and (e) 1,2-bis(6-methyl-2-pyridinyl)ethane as tetradentate ligand. (f) Cyclen, (g) cyclam, and (h) 1,4-bis(pyridinylmethyl)-1,4,7- triazacyclononane represent macrocyclic amino ligands.

Many tridentate amino ligands exhibit aromatic amines, but imines (Schiff bases) as well as amines can be part of tridentate ligands (Figure 23b-d). The aromatic chelator depicted in Figure 23d possesses benzothiazole as fluorescent moiety and di-(2-picolyl)amine as chelating moiety and can therefore be used to follow the body distribution of the chelator.

Due to the distinct coordination number of Cu(II), tridentate ligands are supported by other ligands like chloride or water among many other possible small molecules to achieve a tetra- to hexacoordinated arrangement. On the other hand, tetradentate ligands, e.g., 1,2-bis(6-methyl-2-pyridinyl)ethane (ENDIP, Figure 23e) can form 1:1 complexes with Cu(II) without the help of other ligands.

Macrocyclic ligands are known to be very strong Cu chelators and can therefore be used as competitor agents in order to avoid proteins binding to Cu. Tetradentate macrocycles like cyclen and cyclam have already been used as agents to destabilize Aβ aggregates in AD (Figure 23f,g).[182] Another macrocyclic ligand is 1,4-bis(pyridinylmethyl)-1,4,7-triazacyclononane (DMPTACN, Figure 23h). In this case, the pyridinyl residues are also involved in the complex formation which makes DMPTACN a very strong pentadentate chelator.[183] The macrocycle could be used to destabilize undesired complexes by transmetallation.

The Cu(II)-complexes of the chelators in Figure 23 increase in stability with increasing denticity of the ligands. However, tetramethylethylene diamine (Figure 23a) is an exception, because its complex stability with Cu(II) was determined to be between that of tri- and tetradentate ligands. The reason for this observation is the flexibility of tetramethylethylene diamine in comparison to larger ligands, but also the increased basicity of aliphatic amines compared to aromatic amines determine the stability constant of complexes.[184] Furthermore, other factors of the chelate effect have to be considered for the estimation of the complex stability, which is influenced by the size, charge, and the spatial design of the ligand.

2 Scientific Goals

In order to address the disturbed Cu homeostasis in neurodegenerative diseases (ND), the transport of Cu into CNS can restore the Cu level and reduce the development of ND. Due to their tunable properties, polymer-based drug delivery systems (DDS) are promising candidates for the delivery of Cu ions across the blood-brain barrier (BBB).

The objective of this thesis is the synthesis and investigation of new nanocarriers, which are based on hyperbranched polymers and able to stabilize Cu ions. These nanocarriers are supposed to transport Cu ions across cellular membranes and release them intracellularly to treat Cu deficiency disorders like AD. The PG core will be used because of its low toxicity and high biocompatibility, and bidentate amino ligands will be attached as Cu binding moieties. The nanocarriers should have numerous ligands to be able to encapsulate high amounts of Cu and to increase the local concentration of Cu to obtain a high therapeutic effect in in vivo studies. The Cu binding is supposed to be strong enough for a transport through the blood, but the nanocarrier must also release the Cu in a pH-triggered fashion into the inflamed tissue of the AD brain (Figure 24). Until now, only few examples of nanocarriers exist, which can stabilize metal ions by coordination bonding and their transport behavior across the BBB was not investigated so far.

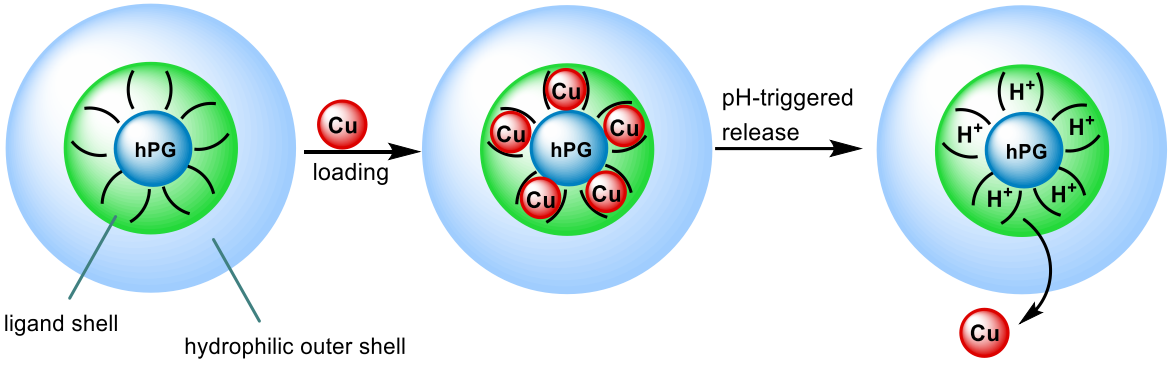

Figure 24. Schematic illustration of core-multishell nanocarriers with hyperbranched core. Nanocarriers are able to transport Cu ions and release them intracellularly.

This work will compare different core-shell and core-multishell architectures in terms of loading capacity, binding strength, and pH-triggered release of Cu ions. Special focus will be given to the biological properties like the transport into cells, increase of cellular Cu level,

cellular accessibility of imported Cu, and the transport across the BBB by using an in vitro model. Furthermore, it will be investigated how the structural design of the nanocarriers impacts the transport behavior of Cu and the cytotoxicity.

In order to enhance the Cu shielding from the environment and prolong blood circulation without losing biocompatibility, PEG units will be attached. PEGylated nanocarriers shall be investigated more from the physicochemical point of view. UV/Vis measurements will be used to determine the maximum Cu loading of the nanocarriers. Since size and charge of the nanocarriers are important factors for permeability through the BBB and blood circulation time, dynamic light scattering (DLS) and zeta potential measurements will be performed. Complex stability can be shown in experiments, where other metal ions like Zn(II) compete with Cu(II) for the amino ligands. Also in this case, investigation of Cu loading and release as well as their cytotoxicity depending on the architectural arrangement of the nanocarriers will also be discussed.

3 Publications and Manuscripts

3.1 Copper Transport Mediated by Nanocarrier Systems in a Blood-Brain Barrier In Vitro Model

This chapter was submitted to *Biomacromolecules*

Susanne Fehse[‡], Sabrina Nowag[‡], Mohiuddin Quadir, Kwang Sik Kim, Rainer Haag[*], Gerd Multhaup[*]

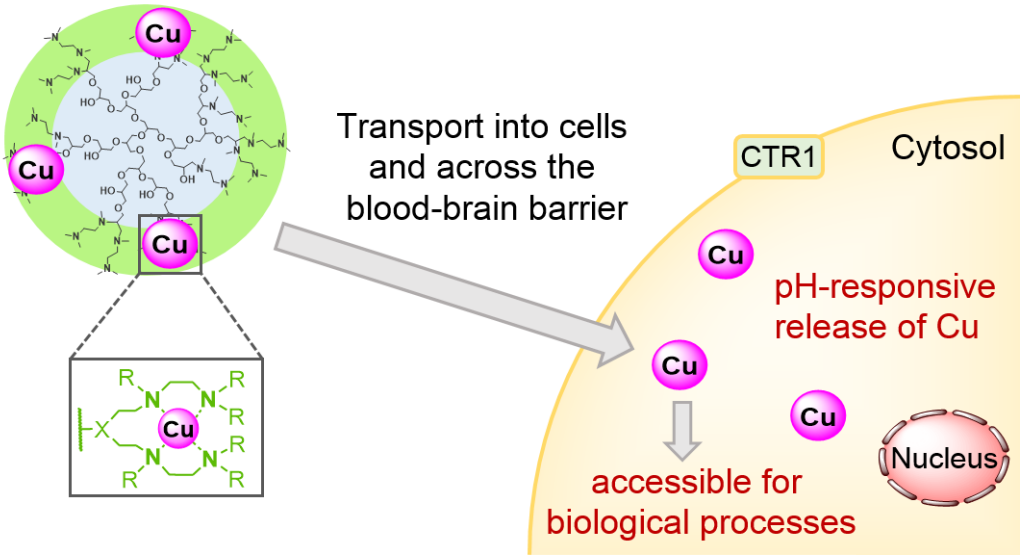

Author's Contribution

- Synthesis of core-shell nanocarrier (CS-NP)
- Loading of the nanocarriers with Cu ions
- Confocal microscopy images
- Redesign of the determination of the Cu level in cells after import together with Susanne Fehse
- Discussion and evaluation of the results
- Manuscript preparation together with Susanne Fehse

Copper Transport Mediated by Nanocarrier Systems in a Blood-Brain Barrier In Vitro Model

Susanne Fehse,[1‡] Sabrina Nowag,[2‡] Mohiuddin Quadir,[2] Kwang Sik Kim,[3] Rainer Haag,[2] Gerd Multhaup*[1]*

[1]Dipl. Biol. Susanne Fehse‡, Freie Universität Berlin, Institut für Chemie und Biochemie, Thielallee 63, 14195 Berlin, Germany. Prof. Dr. Gerd Multhaup*, Department of Pharmacology & Therapeutics, McGill University, 3655 Promenade Sir-William-Osler, McIntyre Building, Room 1325, Montreal, QC Canada H3G 1Y6. Tel. (514) 398 3621, Fax (514) 398 2045, E-mail gerhard.multhaup@mcgill.ca

[2]M. Sc. Sabrina Nowag‡, Dr. Mohiuddin Quadir, Prof. Dr. Rainer Haag*, Freie Universität Berlin, Institut für Chemie und Biochemie, Takustraße 3, 14195 Berlin, Germany

[3]Prof. Dr. Kwang Sik Kim, Johns Hopkins University, School of Medicine, Division of Pediatric Infectious Diseases, 200 North Wolfe St, Baltimore, Maryland 21287, USA

ABSTRACT

Copper (Cu) is a cofactor of various metalloenzymes and has a role in neurodegenerative diseases with disturbed Cu homeostasis, e.g., in Alzheimer's disease (AD) and Menkes disease. To address Cu imbalances, we synthesized two different dendritic nanoparticles (NP) for the transport of Cuions across the blood-brain barrier (BBB). The synthesized NPs show low toxicity and high water solubility and can stabilize high amounts of Cu. The Cu-laden NPs crossed cellular membranes and increased the cellular Cu level. A human brain microvascular endothelial cell (HBMEC) model was established to investigate the permeability of the NPs through the BBB. By comparing the permeability×surface area product (PS_e) of reference substances with those of NPs, we observed that NPs crossed the BBB model two times more effectively than ^{14}C-sucrose and sodium fluorescein (NaFl) and up to 60 times better than Evans Blue labeled albumin (EBA). Our results clearly indicate that NPs cross the BBB model effectively. Furthermore, Cu was shielded by the NPs, which decreased the Cu toxicity. The novel design of the core-shell NP enabled the complexation of Cu in the outer shell and therefore facilitated the pH-dependent release of Cu in contrast to core-multishell NPs, where the Cu ions are encapsulated in the core. This allows a release of Cu into the cytoplasm. In addition, by using a cellular detection system based on a metal response element with green fluorescent protein (MRE-GFP), we demonstrated that Cu could also be released intracellularly from NPs and is accessible for biological processes. Our results indicate that NPs are potential candidates to rebalance metal-ion homeostasis in disease conditions affecting brain and neuronal systems.

KEYWORDS: core-shell nanoparticles, Cu ion transport, Alzheimer's disease, blood-brain barrier, dendritic polyglycerol

INTRODUCTION

Copper (Cu) is an essential element that is needed for various biological functions and its levels are tightly regulated in a systemic environment. In addition, Cu is a cofactor of many important metabolic enzymes and has a role in such essential cellular processes as neuronal activity and signal transduction. The main Cu uptake into eukaryotic cells is mediated by channel-like high-affinity copper transport protein-1 (Ctr1) and partially mediated through low-affinity transport mechanisms.[1] External Cu(I) transported by Ctr1 is then delivered to Cu chaperones. Cu delivery to the Cu/Zn SOD1 requires the Cu chaperone of Cu/Zn superoxide dismutase-1 (CCS), the Cu chaperone Cox17 binds up to four Cu(I) ions and functions in the Cu delivery pathway to cytochrome oxidase[2] and Cu(I) is transferred from the surface of Atox1 to a metal binding domain in the N-terminus of ATPases ATP7A and ATP7B.[3] Mutations in ATP7A or ATP7B cause Menkes or Wilson disease. In Wilson disease, a dysfunction of the Cu transport gene ATP7B causes a Cu accumulation in liver, brain, and even eyes. Oral application of Cu-chelating compounds could restore copper homeostasis in many Wilson-disease-patients.[4] The Menkes disease is characterized by a genetically defective ATP7A, which leads to an intestinal Cu accumulation and a severe Cu deficiency in peripheral tissues including the brain.[5] The disturbed Cu homeostasis with low Cu levels in the brain and decreased activities of Cu-dependent enzymes lead to the typical clinical hallmarks.[4] Menkes disease is a rare disorder seen in childhood that results in progressive neurodegeneration. Cu-histidine is used as a treatment and neurodegeneration can be prevented if treatment starts before two months of age.[6]

In AD, an aberrant Cu homeostasis has been associated with the disease.[7] Key proteins in AD, such as the amyloid precursor protein (APP),[8] the β amyloid peptide (Aβ),[9] which is derived from

APP as a result of proteolytic cleavage by β-site amyloid precursor protein cleaving enzyme-1 (BACE1)[10-11] and presenilin γ-secretase,[12] have been identified as metalloproteins.

APP can act as a Cu transporter[13-14] because the ectodomain of APP contains a Cu-binding site where Cu(II) binds to and is reduced to Cu(I).[8,15] Furthermore, Cu ions can induce oligomerization of the BACE1 transmembrane sequence, which might influence substrate recognition and activity.[11] An imbalanced Cu-homeostasis is a problem in all of these disease conditions. In the case of AD, for example, a dietary oral treatment of AD patients with Cu-orotate had neither a detrimental nor a beneficial effect on AD development in a clinical phase II trial.[16] However, levels of soluble Aβ42, which is used as a biomarker in cerebrospinal fluid (CSF), were slightly higher in treated patients indicating a slower aggregation process than normally observed. It might be possible to improve this beneficial effect with better Cu-transport across the blood-brain barrier (BBB) to provide sufficient amounts bioavailable Cu to the neuronal cells. Transporting Cu across the BBB is most challenging when Cu-deficiency disorders are treated dietarily. Such compounds, however, could be used to achieve efficient transport by controlling an active or carrier-mediated passive mechanism and the supply of small molecules and electrolytes to and from the CNS to systemic circulation. Another challenge is the transport into the cells and intracellular release of Cu(II) ions.

To this end, a suitable carrier system is needed, which can encapsulate Cu(II) ions with substantial stability to ensure the systemic transport of the metal ions in vivo. In addition, the structural design of such carriers should not only facilitate the BBB traffic of the encapsulated Cu(II) but also its release within neuronal cells of the brain, where Cu(II) is needed for biological processes. Different Cu chelating molecules like Clioquinol (CQ) have been studied as a potential therapeutic agent. CQ facilitated the transport of extracellular Cu across cell membranes and

changed soluble Aβ and copper levels in cells and brain tissue,[13,19] but severe side effects excluded CQ from therapeutic applications.[20] Thus, the use of nanometer-sized transporters based on Cu-complexing macromolecules are beneficial, because they can be tailored to optimize their properties such as hydrodynamic size, surface charges, and conductive transport to the area of intended application.[21] A substantial number of drug delivery systems have been developed to bypass the BBB, among which nanoparticle-based systems seem to be most efficient.[22] Due to the substantial loading capacities of the nanocarriers, a high local concentration of the drug can be achieved in specific tissues. There is a scarcity of literature on the transport of metal ions by nanocarriers, and their ability to cross the BBB has largely been overlooked.[23-24]

Herein we report on dendritic core-single shell (CS-NP) and core-multishell nanoparticles (CMS-NP) based on hyperbranched polymers and compare them head-to-head for their chemical, biochemical, and Cu-stabilizing properties relating to the nanoparticle architectures. The transport of Cu into cells, the pH-triggered release of Cu ions from the nanoparticle, and the cytotoxicity and penetration of the nanoparticles in a BBB model are reported.

EXPERIMENTAL SECTION

Materials and Methods

^{1}H NMR and ^{13}C NMR spectra were recorded on ECX 400 (400 MHz for ^{1}H and 100 MHz for ^{13}C). Calibration was performed using the chloroform peak at 7.26 ppm for ^{1}H and 77.0 ppm for ^{13}C. IR spectra of neat samples were recorded on a Nicolet Avatar 320 FT-IR spectrometer (Thermo Fisher Scientific, Dreieich, Germany). UV/Vis spectra were recorded with Scinco S-3150 (range: 190-1100 nm, resolution 1024 points) in fast mode. Calibration was performed at 360.85 and 453.55 nm with holmium oxide glass. The spectra were recorded at r.t. and were evaluated

with Labpro® Plus from Scinco Co., Ltd, Microsoft® Excel 2000, and Origin® 7.0 from Origin Lab Corporation. Microcal VP-ITC microcalorimeter (MicroCal, LLC, Northampton, MA) was used to carry out the calorimetric experiments. Dynamic light scattering (DLS) measurements and Zeta potential were conducted using a Zetasizer Nano-ZS (Malvern Instruments, Ltd, UK) with integrated 4 mW He-Ne laser, $\lambda = 633$ nm. For Zeta potential measurements, doppler anemometry technique was used whereby electric field was applied across the sample solution. All measurements were carried out at 25 °C using folded capillary cells (DTS 1060). The polymer concentration was 5 mg mL^{-1}. Dialysis was performed with Dialysis tubing benzoylated 10 FT from Sigma-Aldrich (molecular weight cut-off 2000 g mol^{-1}). TLC was performed on Merck aluminum sheets with silica (corn size 60) and fluorescence marker (F254). All reagents and solvents were purchased from Acros, Fluka or Sigma Aldrich and used as received.

Synthesis

CS-NP: N^1,N^1,N^2-trimethylethane-1,2-diamine modified dPG (100%):

In a sealed tube, O-tosylpolyglycerol (0.5 g, 3.28 mmol OTs group, 1.0 equiv.) was dissolved in 7 mL of p.a. DMF. N^1,N^1,N^2-trimethylethane-1,2-diamine (1.675 g, 16.4 mmol, 5.0 equiv., 2.1 mL) was added slowly at r.t. and the resulting solution was heated at 120 °C for 4 days. At the end of the reaction, the tube was cooled to r.t. and DMF was removed by cryo-distillation. The residue was dissolved in $CHCl_3$ and extracted three times with sat. Na_2CO_3 solution. The combined organic phase was washed three times with water, dried over MgSO4, concentrated in vacuo, and dialyzed in MeOH for 48 h to give the brown hard paste-like product. Yield: 72% ; Conversion: quant.; ^{1}H NMR (500 MHz, CD_3OD): δ (ppm) = 4.41-3.41 (dPG-groups), 3.42-2.98 (-CHOH-CH_2-N-CH_2-), 2.72-2.49 (-CH_2-N-CH_3), 2.42-2.10 (bs, -N-CH_3); ^{13}C NMR: (D_2O): δ (ppm) = 80.1

- 66.3 (dPG-backbone), 56.6-53.3 (-CH_2-CH_2), 45.3-40.2 (-N-$(CH_3)_2$); IR (KBr) $\bar{\upsilon}$ = 2887, 1687, 1598, 1441, 1387, 1298, 1234 cm^{-1}. M_w = 22 kDa (calculated by NMR), DLS: d = 4 ± 2 nm, Zeta Potential (in PBS, pH 7.4): +18.2 mV.

UV/VIS analysis

To assess the maximum metal cargo capacity of the polymers, an aqueous solution of the nanotransporter was mixed with a solution of $CuSO_4$ to yield a distinct molar [Cu(II):NP] ratio within the range of 0-100. The solutions were incubated for 24 h to reach equilibrium before absorbance at the Cu binding band was monitored at specified wavelengths

Release study was performed with Cu loaded NP (Cu:CS-NP = 60:1 and Cu:CMS-NP = 40:1) in Na acetate solution (100 mM) with pH values from 7 to 3 (acidified with hydrochloric acid). Particular pH-dependent absorption of the Cu:NP complexes was monitored.

Isothermal titration calorimetry

The experimental parameters for titration experiments were number of injections 34, cell temperature 30 °C, stirring speed 290 rpm, cell volume 1.43 mL, injection volume 8 µl, injection duration 16 sec, spacing 300 sec, filter speed 2 sec, and reference power 10 µcal sec^{-1}. NP concentration (cell): 0.5 µM, Cu concentration (syringe): 0.5 mM.

Determination of imported Cu ions by ICP-MS measurements

According to UV/Vis and ITC data, stock solutions of Cu preloaded NPs with a 1:40 (for Cu:CMS-NP) and 1:60 (for Cu:CS-NP) stoichiometry, respectively, using $CuCl_2$ as the Cu source, were prepared in MilliQ-water. In general, SH-SY5Y (human neuroblastoma) cells were cultivated at

37 °C in 5% CO_2 atmosphere and 95% air moisture and the following medium was used: DMEM/MAM's F12, 10% FCS, 1x non-essential amino acids, 2 mM L-glutamine, 100 U/mL penicillin, and 100 µg/mL streptomycin. After seeding the cells in 10-cm plates with $3*10^5$ cells/mL SH-SY5Y cells were grown for at least 24 h. For Cu import analysis SH-SY5Y cells were incubated for 5 h with varying Cu:NPs concentrations. After washing with PBS-EDTA the cells were scraped from the cell plates and a 200-µl sample solution was analyzed per ICP-MS using a Finnigan Element2 Shield Torch system instrument (Thermo Fisher Scientific) as described before.[25] Data were normalized by the amount of cells.

Determination of the cellular uptake of NPs by confocal laser-scanning microscopy (CLSM)

Cellular uptake of dye-labeled CS-NP was monitored by confocal laser scanning microscopy (CLSM). For uptake studies $1*10^5$ cells/mL SH-SY5Y cells were seeded per well of a 24-well plate, in which one glass cover slide was inserted before. Cells were grown as described above for 24 h. After incubation with FITC dye-labeled CS-NP in varying concentrations, cells were washed three times with PBS-EDTA and fixed with DAPI-methanol (1 µg/mL) and Atto Phalloidin 647 in PBS (0.165 µM) for 30 min. The cells were imaged on a dried cover slip that was fixed with Fluoromount-G (SouthernBiotech) using a confocal laser scan Leica TSC SP8 microscope.

Analysis of Cu accessibility using the MRE-GFP detection system

The MRE-GFP (metal responsive elements with green fluorescent protein) detection system was kindly provided by O. Georgiev and W. Schaffner. HEK 293 (human embryonic kidney-293) cells were transient transfected with pMRE-GFP and cultivated at 37 °C in 5% CO_2 atmosphere and 95% air moisture with the following medium: DMEM high glucose, 10% FCS, 2 mM L-glutamine,

1 mM sodium pyruvate, 100 U/mL penicillin, and 100 µg/mL streptomycin. After addition of the Cu:NP complexes in varying concentrations followed by 5 h incubation, the cells were lysed in 25 mM Tris-phosphate, pH 7.8, 2 mM dithiothreitol, 10% glycerol, and 1% Triton X-100 [modified as [26]]. The cells were incubated for 30 min at 4 °C on a distributing jigger and centrifuged for 10 min at 10,000 rpm and 4 °C. The supernatant was measured at 485/535 nm (extinction/emission) for GFP fluorescence. Data were normalized to an untreated control.

Transport studies using an HBMEC model of the blood-brain barrier

We used an in vitro model of the BBB based on the HBMEC cell line. Cells were developed and provided by Prof. K. S. Kim. To create the stable cell line HBMEC, originally primary endothelial cells of human brains were isolated and transfected with SV40-LT (simian virus 40 large T antigen).[27-28] The cells were used up to passage 30 and showed characteristics typical of blood-brain endothelial cells.[27] Cells were cultivated at 37 °C in 5% CO_2 atmosphere and 95% air moisture and the following media was used: RPMI 1640, 10% (v/v) FCS (fetal calf serum), 10% NU-Serum (BD, Germany), 1x non-essential amino acids, 2 mM L-glutamine, 1 mM sodium-pyruvat, 1x vitamine, 100 U/mL penicillin und 100 µg/mL streptomycin.

For permeability experiments specified transwell systems (Corning, USA) with luminal chambers (0.5 mL) and abluminal chambers (1.5 mL) separated with a membrane (pores of 3 µm) were used. The membranes were preincubated with Collagen IV/Fibronectin solution (Sigma-Aldrich, Germany). HBMECs were plated to a density of $2 * 10^5$ cells/mL and grown for four more days. Before adding the Cu:NP solution the TEER value was determined (Millipore, USA). After 20, 40, and 60 minutes of incubation the abluminal wells were replaced by fresh wells to imitate cerebral flow. Afterwards the TEER was measured again. Cell-free wells were used as

controls. The fractions were analyzed for their Cu content via ICP-MS measurements. Transport analyses were performed in OptiMEM. The permeability × surface area product (PS_e) of the substances was calculated as described before.[29]

Statistics

For statistical analysis GraphPad Prism Software was used. First the standard error of the mean (SEM) was calculated. As a normality test the Shapiro Wilk test was used. According to the existence of normal distribution one-way Anova or Kruskal-Wallis tests were performed. Dunnett's or Dunn's multiple comparison test functions were used as a post-hoc test.

RESULTS AND DISCUSSION

Synthesis of Nanocarriers

The aim of this study was (i) to develop novel nanocarriers based on polymeric core-shell nanoparticles and (ii) to test for transport of Cu(II) ions into different cells including a BBB model to address Cu deficiencies and to recover Cu homeostasis. The intracellular release was analyzed as a function of pH. Since oligoamines are known to form strong complexes with Cu(II), we focused on dendritic poly(ethylene imine) (PEI) and diamino-functionalized dendritic polyglycerol (dPG) to fabricate Cu-encapsulating constructs. Both of the dendritic polymers used in this study have already been reported for the synthesis of cores for biocompatible CMS,[30-31] e.g., for the stabilization of metal-NPs, dyes, and drugs.[32-35] The presence of a large number of modifiable functional groups,[30] facile synthesis,[36] low cytotoxicity, high biocompatibility,[37] and

substantial cargo-loading capacities[34] predicted dendritic PEI and dPG based CMS systems as ideal candidates to facilitate the transport of metal-ions across cell membranes.

In this paper, we compared two design architectures: a CS-NP and a CMS-NP. CS-NP is composed of a dPG core (M_w = 10 kDa) coupled to a single shell of trimethylethylene diamine (TMEDA) (Figure S1). Since amines can be toxic in high concentrations, the ligands were bound to a nontoxic dPG core to increase the biocompatibility of the nanocarrier. Due to protonation of amines in aqueous solution, the NPs complied with the requirements to enter cells by adsorptive endocytosis.

CMS-NP (Figure 1A) is composed of a dendritic poly(ethylene imine) (PEI) core (M_w = 5 kDa) attached to linear amphiphilic building blocks comprised of C_{18}-alkyl diacids which in turn is connected to monomethyl poly(ethylene glycol) (mPEG) chain (M_w = 550 Da). The double-shell concept was introduced to mask the amino ligands and increase the biocompatibility. The degree of functionalization of the PEI core was maintained within the range of 40 – 45% according to a previously reported procedure.[36] These particles had a molecular weight of ~20 kDa and a hydrodynamic diameter of 5 nm as determined by ^{1}H-NMR and dynamic light scattering (DLS), respectively.

For the synthesis of TMEDA-functionalized CS-NPs the dPG cores were reacted with tosyl chloride in pyridine to convert the hydroxyl group to a highly efficient tosyl leaving group (see Figures 1B and S1). ^{1}H-NMR-analysis of CS-NP was performed to investigate the degree of functionalization. After substitution of tosyl group with TMEDA, the complete absence of aromatic signals and appearance of signals due to TMEDA alkyl functionalities within the dPG backbone indicated the successful completion of the reaction. The molecular weight calculated

from ^{1}H-NMR for this system was ~22 kDa and dynamic light scattering (DLS) measurements of the resulting CS-NPs showed a hydrodynamic diameter was in the order of 4 nm.

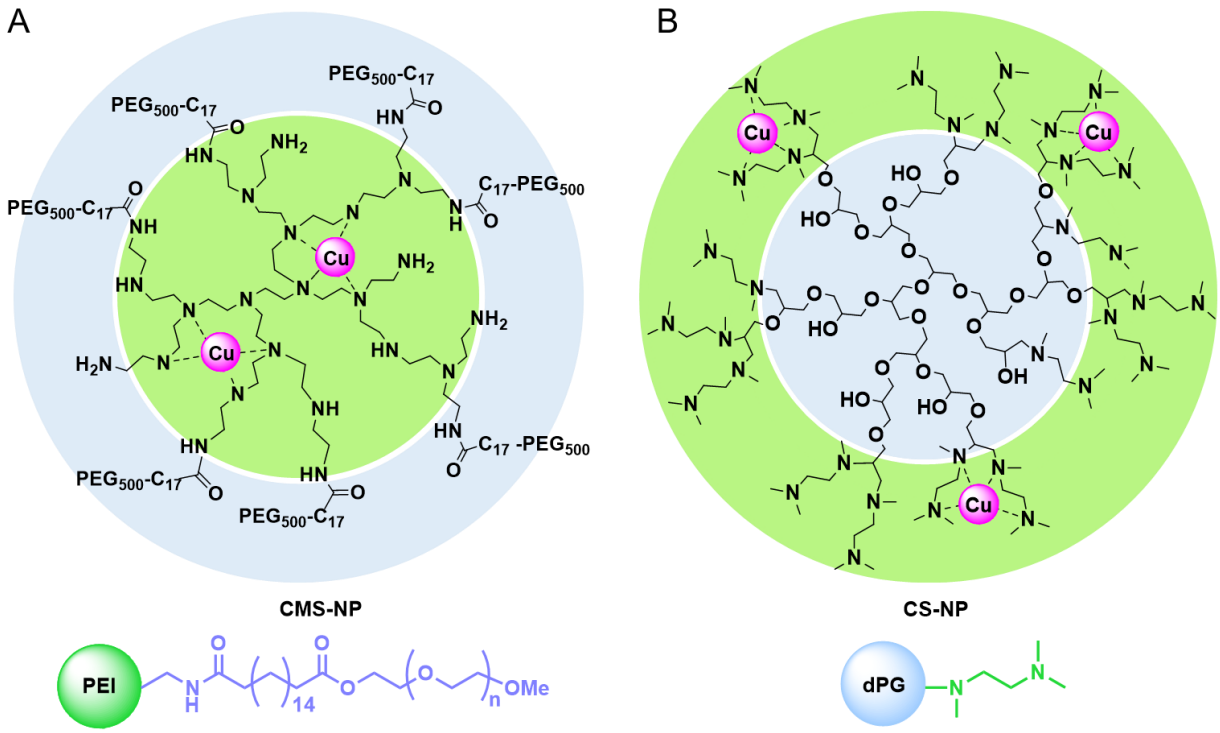

Figure 1. Structures and Cu(II) complexation of the different NP architectures. (A) CMS-NP complexes Cu(II) inside the PEI core, (B) CS-NP stabilizes Cu(II) ions in its amino ligand shell.

Although CMS-NP were able to import Cu into eukaryotic cells,[23] the structural effects, the potential of these constructs to cross the BBB and the cellular accessibility of the introduced Cu had never been addressed before. In spite of the low LD_{50} value of CMS-NPs, the intrinsic toxicity associated with a PEI core of such particles may lead to side effects in in vivo situations.[38] We therefore wanted to develop more biocompatible core-shell NP systems based on a dPG core. In contrast to PEI, the dPG core which is composed of an all polyether backbone is non-toxic and non-immunogenic.[35,38-40] Since bare dPG has a very low Cu-complexing property, we attached

TMEDA, a strong Cu-binding ligand, to the primary and secondary hydroxyl groups of the dPG. The amino ligands enabled dPG to stabilize Cu ions in the same manner as PEI stabilizes metal ions (Fig. 1) but with a significantly four times lower cytotoxicity. Furthermore, the complexation in the outer shell of the CS-NP should facilitate the intracellular Cu release. Thus, Cu should be more accessible for intracellular processes when released from CS-NP. In contrast, CMS-NP contains the Cu-binding amines in the core of the macromolecular scaffold (see Fig. 1), which could hinder the release of Cu.

Cu loading capacity and enthalpies of Cu-NP complexes

Encapsulation of a sufficient amount of Cu is an essential prerequisite for Cu-NP complexes to achieve significant biological effects. Thus, both CS- and CMS-NPs were analyzed for their spontaneous encapsulation property towards Cu ions. The maximum loading capacity of the individual NP was investigated by spectroscopic and microcalorimetric titration of the NPs with $CuSO_4$ as an initial test. Spectroscopically, in the absence of a polymer with complexation capabilities, Cu(II) primarily exists as $[Cu(H_2O)_6]^{2+}$ in aqueous solutions, which gives rise to a broad, weak absorption band at 810 nm associated with a d-d transition ($\varepsilon \sim 10$). In the presence of Cu-encapsulating groups as polyethylene imine (in CMS-NP) or TMEDA (in CS-NP), λ_{max} for the Cu(II) d-d transition is shifted to 600-650 nm with another strong ligand-to-metal-charge-transfer (LMCT) transition band appearing in the 280-300 nm region. With a higher ratio of Cu(II) to polymer, the spectrum shows a tendency to shift towards the longer wavelength. This change in UV/Vis spectrum allows one to follow the Cu(II) ion binding with different nanoparticle systems containing Cu-encapsulating properties. In this experiment, the absorbance at λ_{max} = 630 nm increased with increasing Cu:NP ratio until a critical value is reached, above which the absorbance

only increased slowly (Figure 2A). An UV/Vis spectroscopic experiment revealed that the highest number of 40 Cu ions were encapsulated by the CMS-NP[23] while the CS-NP accommodated 60 Cu ions.

The discrepancy in Cu loading stoichiometry between CMS- and CS-NP is most likely due to the presence of the polyamine core in CMS-NP, which stabilizes most of the Cu ions in a more sterically challenging environment compared to CS-NPs, because of the presence of C_{18}-alkyl and mPEG functionalization. CS-NPs, on the other hand, are more easily accessible for incoming Cu(II) ions since the ions are bound to the outermost TMEDA shell with relative ease (Figure 1). This observation was further supported by the fact that the loading capacity of TMEDA functionalized dPG core towards Cu is linearly dependent on the degree of core-functionalization with the amine moiety (data not shown). We postulate that the higher loading capacity for CS-NP compared to CMS-NPs is mostly because the Cu ions can easily access the amine-dense area within the nanoparticle interior.

The Cu-encapsulation stoichiometry of CS-NP (Cu:CS-NP = 60:1) is much higher compared to currently used monomeric Cu-chelators such as CQ or glyoxalbis(N-(4)-methylthiosemi-carbazonate) (gtsm), which exhibit stoichiometry of 1:2 for Cu:CQ or 1:1 for Cu(II):gtsm.[18,41] Using polymer-based Cu-complexing agents like for CMS- or CS-NPs it is possible to transport higher amounts of Cu ions and to increase the local concentration of Cu(II) in the targeted regions and reduce off-target deposition. All effects are beneficial for increasing the therapeutic efficacy.

The energetics of complexation is of critical importance for the development of metal ion delivery systems since it influences the in vivo stability of the complex in fluctuating conditions before it reaches the target tissue. The Cu:NPs need to be engineered so that the complexes are stable enough to transport Cu through the blood without premature Cu-release, and at the same

time, only carry the guest ion under controlled conditions within the cellular microenvironment. To this end, the thermodynamics and stoichiometry of this complexation was investigated and isothermal titration calorimetry (ITC) experiments[42] were carried out between the nanoparticles and the metal ion. In the enthalpogram (Figure 2B, inset) of the titration of Cu(II) to individual NP in water strong interactions were observed as indicated by the strong heat flow signal (μcal sec^{-1}) from the baseline. The resulting binding isotherm (Figure 2B, 2C) is hyperbolic in nature with a strong initial exothermic interaction between Cu and NP that shows a plateau indicating the saturation of the Cu-binding to the NP architecture. ITC experiment revealed that CS-NPs encapsulated Cu(II) with a heat of binding of ΔH ~ -3 kcal mol^{-1} (Figure 2B). For CMS-NP, ΔH was found to be -7 kcal mol^{-1} (Figure 2C).

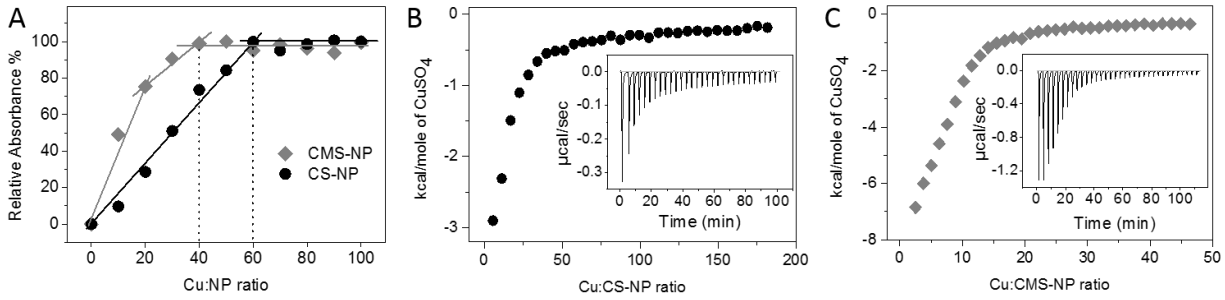

Figure 2. Complexation of Cu(II) ions by NPs. (A) UV/Vis measurements monitored the absorbance maximum of the Cu binding band at 630 nm during a titration of $CuSO_4$ solution into NP solution to determine the maximum loading. Absorbance maximum reached saturation at 60 Cu ions per CS-NP and 40 Cu ions for CMS-NP. (B+C) Binding isotherm of Cu:CS-NP (B) and Cu:CMS-NP (C) interaction obtained by ITC measurements. (B) Binding enthalpy for CS-NP was found to be -3 kcal $mole^{-1}$. (C) Binding enthalpy for CMS-NP was found to be -7 kcal mol^{-1}. Raw ITC data (insets of B and C) shows a strong exothermic interaction between Cu(II) and CS-NP.

As evident from Figure 2B, CS-NP spontaneously encapsulates Cu ions with $\Delta H \sim 3$ kcal mol^{-1}. The heat of complex stabilization for CS-NP was less than for CMS-NP ($\Delta H \sim 7$ kcal mol^{-1}) which indicated a relatively stronger (two-fold) interaction between the Cu and CMS-NP systems (Figure 2C). For both of the NPs, the enthalpogram shows that the association between the metal ion and polymer is enthalpy-driven with a decrease in entropy which essentially involves the restriction of mobility of Cu(II) ion within the complexation network. The strong release of exothermic energy is an inherent characteristic of electrostatic interaction. The fact that the Cu(II) ion is encapsulated in CMS-NP with higher stability should also be reflected in the pH-responsive release profile of Cu from both the NPs.

Cytotoxicity

The nanocarriers were designed to shield the Cu from its environment hence avoiding cytotoxicity. To study the influence of the nanocarriers on the toxicity of Cu, MTT assays in SH-SY5Y cells have been performed with Cu loaded nanocarriers. Free Cu ions are toxic to SY5Y cells at 10 μM (LD_{50}), whereas other cell lines are more resistant.[23] When Cu was stabilized in CS-NP the cytotoxicity of Cu decreased tremendously to a LD_{50} value of 600 μM. Cu/CMS-NP exhibited a LD_{50} value of 120 μM with respect to Cu (Figure 3). The unloaded NPs showed a similar toxicity respectively with a LD_{50} value of 3 μM for CMS-NP and 10 μM for CS-NP (data not shown). Cu/CS-NP is therefore less toxic and likely more appropriate for in vivo studies than Cu/CMS-NP. Since both nanocarriers showed decreased cytotoxicity compared to free Cu, the carriers successfully shielded the ion from the environment. In comparison with CS-NP, the increased cytotoxicity of CMS-NP can be more attributed to the PEI-core of the carrier scaffold than to

bound Cu. It must be noted that a daily intake of 60 mg Cu would lead to severe liver cirrhosis,[43] which further illustrates the importance of shielding and the transport of controlled amounts.

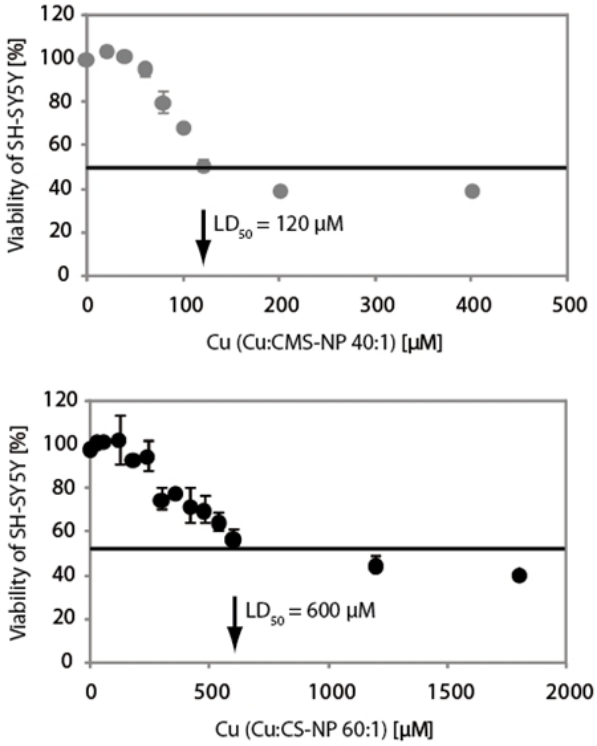

Figure 3. LD_{50} values of Cu:NPs to SH-SY5Y cells.

Uptake and increase of cellular Cu level

Neuroblastoma SH-SY5Y cells were treated with fluorescent dye-conjugated CS-NPs and their intracellular colocalization was investigated by confocal laser-scanning microscopy (CLSM). Confocal scanning revealed that FITC-tagged CS-NP system (red), which was detected in the subcellular compartments (Figure 4A) except the nucleus (Figure 4B). Furthermore, confocal z-stack analysis proved that NPs were not located within the nucleus (data not shown). The potential uptake mechanism of CMS-NPs was described earlier.[23]

For further analysis of intracellular Cu, SH-SY5Y cells were incubated with increasing concentrations of both Cu:NP complexes. Inductively coupled Plasma Mass Spectrometry (ICP-MS) measurements of cellular Cu revealed an increase of the intracellular Cu in a concentration-dependent manner for both NPs (Figures 4C, 4D). The untreated control unraveled an amount of intracellular Cu of 20 fg Cu/cell. This Cu level was increased by up to 10 times (about 200 fg Cu/cell), when the cells were incubated with Cu:CMS-NPs containing 40 µM Cu (Cu:CMS-NP 40:1) (Figure 4C). A higher Cu level could be reached with a treatment of 100 µM Cu (Cu:CS-NP 60:1), which resulted in 500 fg Cu/cell, which is 25 times more than the Cu content of the control (Figure 4D). CS-NP could be loaded with a higher amount of Cu as it is less toxic than the CMS-NP counterpart at the same NP concentration. Thus, a higher level of the intracellular Cu content could be reached with Cu:CS-NP due to the fact that more Cu was taken up by the cells in the particle-encapsulated form although a cytotoxic effect was not observed due to the chelation by CS-NP. The comparison of both carriers loaded with 10 µM Cu revealed, furthermore, that the uptake of CS-NP must be faster than of CMS-NP. While CS-NP transported 50 fg Cu into a cell, CMS-NP failed to show significant transport activity at this concentration. Our previous study revealed a cellular increase of Cu as a result of Cu:CMS-NP treatment in yeast cells.[23] Subsequently we have been able to prove that the Cu import also occurred in eukaryotic SH-SY5Y cells although the import of Cu was less than with Cu:CS-NP. Furthermore, compared to simple chelators transporting Cu, substantially higher Cu concentrations could be brought into the cells with CMS-NPs or CS-NPs. For example, Cu(II)-gtsm complexes were used with a concentration of 25 µM for SH-SY5Y cells,[18] which is at least four times lower than that of the amount of Cu used with Cu:CS-NP complexes.

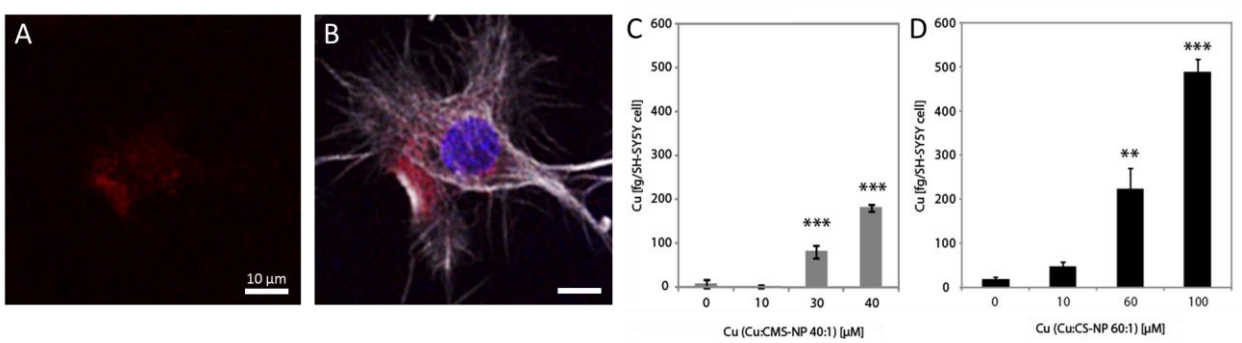

Figure 4. Cellular import of CS-NP and cellular increase of the Cu level of SH-SY5Y after Cu:NP treatment. Incubation of CS-NP with SH-SY5Y cells for 30 min revealed a cellular uptake CS-NP-FITC (A+B). Magnification 63x, scale bar in all images 10 µm. Incubation of SH-SY5Y cells for 5 h with varying Cu:NP concentrations yielded a concentration-dependent increase of the cellular Cu level quantified via ICP-MS measurements (C+D). Statistics: one-way ANOVA, Dunnett's multiple comparison test, *$p < 0.05$, **$p < 0.01$, ***$p < 0.001$, $n \geq 4$.

Previous and current experiments have indicated that several mechanisms can play a role for the uptake of CMS- and CS-NP systems. While CMS-NPs undergo an active, clathrin-mediated transport,[23] no active transport mechanism was evident for CS-NPs. In experiments where endocytosis was inhibited by inhibitors or temperature, an uptake of Cu by Cu:CS-NP was still observed (Figure S3). Since both NPs were similar in size and in diameter, the difference in the uptake processes can be attributed instead to the difference in their chemical composition. It is most likely that CS-NPs' uptake is mediated, to a large extent, by a non-specific diffusion-like mechanism, i.e., possibly a passive transport enabled by exposed tertiary amines and subsequent positive surface charge of the NPs (Figures S1 and S2). Therefore, it can be expected that CS-NP uptake is not limited compared to CMS-NPs, since there is no energy required.

Cu release and intracellular accessibility of imported Cu

Normally, Cu is bound to proteins and amino acids and free Cu in a single cell is in the order of 10^{-9} atoms which is extremely minuscule, because free Cu is toxic to the cells.[44] Furthermore, cells avoid excess Cu by a tightly regulated homeostasis including a secretion mechanism. Thus, the primary challenges for our approach is to bypass the cellular control mechanisms by minimizing the premature release and access to excretion systems.

In order to use Cu loaded NPs for therapeutic applications, the influence of the cellular microenvironment, especially the effect of different pH values on the stability of Cu:NP complexes, was investigated as a controllable system. To this end, nanoparticles with maximum Cu:NP ratio were incubated in acetate-buffered solution of different pH (3.0 – 7.0) and the absorption intensity of the Cu-complex with polymer structure at 650 nm (for CMS-NPs) and 700 nm (for CS-NPs) were systematically measured by UV/Vis spectrophotometry. A reduction in the maximum intensity at these wavelengths indicated a reduced amount of Cu:NP complexes present in the solution due to the release of the free Cu ions from the complex. As illustrated in Figure 5A, CS-NP showed a more gradual dependence of Cu-release with changing pH values, while CMS-NPs remained stable throughout the entire pH range tested. The two analyzed NPs differ in their chemical structure and therefore also in their Cu complexation stability. CMS-NPs have the capacity to bind Cu at the core, whereas the primary location of Cu for CS-NPs is in the shell (Figure 1). These different modes of binding are responsible for the difference observed in the release profiles. The encapsulation of the Cu inside the core of CMS-NP, along with its alkyl and mPEG shells, seems to protect Cu from release. Subsequently, CMS-NP, which encapsulated Cu at the expense of more enthalpic energy, is mostly unresponsive to pH-change in the environment and only releases the metal ion at pH $\leq$ 3. In contrast, CS-NP rapidly responds to

mildly acidic conditions at pH 5 since Cu(II) is bound to the ion complexing shell which is sterically more accessible to protonation of the amines resulting in acid-sensitive destabilization of the Cu-complexing domain. Assuming a lower pH in an Alzheimer patient's brain due to hyperperfusion,[45] an in vivo release of the Cu cargo from CS-NPs is expected. Furthermore, cell compartments as lysosomes or late endosomes exhibit lower pH values (~pH 4.5-5).[46] To this end, CS-NP should be more suitable to enhance a targeted Cu release in the cytoplasm of cells at pH 5.

To investigate the accessibility of Cu ions imported into cells by NPs, we adopted a MRE-GFP-detection system (metal response element with green fluorescent protein, developed and kindly provided by O. Georgiev and W. Schaffner). The principle of the MRE-GFP-detection system involves an indirect signal cascade, in which Cu ions replace Zinc (Zn) ions of metallothionein (MT). This leads to a binding of the released Zn ions to metal-responsive transcription factor-1 (MTF-1) followed by the activation of the MREs which are connected to GFP expression (Figure 5B).[47-48] To activate the GFP-expression via this indirect cascade the Cu ions have to be accessible as free Cu ions. Therefore increased GFP-expression in the cell-lines as a result of Cu loaded NP treatment clearly involves the release of Cu ions in their bioavailable form within the cytosol.

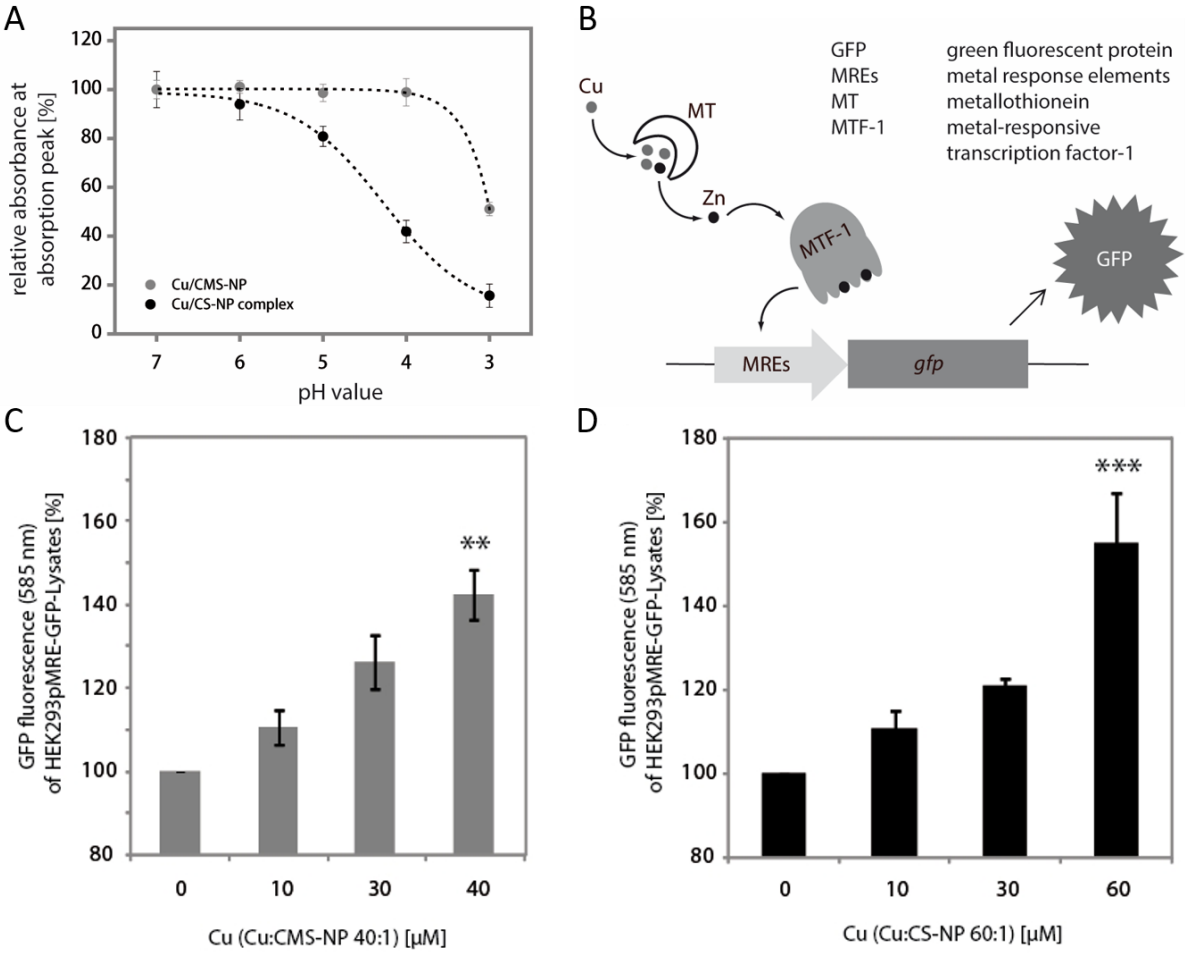

Figure 5. Release and accessibility of Cu ions. (A) pH-dependent release of Cu(II) from CMS-NP and CS-NP. Measurements of maximum absorption band of the Cu:NP complexes in 100 mM Na acetate with pH values ranging from 7 to 3. CS-NP released Cu already under mild acidic conditions at pH of 5, while Cu:CMS-NP complex disassembled at pH 3, reflecting the release of Cu under more acidic conditions. (B) Schematic illustration of the principle of the MRE-GFP-detection system. Increased cellular Cu levels led to a replacement of Zn ions bound to MT. Released Zn ions bonded to MTF-1 and trigger activation of MREs combined with gfp-expression. MRE-GFP system was used as a reporter in cells. The observed increase in GFP fluorescence indicates the release and accessibility of Cu ions. (C, D) Cu accessibility determined by this system. HEK 293 transient transfected with MRE-GFP were incubated for 5 h with Cu:CMS-NP

(C) and Cu:CS-NP (D). Quantitative fluorescence measurements of cell lysates at 485/535 nm showed a concentration-dependent increase of GFP fluorescence equally with the increase of Cu accessibility. Statistics: Kruskal-Wallis test (C, D), Dunn's multiple comparison test, *$p < 0.01$, ***$p < 0.001$, $n \geq 4$ (A,D), $n \geq 6$ (C).

To assess the amount of accessible Cu within intracellular environment, HEK 293 cells transfected with MRE-GFP construct were treated with both variants of Cu loaded NPs. A concentration-dependent increase of GFP-fluorescence was observed due to an increase of released Cu. Incubation of 40 μM Cu (Cu:CMS-NP 40:1) led to an increase of 40% in GFP fluorescence while incubation of 60 μM Cu (Cu:CS-NP 60:1) resulted in an fluorescence increase of 60% (Figures 5C and 5D). Treatment of empty NP did not show any significant difference in Cu levels compared to untreated control (data not shown).

The results indicated an intracellular Cu release and accessibility from the NPs and therefore the in vivo potential of these nanocarriers. Due to the lower toxicity, CS-NPs can be applied in higher concentrations and then release more accessible Cu than CMS-NPs. The fact that CS-NPs can also complex more Cu ions which are readily available for intracellular processing suggests that this nanocarrier design is a more suitable therapeutic candidate than their CMS-NP counterpart. It is equally important to note that the accessibility of both NPs was in the same range, when the same amount of Cu was incubated (see Figures 5C and 5D) even though the pH-dependent Cu release from CMS-NP requires slightly more acidic conditions.

The increased Cu accessibility after Cu:NP treatment is in line with the findings of a previous study, where it was shown that Cu loaded nanocarrier including CMS-NP led to enhanced SOD1 activity, which could then function as a reliable marker for bioavailable cellular Cu in yeast cells.[23]

Since our analyses were done in a eukaryotic SH-SY5Y cell line, we additionally were able to prove that these nanocarriers worked efficiently in higher developed cells.

Furthermore, SOD1 activity was restored after oral treatment with Cu sulfate in an AD mouse model. Not only did the treated AD mice have a restored Cu level, but also lower endogenous CNS Aβ levels and reduced Aβ plaques.[49] Since our NPs were able to transport high amounts of bound Cu and could thus increase the local concentration of Cu on a cellular level, they are promising candidates for further in vivo investigations.

Permeability of NPs through the blood-brain barrier using a HBMEC-model

Targeting the brain or the CNS is a major challenge for designing therapeutics addressing neuronal pathology. Only 5% of the drugs listed in the Comprehensive Medicinal Chemistry database target the CNS.[50] Therefore, the transport of Cu ions over the BBB is a critical issue for our therapeutic approach.

To analyze the permeability of NPs through the tightly closed BBB, we established an in vitro model using a human brain microvascular endothelial cell line (HBMEC, provided by K.S. Kim). A two-chamber transwell system was separated by a membrane as barrier on which HBMEC were cultured (Figure 6A). After adding Cu:NP-complexes, the amount of complex passing this barrier was determined by quantifying the amount of Cu after specific time intervals using ICP-MS. Time points were used to calculate the ability of permeation as PS_e (permeability × surface area product) which had been previously used.[29]

At first, the density of the HBMEC barrier was tested by determining the PS_e of frequently used and established marker substances. PS_e values were respectively calculated to be 61, 1720, and 1488 $*10^{-6}$ cm min^{-1} for Evans Blue labeled albumin (EBA), ^{14}C-sucrose and sodium fluorescein

(NaFl), which is in accordance with previously published data (Table 1).[29,51-56] In addition, an immunofluorescence analysis of the tight junction protein ZO1 confirmed that the tight junctions had correctly assembled (data not shown). Through this standardized HBMEC model, Cu loaded CS-NPs showed a PS_e value of 3600 ± 487 $*10^{-6}$ cm min^{-1}, while a PS_e value of 3584 ± 695 $*10^{-6}$ cm min^{-1} was determined for the Cu loaded CMS-NP system. The results show that the PS_e of both NPs did not significantly differ (see Figure 6B) which means they should both be able to cross the BBB. A comparison of the NPs with the marker substances showed that the PS_e of both NPs was twice as high as for ^{14}C-sucrose and NaFl and up to 60 times higher than for EBA (see Figure 6B). Since high PS_e values are related to elevated permeability, we could prove that both NPs can cross the in vitro model of the BBB with substantial speed compared to the reference substances investigated.

Table 1. PS_e values for EBA, ^{14}C-sucrose, and NaFl in the used HBMEC-model compared to various BBB-models in published data.

Substance	PS_e (10^{-6} cm min^{-1})	Cell line	Reference
CS-NP	3600	HBMEC	present study
CMS-NP	3584	HBMEC	present study
EBA	61	HBMEC	present study
	20	BMEC/MBGC	[56]
	113	CEC/C6 glyoma cells	[29]
^{14}C-sucrose	1720	HBMEC	present study
	1602	HPBEC	[51]
	620	PBEC/CRA	[55]
NaFl	1488	HBMEC	present study
	1812	CEC/C6 glyoma cells	[29]
	3200		
		HCEC	[53]

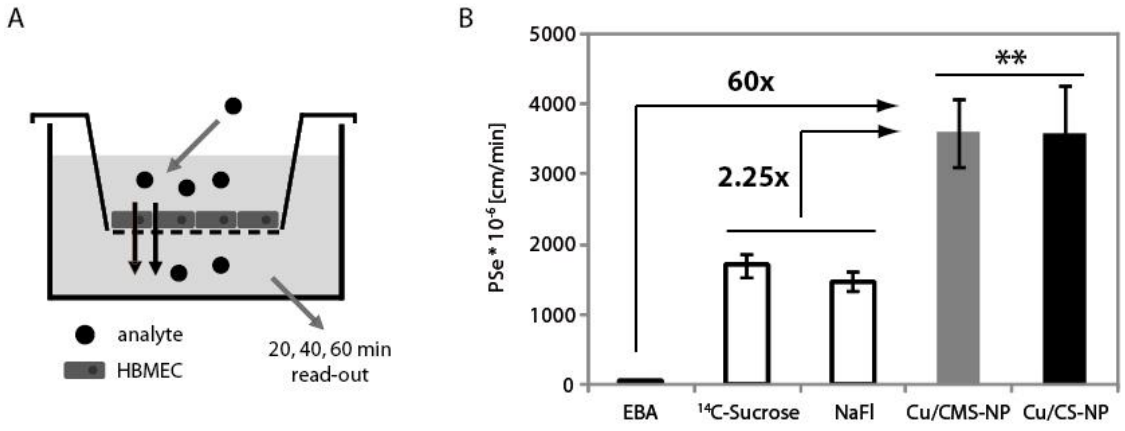

Figure 6. HBMEC in vitro model of the BBB. (A) Scheme of the HBMEC in vitro model. Cells were grown on the filter insert. Compounds added to the upper (luminal) compartment were determined after 20, 40, and 60 min in the lower (abluminal) compartment. (B) Comparison of the permeability (PS_e values in 10^{-6} cm min^{-1}) of the test compounds EBA, ^{14}C-sucrose, and NaFl with both NPs. Both NPs showed a PS_e around 3600 * 10^{-6} cm min^{-1}, which is about two-fold higher than with ^{14}C-sucrose (1720±168 * 10^{-6} cm min^{-1}) and NaFl (1488±146 * 10^{-6} cm min^{-1}) and 60 times higher than EBA (61±2 * 10^{-6} cm min^{-1}). Hence, both NPs were able to cross the in vitro BBB model. Statistics: Kruskal-Wallis test, Dunn's multiple comparison test, $n \geq 6$.

PS_e values are known for various substances in other BBB models. For example, they were 13782 * 10^{-6} cm min^{-1} and 17358 * 10^{-6} cm min^{-1} for caffeine and nicotine.[52] A PS_e of 540 * 10^{-6} cm min^{-1} was determined for acetylsalicylic acid.[52] Morphine, which crosses easily, showed a PS_e of around 1500 * 10^{-6} cm min^{-1} in in vitro models of the BBB.[52,55] The ability of CS- and CMS-NPs to cross the BBB model is lower than that of caffeine or nicotine. However, compared to morphine or acetylsalicylic acid, the ability of NPs to permeate the BBB was two or six times higher. Morphine and acetylsalicylic acid are known to be active substances in the brain.

Furthermore, less than 4% of orally applied acetylsalicylic acid is available in plasma and reaches the brain. However, this low concentration is still potent enough to be active in the brain.[57] Therefore it is perceivable that the CS- and CMS-NPs will most likely be able to show a suitable effect in the brain in an in vivo model.

Interestingly, with respect to the PS_e values, no significant difference occurred between the two NPs. Since they were similar in size, it is likely that both could be transported via identical transport routes through the BBB. Size is a problem in BBB permeability because most molecules with M_w bigger 400 Da cannot pass the BBB. However, a transfer of large hydrophilic molecules like CMS-NP and CS-NP is possible by receptor-mediated or adsorptive-mediated transcytosis.[58] Another factor that influences permeability is charge. A study comparing positively-charged with negatively-charged tripalmitin nanoparticles showed that those with cationic character had an up to 14 times increased ability to cross the BBB.[22,59-60] The surface charge of empty and Cu loaded CS-NP analyzed by zeta potential measurements showed that empty CS-NPs were positively charged (+18.2 mV) and that Cu loading decreased the surface charge of these particles to +12.1 mV (see Figure S2). Although the addition of Cu up to Cu:CS-NP ratios of 120 further decreased the surface charge, it did remain well above neutrality. This positive surface charge of the NPs most likely compensates the molecular weight restriction and thus allow the NPs to pass the BBB.

CONCLUSION

We reported and compared the design and the synthesis of novel dendritic polymer-based CS-NPs in comparison to multishell nanoparticles (CMS-NPs). As both types of nanocarriers were found

to bind significant amounts of Cu ions and release them under endosomal pH condition, this approach could very well be therapeutically relevant for addressing Cu imbalances. The chemical structure of the Cu complexing NPs were found to play a pivotal role in the 'load and release' characteristics of the NPs. In CS-NP, the Cu-chelating moieties are in the outer shell and Cu is easily encapsulated, which facilitates a release of Cu at moderately lower pH values than in CMS-NP, which requires unphysiological pH-values. Moreover, CS-NP is less toxic than CMS-NP and can shield Cu from its biological environment to decrease the intrinsic toxicity exerted by free Cu ions. Both NPs were shown to increase the intracellular Cu levels in neuroblastoma cells at nontoxic NP concentrations. When stabilized in NPs, Cu is less toxic than free Cu ions. Furthermore, it was established with a cellular BBB model that NPs can transport Cu ions across the BBB in a HBMEC model. The permeation of NPs was up to 60 times higher than that of reference substances. These results indicate that CS- and CMS-NPs can be potentially used in vivo to increase the Cu levels, e.g., in the brain. CS-NPs seem to be more suitable for the treatment of Cu deficiency disorders because of their lower toxicity, higher Cu loading, and release under mildly acidic conditions of pH 5 indicating a better bioavailability of Cu for enzymes in the cytoplasm and thereby the accessibility for cellular processes.

ASSOCIATED CONTENT

Supporting Information

Figure S1. Synthesis of CS-NP. Figure S2. Change in Zeta potential with increasing concentration of Cu(II) ions in the presence of CS-NP. Figure S3. Cellular uptake studies of Cu:CS-NP analyzed by ICP-MS. This material is available free of charge via the Internet at http://pubs.acs.org.

AUTHOR INFORMATION

Corresponding Authors

* Fax: (+)49-30-838-53-357, E-mail: haag@chemie.fu-berlin.de. *Gerhard Multhaup, Department of Pharmacology & Therapeutics, McGill University, 3655 Promenade, Sir-William-Osler McIntyre Building, Room 1325, Montreal, QC Canada H3G 1Y6, Tel. (514) 398 3621 Fax (514) 398 2045, E-mail: gerhard.multhaup@mcgill.ca

Author Contributions

‡These authors contributed equally.

ABBREVIATIONS

AD, Alzheimer's disease; NP, nanoparticles; BBB, blood-brain barrier; HBMEC, human brain microvascular endothelial cells; PS_e, permeability×surface area product; NaFl, sodium fluorescein; EBA, Evans Blue labeled Albumin; MRE-GFP, metal response element with green fluorescent protein; Ctr1, copper transporter protein-1; Cu, copper; SOD1, superoxide dismutase-1; CCS, Cu chaperone of SOD1, Cox-17, Cyto oxidase complex; Cytox, Cytochrome C oxidase; Atox1, antioxidant protein-1; ATP7A/B, Cu transport ATPasen; CNS, central nervous system; APP, amyloid precursor protein; Aβ, β-amyloid peptide; BACE1, β-site precursor protein cleaving enzyme-1; CSF, cerebrospinal fluid; CQ, clioquinol; CS-NP, core-shell nanoparticle; CMS-NP, core-multishell nanoparticle; dPG, dendritic polyglycerol; PEI, poly(ethylene imine); TMEDA, trimethylethylene diamine; DLS, dynamic light scattering; mPEG, methoxy poly(ethylene glycol); LMCT, ligand-to-metal-charge-transfer; gtsm, glyoxalbis(*N*(4)-methylthiosemicarbazonate); ITC, isothermal titration calorimetry; CLSM, confocal laser-

scanning microscopy; Zn, zinc; MT, metallothionein; MTF-1, metal-responsive transcription factor-1.

ACKNOWLEDGMENT

The authors thank the ANR-DFG program for financial support, Oleg Georgiev and Walter Schaffner for MRE-GFP construct, Gerd Buchlow and Andrea Senge, Frank Kuppler, and Thomas Wons for technical and experimental assistance and Vivienne Engelschalt for helpful discussions.

REFERENCES

1. Lee, J.; Petris, M. J.; Thiele, D. J. *J. Biol. Chem.* **2002,** *277,* 40253-40259.
2. Cobine, P. A.; Pierrel, F.; Bestwick, M. L.; Winge, D. R. *J. Biol. Chem.* **2006,** *281,* 36552-36559.
3. Pufahl, R. A.; Singer, C. P.; Peariso, K. L.; Lin, S. J.; Schmidt, P. J.; Fahrni, C. J.; Culotta, V. C.; PennerHahn, J. E.; Ohalloran, T. V. *Science* **1997,** *278,* 853-856.
4. Desai, V.; Kaler, S. G. *Am. J. Clin. Nutr.* **2008,** *88,* 855S-858S.
5. Voskoboinik, I.; Camakaris, J. *J. Bioenerg. Biomembr.* **2002,** *34,* 363-371.
6. Tümer, Z.; Moller, L. B. *Eur. J. Hum. Genet.* **2010,** *18,* 511-518.
7. Deibel, M. A.; Ehmann, W. D.; Markesbery, W. R. *J. Neurol. Sci.* **1996,** *143,* 137-142.
8. Multhaup, G.; Schlicksupp, A.; Hesse, L.; Beher, D.; Ruppert, T.; Masters, C. L.; Beyreuther, K. *Science* **1996,** *271,* 1406-9.
9. Bush, A. I.; Pettingell, W. H.; Multhaup, G.; Paradis, M. D.; Vonsattel, J. P.; Gusella, J. F.; Beyreuther, K.; Masters, C. L.; Tanzi, R. E. *Science* **1994,** *265,* 1464-1467.
10. Angeletti, B.; Waldron, K. J.; Freeman, K. B.; Bawagan, H.; Hussain, I.; Miller, C. C. J.; Lau, K.-F.; Tennant, M. E.; Dennison, C.; Robinson, N. J.; Dingwall, C. *J. Biol. Chem.* **2005,** *280,* 17930-17937.
11. Munter, L. M.; Sieg, H.; Bethge, T.; Liebsch, F.; Bierkandt, F. S.; Schleeger, M.; Bittner, H. J.; Heberle, J.; Jakubowski, N.; Hildebrand, P. W.; Multhaup, G. *J. Am. Chem. Soc.* **2013,** *135,* 19354-19361.
12. Southon, A.; Greenough, M. A.; Ganio, G.; Bush, A. I.; Burke, R.; Camakaris, J. *PLOS ONE* **2013,** *8,* 7.
13. Treiber, C.; Simons, A.; Strauss, M.; Hafner, M.; Cappai, R.; Bayer, T. A.; Multhaup, G. *J. Biol. Chem.* **2004,** *279,* 51958-51964.
14. Barnham, K. J.; McKinstry, W. J.; Multhaup, G.; Galatis, D.; Morton, C. J.; Curtain, C. C.; Williamson, N. A.; White, A. R.; Hinds, M. G.; Norton, R. S.; Beyreuther, K.; Masters, C. L.; Parker, M. W.; Cappai, R. *J. Biol. Chem.* **2003,** *278,* 17401-17407.
15. Hesse, L.; Beher, D.; Masters, C. L.; Multhaup, G. *FEBS Lett.* **1994,** *349,* 109-116.

16. Kessler, H.; Pajonk, F.-G.; Bach, D.; Schneider-Axmann, T.; Falkai, P.; Herrmann, W.; Multhaup, G.; Wiltfang, J.; Schäfer, S.; Wirths, O.; Bayer, T. *J. Neural Transm.* **2008,** *115,* 1651-1659.
17. Borchardt, T.; Camakaris, J.; Cappai, R.; Masters, C. L.; Beyreuther, K.; Multhaup, G. *Biochem. J.* **1999,** *344,* 461-467.
18. Crouch, P. J.; Hung, L. W.; Adlard, P. A.; Cortes, M.; Lal, V.; Filiz, G.; Perez, K. A.; Nurjono, M.; Caragounis, A.; Du, T.; Laughton, K.; Volitakis, I.; Bush, A. I.; Li, Q. X.; Masters, C. L.; Cappai, R.; Cherny, R. A.; Donnelly, P. S.; White, A. R.; Barnham, K. J. *Proc. Natl. Acad. Sci. USA* **2009,** *106,* 381-386.
19. Cherny, R. A.; Atwood, C. S.; Xilinas, M. E.; Gray, D. N.; Jones, W. D.; McLean, C. A.; Barnham, K. J.; Volitakis, I.; Fraser, F. W.; Kim, Y.-S.; Huang, X.; Goldstein, L. E.; Moir, R. D.; Lim, J. T.; Beyreuther, K.; Zheng, H.; Tanzi, R. E.; Masters, C. L.; Bush, A. I. *Neuron* **2001,** *30,* 665-676.
20. Schäfer, S.; Pajonk, F. G.; Multhaup, G.; Bayer, T. A. *J. Mol. Med.* **2007,** *85,* 405-413.
21. Fleige, E.; Quadir, M. A.; Haag, R. *Adv. Drug Delivery Rev.* **2012,** *64,* 866-884.
22. Kozlovskaya, L.; Stepensky, D. *J. Control. Release* **2013,** *171,* 17-23.
23. Treiber, C.; Quadir, M. A.; Voigt, P.; Radowski, M.; Xu, S. J.; Munter, L. M.; Bayer, T. A.; Schaefer, M.; Haag, R.; Multhaup, G. *Biochemistry* **2009,** *48,* 4273-4284.
24. Vincent, J. B.; Love, S. *Biochim. Biophys. Acta - Gen. Subjects* **2012,** *1820,* 362-378.
25. Mainz, A.; Bardiaux, B.; Kuppler, F.; Multhaup, G.; Felli, I. C.; Pierattelli, R.; Reif, B. *J. Biol. Chem.* **2012,** *287,* 1128-1138.
26. Dandekar, D. H.; Kumar, M.; Ladha, J. S.; Ganesh, K. N.; Mitra, D. *Anal. Biochem.* **2005,** *342,* 341-344.
27. Stins, M. F.; Badger, J.; Sik Kim, K. *Microb. Pathog.* **2001,** *30,* 19-28.
28. Stins, M. F.; Gilles, F.; Kim, K. S. *J. Neuroimmunol.* **1997,** *76,* 81-90.
29. Deli, M. A.; Abraham, C. S.; Niwa, M.; Falus, A. *Inflamm. Res.* **2003,** *52,* S39-S40.
30. Burakowska, E.; Haag, R. *Macromolecules* **2009,** *42,* 5545-5550.
31. Krämer, M.; Kopaczynska, M.; Krause, S.; Haag, R. *J. Polym. Sci. Pol. Chem.* **2007,** *45,* 2287-2303.
32. Keilitz, J.; Schwarze, M.; Nowag, S.; Schomäcker, R.; Haag, R. *ChemCatChem* **2010,** *2,* 863-870.
33. Keilitz, J.; Radowski, M. R.; Marty, J. D.; Haag, R.; Gauffre, F.; Mingotaud, C. *Chem. Mater.* **2008,** *20,* 2423-2425.
34. Quadir, M. A.; Radowski, M. R.; Kratz, F.; Licha, K.; Hauff, P.; Haag, R. *J. Control. Release* **2008,** *132,* 289-294.
35. Calderón, M.; Quadir, M. A.; Sharma, S. K.; Haag, R. *Adv. Mater.* **2010,** *22,* 190-218.
36. Radowski, M. R.; Shukla, A.; von Berlepsch, H.; Böttcher, C.; Pickaert, G.; Rehage, H.; Haag, R. *Angew. Chem. Int. Ed.* **2007,** *46,* 1265-1269.
37. Petersen, H.; Fechner, P. M.; Fischer, D.; Kissel, T. *Macromolecules* **2002,** *35,* 6867-6874.
38. Khandare, J.; Mohr, A.; Calderón, M.; Welker, P.; Licha, K.; Haag, R. *Biomaterials* **2010,** *31,* 4268-4277.
39. Kainthan, R. K.; Janzen, J.; Levin, E.; Devine, D. V.; Brooks, D. E. *Biomacromolecules* **2006,** *7,* 703-709.
40. Huang, Y.-C.; Royappa, A. T.; Tundel, S.; Tsukamoto, K.; Sharma, V. *J. Appl. Polym. Sci.* **2009,** *111,* 2275-2278.

41. Di Vaira, M.; Bazzicalupi, C.; Orioli, P.; Messori, L.; Bruni, B.; Zatta, P. *Inorg. Chem.* **2004,** *43,* 3795-3797.
42. Zysk, G.; Schneider-Wald, B. K.; Hwang, J. H.; Bejo, L.; Kim, K. S.; Mitchell, T. J.; Hakenbeck, R.; Heinz, H.-P. *Infect. Immun.* **2001,** *69,* 845-852.
43. Odonohue, J. W.; Reid, M. A.; Varghese, A.; Portmann, B.; Williams, R. *Eur. J. Gastroen. Hepat.* **1993,** *5,* 561-562.
44. Lippard, S. J. *Science* **1999,** *284,* 748-749.
45. Broussard, G. J.; Mytar, J.; Li, R. C.; Klapstein, G. J. *Inflammopharmacol.* **2012,** *20,* 109-126.
46. Li, Z.; Wu, S.; Han, J.; Yang, L.; Han, S. *Talanta* **2013,** *114,* 254-260.
47. Balamurugan, K.; Schaffner, W. *Biochim. Biophys. Acta-Mol. Cell. Res* **2006,** *1763,* 737-746.
48. Günther, V.; Lindert, U.; Schaffner, W. *Biochim. Biophys. Acta-Mol. Cell. Res* **2012,** *1823,* 1416-1425.
49. Bayer, T. A.; Schafer, S.; Simons, A.; Kemmling, A.; Kamer, T.; Tepest, R.; Eckert, A.; Schussel, K.; Eikenberg, O.; Sturchler-Pierrat, C.; Abramowski, D.; Staufenbiel, M.; Multhaup, G. *Proc. Natl. Acad. Sci. USA* **2003,** *100,* 14187-14192.
50. Pardridge, W. M. *Drug Discov. Today* **2007,** *12,* 54-61.
51. Giese, H.; Mertsch, K.; Blasig, I. E. *Neurosci. Lett.* **1995,** *191,* 169-172.
52. Lundquist, S.; Renftel, M.; Brillault, J.; Fenart, L.; Cecchelli, R.; Dehouck, M. P. *Pharm. Res.* **2002,** *19,* 976-81.
53. Muruganandam, A.; Tanha, J.; Narang, S.; Stanimirovic, D. *FASEB J.* **2002,** *16,* 240-2.
54. Descamps, L.; Coisne, C.; Dehouck, B.; Cecchelli, R.; Torpier, G. *Glia* **2003,** *42,* 46-58.
55. Garberg, P.; Ball, M.; Borg, N.; Cecchelli, R.; Fenart, L.; Hurst, R. D.; Lindmark, T.; Mabondzo, A.; Nilsson, J. E.; Raub, T. J.; Stanimirovic, D.; Terasaki, T.; Öberg, J. O.; Österberg, T. *Toxicol. In Vitro* **2005,** *19,* 299-334.
56. Gesuete, R.; Zanier, E. R.; Orsini, F.; Garzetti, L.; Deli, M.; De Simoni, M. G. *J. Cerebr. Blood F. Met.* **2009,** *29,* S83-S84.
57. Kato, H.; Yoshimoto, K.; Kobayashi, M.; Sakabe, M.; Funaki, H.; Ikegaya, H. *Eur. J. Pharmacol.* **2010,** *635,* 184-187.
58. Abbott, N. J.; Ronnback, L.; Hansson, E. *Nat. Rev. Neurosci.* **2006,** *7,* 41-53.
59. Lu, W.; Wan, J.; She, Z.; Jiang, X. *J. Control. Release* **2007,** *118,* 38-53.
60. Reddy, L. H.; Sharma, R. K.; Chuttani, K.; Mishra, A. K.; Murthy, R. R. *AAPS J.* **2004,** *6,* e23.

Supporting Information

Copper Transport Mediated by Nanocarrier Systems in a Blood-Brain Barrier In Vitro Model

Susanne Fehse[1‡], Sabrina Nowag[2‡], Mohiuddin Quadir[2], Kwang Sik Kim[3], Rainer Haag[2], Gerd Multhaup*[1†]*

[1]Dipl. Biol. Susanne Fehse‡, Freie Universität Berlin, Institut für Chemie und Biochemie, Thielallee 63, 14195 Berlin, Germany. Prof. Dr. Gerd Multhaup*, Department of Pharmacology & Therapeutics, McGill University, 3655 Promenade, Sir-William-Osler McIntyre Building, Room 1325, Montreal, QC Canada H3G 1Y6. Tel. (514) 398 3621, Fax (514) 398 2045, E-mail gerhard.multhaup@mcgill.ca

[2]M. Sc. Sabrina Nowag‡, Dr. Mohiuddin Quadir, Prof. Dr. Rainer Haag*, Freie Universität Berlin, Institut für Chemie und Biochemie, Takustraße 3, 14195 Berlin, Germany

* Fax: (+)49-30-838-53-357. E-mail: haag@chemie.fu-berlin.de

[3]Prof. Dr. Kwang Sik Kim, Johns Hopkins University, School of Medicine, Division of Pediatric Infectious Diseases, 200 North Wolfe St, Baltimore, Maryland 21287, USA

SUPPORTING EXPERIMENTAL SECTION

Synthesis of CS-NP:N,N,N'-trimethylethane-1,2-diamine modified dPG (100%):

In a sealed tube, O-tosylpolyglycerol (0.5 g, 3.28 mmol OTs group, 1.0 equiv.) was dissolved in 7 mL of p.a. DMF. *N*,*N*,*N*'-trimethylethane-1,2-diamine (1.675 g, 16.4 mmol, 5.0 equiv., 2.1 mL) was added slowly at r.t. and the resulting solution was heated at 120 °C for 4 days. At the end of the reaction, the tube was cooled to r.t. and DMF was removed by cryo-distillation. The residue was dissolved in $CHCl_3$ and extracted three times with sat. Na_2CO_3 solution. The combined organic phase was washed three times with water, dried over $MgSO_4$, concentrated in vacuo, and dialyzed in MeOH for 48 h to give the brown hard paste-like product. Yield: 72% ; Conversion: quant.; ^{1}H NMR (500 MHz, CD_3OD): δ (ppm) = 4.41-3.41 (dPG-groups), 3.42-2.98 (-CHOH-C*H*$_2$-N-CH_2-), 2.72-2.49 (-C*H*$_2$-N-CH_3), 2.42-2.10 (bs, -N-C*H*$_3$); ^{13}C NMR: (D_2O): δ (ppm) = 80.1 - 66.3 (dPG-backbone), 56.6-53.3 (-*C*H_2-CH_2), 45.3-40.2 (-N-(*C*H_3)$_2$); IR (KBr) $\bar{\upsilon}$ = 2887, 1687, 1598, 1441, 1387, 1298, 1234 cm^{-1}. M_w = 22 kDa (calculated by NMR), DLS: d = 4 ± 2 nm, Zeta Potential (in PBS, pH 7.4): +18.2 mV.

SUPPORTING FIGURES

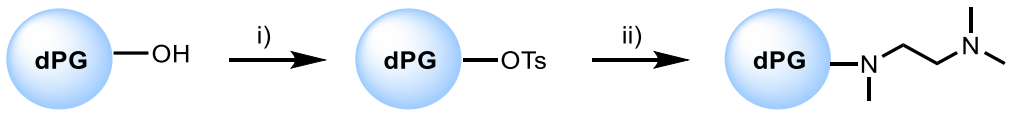

Figure S1. Synthesis of CS-NP. i) 0.7 equiv. TsCl, pyridine, ii) 5 equiv. TMEDA, DMF, 120 °C, 4 d.

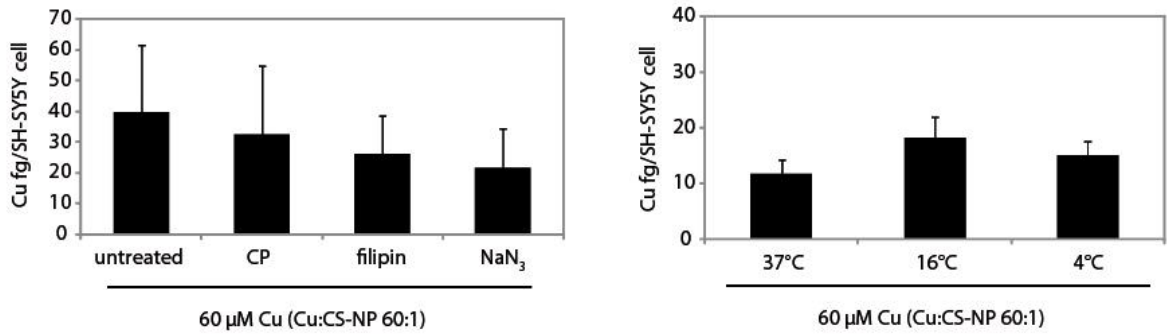

Figure S2. Cellular uptake studies of Cu:CS-NP analyzed by ICP-MS. Neither inhibitors, which are known to block endocytosis, nor low temperature (16 °C and 4 °C) could inhibit the Cu transport of Cu:CS-NP into the cell. Statistics: one-way ANOVA, Dunnett's multiple comparison test, $n \geq 3$.

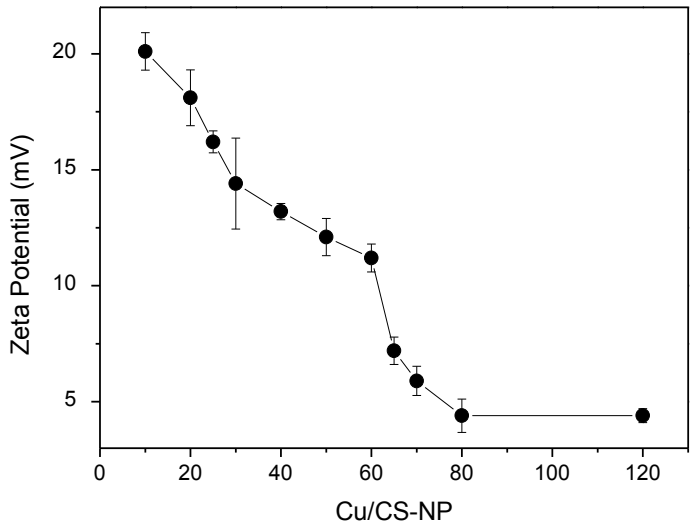

Figure S3. Change in Zeta potential with increasing concentration of Cu(II) ions in the presence of CS-NP. Measurements were performed in 0.01 M PBS at pH 7.4 with 5 mg/mL NP. To assess the effect of Cu(II) on surface charge of NPs, the NPs were loaded with maximum stoichiometric amount of Cu (evaluated from ITC and UV-Vis titration). After incubation, free Cu was removed from the polymer encapsulated species by dialysis. The retentate solution was freeze-dried and subsequently redissolved in a specific volume of PBS of pH 6.5.

3.2 Biocompatible, Hyperbranched Nanocarriers for the Transport and Release of Copper Ions

This chapter was submitted to *Journal of Materials Chemistry B*

S. Nowag, C. Frangville, G. Multhaup, J.-D. Marty, C. Mingotaud, R. Haag*

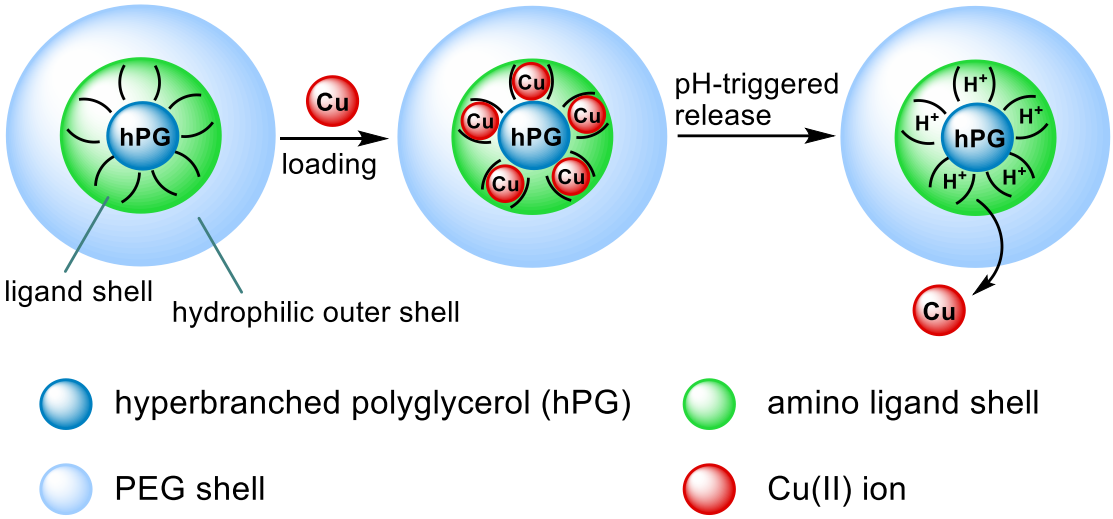

Author's Contribution

- Development of synthetic procedure and synthesis of core-multishell and core-randomshell nanocarriers
- Loading of nanocarriers with Cu ions
- UV/Vis for the determination of maximum loading capacity and pH-dependent release
- Dynamic light scattering and zeta potential experiments
- In vitro experiments
- Confocal microscopy images together with Katharina Achazi
- Preparation of the manuscript

Journal of Materials Chemistry B

RSCPublishing

COMMUNICATION

Biocompatible, Hyperbranched Nanocarriers for the Transport and Release of Copper Ions

Cite this: DOI: 10.1039/x0xx00000x

S. Nowag [a], C. Frangville[b], G. Multhaup[c], J.-D. Marty[b], C. Mingotaud[b], R. Haag [a,*]

Received 00th January 2012,
Accepted 00th January 2012

DOI: 10.1039/x0xx00000x

www.rsc.org/

Core-shell and core-multishell nanocarriers were designed to transport copper ions into cells. Herein, we present their synthesis and physicochemical characterization and demonstrate the high influence of their architectures on the loading and release of copper. Their low toxicity may open a new way to balance the Cu-homeostasis in neurodegenerative diseases.

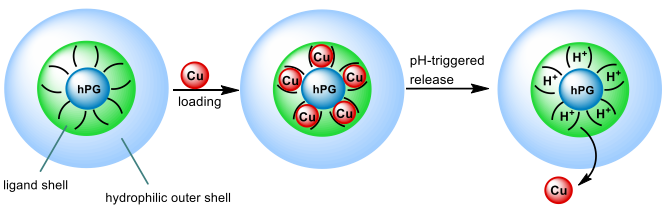

Scheme 1. Encapsulation and release of Cu ions in nanocarrier systems.

Copper (Cu) is an important biological cofactor for a number of metalloenzymes and plays a key role in many neurodegenerative diseases,[1] e.g., Alzheimer's disease (AD) and Parkinson's disease. Particularly in the case of AD, a disturbed homeostasis of Cu leads to a Cu deficiency in the central nervous system (CNS). Exogenous supply of Cu to brain or CNS is one of the many therapeutic approaches for addressing such deficiency symptoms.[2] For such a purpose, copper supply needs to bypass the blood-brain barrier (BBB), which remains an unsolved problem. Additionally, hyperperfusion in AD brain leads to decreased pH and inflammatory processes in the CNS.[3] All the previous information shepherds the design of smart nanocarriers capable of performing Cu pH-triggered delivery across the BBB (see Scheme 1). Hyperbranched polymers are promising representatives of size controllable nanoscaffolds for transport and drug delivery.[4-7] In previous works, hyperbranched poly(ethylene imine) (PEI) has been used to develop Cu-encapsulating nanocarriers.[8] However, the poor biocompatibility due to the presence of large number of amine groups within the PEI limited the applications of such systems.

To enhance biocompatibility, new core-multishell nanocarriers with lower toxicity are required, e.g., functionalized, hyperbranched polyglycerol (hPG). As a macromolecule, hPG possesses a highly branched globular, dendritic structure of a stable polyether scaffold and can be synthesized in a one-step process.[9] It exhibits similar properties to the well-used and FDA-approved poly(ethylene glycol) (PEG), as it is non-toxic, biocompatible, and not recognized by the immune system.[10] Furthermore, a modification of hPG is facile due to its large number of peripheral hydroxyl groups. These functionalized hPG can therefore be tailored to required properties such as size, charge, or molecular weight, respectively.[5, 11-15] By the attachment of shells, specialized architectures can be designed for a wide variety of applications.[16-20]

Herein, we present the synthesis and properties of different modified hPG to develop biocompatible Cu–nanocarriers as potential candidates in therapy of Cu deficiency disorders. An hPG with a molecular weight of 10 kDa was selected for the core in order to get nanocarriers of few tenths of nanometers. Cu-binding ligands to be attached on hPG cores were then reviewed to fit in our specifications. One example for Cu-binding ligands are triazacyclononanes, because they are known to form very strong complexes with Cu which are irreversible under

a Institut für Chemie und Biochemie, Organische Chemie, Freie Universität Berlin, Takustr. 3, 14195 Berlin, GERMANY.
b Laboratoire des Interactions Moléculaires et Réactivités Chimiques et Photochimiques, Université de Toulouse, CNRS UMR 5623, 31062 Toulouse Cedex 09, FRANCE.
c Department of Pharmacology and Therapeutics, McGill University, 3655 Promenade Sir-William-Osler, Montréal, QC H3G 1Y6, CANADA.
Electronic Supplementary Information (ESI) available: Experimental section, Cu and Zn loading capacity, pH-triggered Cu release, Colloidal behavior in water, Metal ion competition. See DOI: 10.1039/c000000x/

This journal is © The Royal Society of Chemistry 2012

physiological conditions.[21] Clearly, copper-release into CNS acidic conditions requires a weaker ligand for a pH-triggered release of Cu. Tri- or dimethylethylene diamine moieties (TMEDA or DMEDA, respectively) have been chosen as suitable candidates.[22] They form square planar bidentate Cu-complexes with moderate interactions, which enable pH-dependent Cu release. Furthermore, in order to increase biocompatibility, to enhance the retention time within blood circulation, or to hide the Cu from the environment, attachment of poly(ethylene glycol) chains (PEG) in the outer sphere is required (see Scheme 1). Two kinds of attachments were chosen to investigate the influence of structural design of nanocarriers on Cu-loading and release, as well as their biocompatibility. Thus, hydrophilic PEG chains were bound to amine building blocks leading to a core-multishell structure (CMS) or directly to the hPG core for a core-random shell architecture (CRS) (see Scheme 2). Finally, hPG fully modified by TMEDA (CS structure in Scheme 2) was used as a reference system.[23]

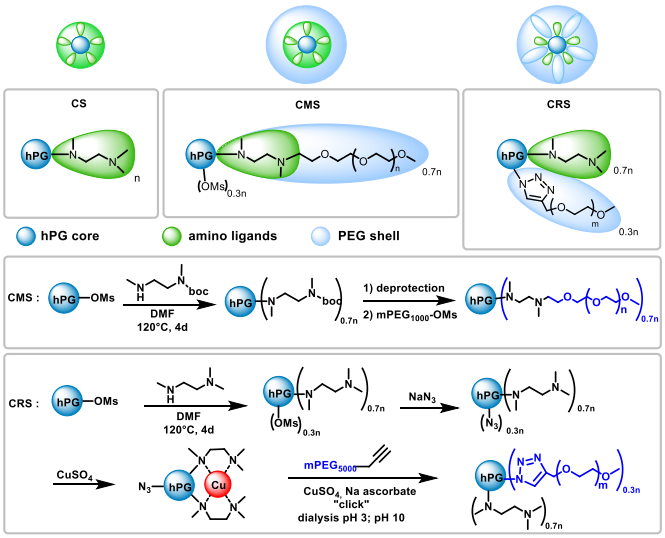

Scheme 2. Structure and synthesis scheme of CS, CMS and CRS.

For the CMS synthesis, boc-protected DMEDA was first reacted with hPG to cover 70% of the hydroxyl groups of hPG's surface. After deprotection, PEG_{1000}-OMs chains were attached to the amino ligands. For the CRS, reaction of hPG with TMEDA was controlled to yield a degree of functionalization on hPG's surface of 70% (similar to that of CMS). The remaining mesylates were then substituted by azides, which could be used in a click reaction to attach propargylated PEG_{5000} (see characterization of CMS and CRS in ESI).

UV/Vis spectroscopic experiments were then carried out to determine the maximum Cu-loading capacity of the nanocarrier in water. A stock solution of the polymer was mixed with an increasing amount of Cu(II) to achieve different Cu:polymer molar ratios. Regardless of the polymer structure, an increase of the absorbance at 580 nm was observed and should be related to the d-d transition of copper ions complexed by amine functions (see Figure S1 in ESI). This demonstrated the complexation of Cu inside the nanocarriers. Above a certain concentration of copper, the absorbance at 580 nm became constant and a new band around 800 nm related to aqueous copper ions grew in size. This behavior is evidence for the saturation of nanocarriers and that the later added copper ions remained free in solution. The plot of the absorbance at 580 nm for increasing Cu:polymer ratio reveals that the CMS structure can load more copper ions than the CRS polymer (see Figure 1a). The close fit of these curves (see ESI) leads to a more quantitative evaluation of this maximum loading (see Table 1).

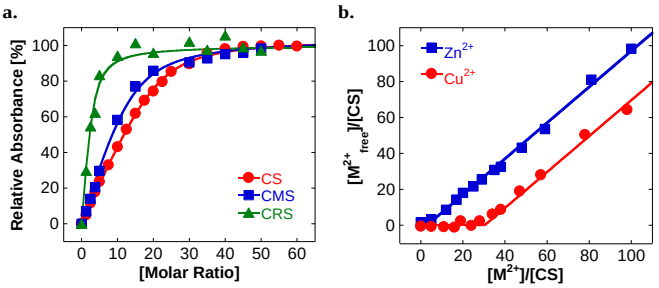

Figure 1. Determination of the maximum loading of polymers by UV-visible measurements. (a) Influence of the Cu:nanocarriers molar ratio on the relative absorbance at 580 nm at room temperature with a constant polymer concentration (80 µM). (b). Free metal ions concentration depending on metal:CS molar ratios at room temperature with CS concentration (6.2 µM).

To check this loading capacity, we developed a second method based on centrifugal filtration of the metal ion/polymer solution. Titration of the metal ion was performed on the filtrate using a well known spectroscopic method based on Zincon indicator (see Figure S2 in ESI).[24] As seen in Figure 1b, CS system retains copper ions until a maximum loading of approx. 30. This is quite comparable with the direct evaluation by UV/Vis spectroscopy. Assuming a binding site of two ligands per copper, one can estimate the maximum theoretical number of sites per polymer and therefore the percentage of active sites. As seen in Table 1, similar values were found for CS and CMS structures. On the contrary, the architecture of the CRS polymer is less favorable for the complexation of Cu metal ions, which can be related to higher steric hindrance due to the attachment of PEG-chains between TMEDA-ligand units as well as aggregation of CRS. The binding kinetic was fast and equilibrium was reached only after few minutes (see Figure S1 in ESI). All these results indicated a behavior highly related to the architecture of the nanocarrier.

After addition of copper ions into a polymer solution, reaching the equilibrium was a slower process for CRS than CMS or CS (see Table 1). This may be partially due to the PEG layer (larger in CRS than in CMS), which should have decreased the accessibility of ions toward the ligand shell.

The ability for such structures to interact with other ions may be providential for the delivery of copper in a controlled manner. To evaluate such possibility, a large excess of different ions (Ca, Mg, Mn, Co, Zn, Ni) was added to Cu-loaded nanocarriers solutions (see Figure S6 in ESI). None of the metal ions were able to displace copper ions from the hyperranched structures.

This journal is © The Royal Society of Chemistry 2012

Table 1. Properties of the CS, CMS and CRS structures.

	CS	CMS	CRS
Loading capacity[a]	22 ± 4	14 ± 3	5 ± 2
Percentage of active sites[b]	46 ± 9%	42 ± 9%	15 ± 6%
Relative intake kinetic[c]	1	11	36
Size (nm)[d]	12/8	8/5	360[e]/6
pH for 10% of copper release	4	4	7
Relative pH-release kinetic[c]	1	2	3
Cytotoxicity of the polymer loaded with copper (IC50)[f]	38.1 mg Cu/L 220 mg CS/L	4.8 mg Cu/L 415 mg CMS/L	4.1 mg Cu/L 2.9 g CRS/L

a. Determined by UV-visible spectroscopy (see text). **b.** Ratio between the experimental loading capacity and the maximum theoretical number of sites per polymer estimated as half the number of ligand ethylene diamine per polymer. **c.** Determined by UV-visible spectroscopy (see ESI). **d.** Hydrodynamic radius (nanocarriers/Cu-loaded nanocarriers) determined by DLS with an analysis in number from 80 µM nanocarrier solutions. **e.** Aggregation. **f.** Determined on human neuroblastoma cell line SH-SY5Y.

Moreover, no direct complexation could be evidenced for zinc ions, another ion of interest in the case of AD,[25] as shown in Figure 1b. Thus, the obtained nanocarriers were of special interest for the specific complexation and delivery of copper.

Blood clearance for molecules below 60 kDa and 6 nm is fast, while bigger particles remain longer in the blood.[26, 27] However, particles bigger than 200 nm are likely renal excreted.[28] Since size also has a big impact on permeability of the BBB of substances,[29-31] size of empty and Cu-loaded nanocarriers were investigated by dynamic light scattering (see Figure S4 in ESI). Empty nanocarriers in solution as unimer were found to have a hydrodynamic diameter close to 10 nm (see Table 1). When CMS was only in the form of unimer, CS and CRS nanocarriers were more or less present as polydisperse aggregates in solutions (R_h above 100 nm). When Cu was stabilized inside nanocarriers, a significant decrease of the aggregation and a slight change in the size of the unimer was observed. Thus, the nanocarriers presented here having molecular weights above 80 kDa and diameters $d \geq 8$ nm are in the right range for application as a delivery system. However, the permeation through the BBB might be critical, since it has been postulated that most molecules bigger 400 Da are not able to pass the BBB.[29] On the other hand, it was observed that the ability to cross the BBB is much higher for NPs with cationic character.[30-32] Due to this, zeta potentials of empty and Cu-loaded nanocarriers were studied at pH values ranging from 7 to 3 in buffer solution. At pH 7, zeta potential of empty CS was found at 30 mV ± 9 mV. As expected, grafting of PEG chains induced a significant decrease of zeta potential that remained slightly positive for both CRS (+13.9 ± 0.8 mV) and CMS (+9.2 ± 1.0 mV) (see Figure S5 in ESI). Partial protonation of amine groups may have been responsible for this observation. Therefore, the highest zeta potentials were measured at pH 3 due to the increase of protonation level at lower pH. Interestingly, the surface charge at all the pH values did not significantly evolve when Cu ions were stabilized inside the nanocarriers. Therefore, these positively charged nanocarriers have a high potential to cross the BBB.

To prove whether nanocarriers were able to release copper ions at low pH, UV/Vis spectroscopy experiments were performed. Cu-loaded nanocarriers were transferred in Britton Robinson universal buffer aliquots with pH-values from 8 to 2 and absorbance was monitored (see Figure S3 in ESI). Figure 2 shows the percentage of Cu-release as a function of pH. As a result, Figure 2 shows that CRS nanocarriers continuously released Cu with decreasing pH. This profile of release highlights the weakness of these nanocarriers due to the random architecture as above discussed and might be too prompt, since the release already started at pH 7. For an application in biological systems a controlled release is therefore not possible presumably due to Cu leakage before the required target was reached. On the other hand, Cu-complexes integrity in CS and CMS structures remained until lower pH values. This indicates a stronger Cu binding in this architecture which makes it a good candidate for carrying its entire load to the target, after which a sharp and fast Cu release could occur according to Figure 2 and kinetics data (see Figure S3 in ESI).

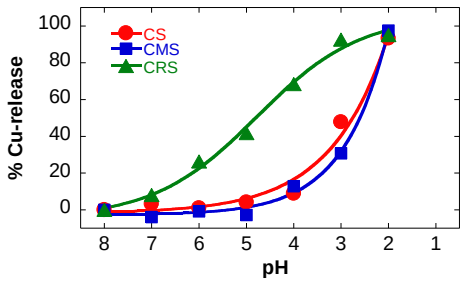

Fig. 2. %Cu-release based on relative absorbance at 580 nm of CMS or CRS polymer (80 µM) in Britton Robinson Buffers, 0.1 M NaCl at 37 °C

Toxicity of Cu-loaded and empty nanocarriers in human neuroblastoma (SH-SY5Y) cells was then investigated by MTT assay (see experimental procedures in ESI). IC50 value of CRS was found to be 22.4 g/L, which was much higher and therefore less toxic than CMS (IC50 ca. 415 mg/L). It is known that long PEG-chains lead to higher biocompatibility.[33] Hence, we assume that CRS with longer mPEG-chains shows less toxicity than CMS, i.e., shielding of the amino ligands by mPEG-chains determines the toxicity of the cargo in living cells. Both nanocarriers in the present study were less toxic than the previously described PEI-based CMS[8] which supported our earlier assumption that hPG-based nanocarrier has a higher compatibility than nanocarriers with a PEI core. Investigation on the toxicity of Cu-loaded nanocarriers showed the same result for CMS as for empty particles regarding the nanocarrier concentration (IC50 [Cu:CMS = 15:1] = 415 mg/L). In contrast, the cytotoxicity of Cu-loaded CRS increased to IC50 [Cu:CRS = 5:1] = 2.9 g/L in comparison to unloaded CRS. Regarding the Cu concentration, however, Cu-loaded CMS was in the same range as Cu:CRS in terms of cytotoxicity (see Table 1). Both nanocarriers could reduce the toxicity of Cu by factor 7.[8] The

compatibility at high loading is especially of importance for in vivo applications when a high local concentration of Cu is required. According to these results, it seems that CMS is a better candidate for treatment of Cu deficiency disorders.

Conclusions

By designing new core-shell polymeric structures, we were able to obtain nanocarriers that had a high binding affinity for copper ions and were able to release these ions at low pH. We demonstrate that the exact architecture of the core-shell system is a paramount parameter to control the maximum loading, the strength of complexation, and the release profile of copper into the solution. The CMS structure proves to be the most promising structure for Cu complexation and release. The CMS structure will now be studied to estimate their transport through the BBB and tested in vivo for the release of copper.

Acknowledgements

This work was financially supported by the ANR-DFG program (ANR-11-INTB-1004, "Dendrion-Bio"). The authors wish to thank the SFB 1112 and the Helmholtz portfolio project "Technologie und Medizin" for financial support and Christina Kühl for technical assistance.

Notes and References

1. M. A. Telpoukhovskaia and C. Orvig, *Chem. Soc. Rev.*, 2013, **42**, 1836-1846.
2. D. J. Waggoner, T. B. Bartnikas and J. D. Gitlin, *Neurobiol. Dis.*, 1999, **6**, 221-230.
3. G. J. Broussard, J. Mytar, R. C. Li and G. J. Klapstein, *Inflammopharmacol.*, 2012, **20**, 109-126.
4. M. Calderón, M. A. Quadir, S. K. Sharma and R. Haag, *Adv. Mater.*, 2010, **22**, 190-218.
5. M. A. Quadir and R. Haag, *J. Control. Release*, 2012, **161**, 484-495.
6. F. Aulenta, W. Hayes and S. Rannard, *Eur. Polym. J.*, 2003, **39**, 1741-1771.
7. M. Krämer, J. F. Stumbe, H. Turk, S. Krause, A. Komp, L. Delineau, S. Prokhorova, H. Kautz and R. Haag, *Angew. Chem. Int. Ed.*, 2002, **41**, 4252-4256.
8. C. Treiber, M. A. Quadir, P. Voigt, M. Radowski, S. J. Xu, L. M. Munter, T. A. Bayer, M. Schaefer, R. Haag and G. Multhaup, *Biochemistry*, 2009, **48**, 4273-4284.
9. D. Wilms, S.-E. Stiriba and H. Frey, *Acc. Chem. Res.*, 2009, **43**, 129-141.
10. R. K. Kainthan, J. Janzen, E. Levin, D. V. Devine and D. E. Brooks, *Biomacromolecules*, 2006, **7**, 703-709.
11. D. Gröger, F. Paulus, K. Licha, P. Welker, M. Weinhart, C. Holzhausen, L. Mundhenk, A. D. Gruber, U. Abram and R. Haag, *Bioconjug. Chem.*, 2013, **24**, 1507-1514.
12. S. Reichert, P. Welker, M. Calderon, J. Khandare, D. Mangoldt, K. Licha, R. K. Kainthan, D. E. Brooks and R. Haag, *Small*, 2011, **7**, 820-829.
13. D. Steinhilber, S. Seiffert, J. A. Heyman, F. Paulus, D. A. Weitz and R. Haag, *Biomaterials*, 2011, **32**, 1311-1316.
14. Z. Chen, L. Zhou, F. Zhang, C. Yu and Z. Wei, *Appl. Surf. Sci.*, 2012, **258**, 5291-5298.
15. J. Khandare, A. Mohr, M. Calderón, P. Welker, K. Licha and R. Haag, *Biomaterials*, 2010, **31**, 4268-4277.
16. M. Seiler, *Fluid Phase Equilibr.*, 2006, **241**, 155-174.
17. Y. Xu, C. Gao, H. Kong, D. Yan, P. Luo, W. Li and Y. Mai, *Macromolecules*, 2004, **37**, 6264-6267.
18. C. R. Yates and W. Hayes, *Eur. Polym. J.*, 2004, **40**, 1257-1281.
19. D. Appelhans, H. Komber, M. A. Quadir, S. Richter, S. Schwarz, J. van der Vlist, A. Aigner, M. Muller, K. Loos, J. Seidel, K. F. Arndt, R. Haag and B. Voit, *Biomacromolecules*, 2009, **10**, 1114-1124.
20. D. Steinhilber, T. Rossow, S. Wedepohl, F. Paulus, S. Seiffert and R. Haag, *Angew. Chem. Int. Ed.*, 2013, **52**, 13538-13543.
21. G. Gasser, L. Tjioe, B. Graham, M. J. Belousoff, S. Juran, M. Walther, J.-U. Kunstler, R. Bergmann, H. Stephan and L. Spiccia, *Bioconjug. Chem.*, 2008, **19**, 719-730.
22. X. Wang and D.-S. Yang, *J. Phys. Chem. A*, 2006, **110**, 7568-7576.
23. M. A. Quadir, Dendritic Polymers for Nanoscale Delivery of Metal Ion and Drugs (Doctoral Dissertation), Freie Universität Berlin, 2010.
24. R. M. Rush and J. H. Yoe, *Anal. Chem.*, 1954, **26**, 1345-1347.
25. H. Kozlowski, M. Luczkowski, M. Remelli and D. Valensin, *Coord. Chem. Rev.*, 2012, **256**, 2129-2141.
26. H. Soo Choi, W. Liu, P. Misra, E. Tanaka, J. P. Zimmer, B. Itty Ipe, M. G. Bawendi and J. V. Frangioni, *Nat. Biotechnol.*, 2007, **25**, 1165-1170.
27. M. J. Knauf, D. P. Bell, P. Hirtzer, Z. P. Luo, J. D. Young and N. V. Katre, *J. Biol. Chem.*, 1988, **263**, 15064-15070.
28. P. J. Crouch, L. W. Hung, P. A. Adlard, M. Cortes, V. Lal, G. Filiz, K. A. Perez, M. Nurjono, A. Caragounis, T. Du, K. Laughton, I. Volitakis, A. I. Bush, Q. X. Li, C. L. Masters, R. Cappai, R. A. Cherny, P. S. Donnelly, A. R. White and K. J. Barnham, *Proc. Natl. Acad. Sci. USA*, 2009, **106**, 381-386.
29. W. M. Pardridge, *Drug Discov. Today*, 2007, **12**, 54-61.
30. W. Lu, J. Wan, Z. She and X. Jiang, *J. Control. Release*, 2007, **118**, 38-53.
31. L. H. Reddy, R. K. Sharma, K. Chuttani, A. K. Mishra and R. R. Murthy, *AAPS J.*, 2004, **6**, e23.
32. L. Kozlovskaya and D. Stepensky, *J. Control. Release*, 2013, **171**, 17-23.
33. H. Petersen, P. M. Fechner, D. Fischer and T. Kissel, *Macromolecules*, 2002, **35**, 6867-6874.

 This journal is © The Royal Society of Chemistry 2012

Supplementary Information

BIOCOMPATIBLE, HYPERBRANCHED NANOCARRIERS FOR THE TRANSPORT AND RELEASE OF COPPER IONS

S. Nowag [a], C. Frangville[b], G. Multhaup[c], J.-D. Marty[b], C. Mingotaud[b], R. Haag [a]

a Institut für Chemie und Biochemie, Organische Chemie, Freie Universität Berlin, Takustr. 3, 14195 Berlin, GERMANY.

b Laboratoire des Interactions Moléculaires et Réactivités Chimiques et Photochimiques, Université de Toulouse, CNRS UMR 5623, 31062 Toulouse Cedex 09, FRANCE.

c Department of Pharmacology and Therapeutics, McGill University, 3655 Promenade Sir-William-Osler, Montréal, PQ H3G 1Y6, CANADA.

Index

A. Experimental....S3
A.1. General. S3
A.2. Synthesis....S3
A.3. Cu-loading by UV/Vis spectroscopy. S4
A.4. Cu-loading kinetics by UV/Vis spectroscopy....S4
A.5. Zincon titration procedure. S4
A.6. pH-triggered release study. S5
A.7. pH-triggered release kinetic. S5
A.8. DLS....S5
A.9. Metal ions competition S5
A.10. Biological studies S5
A.11. Fit equations S6
B. Results and discussion S7
B.1. Cu and Zn loading capacity S7
Figure S1. UV/Vis of Cu loading capacities and loading kinetics of CS, CMS, and CRS. S7
Figure S2. Zincon procedure S8
B.2. pH-triggered Cu release S8
Figure S3. UV/Vis and ITC analysis of Cu loading capacities and pH triggered release of CS. S9
B.3. Colloidal behavior in water solution....S9
Figure S4. DLS measurements of CS, CMS and CRS. S10
Figure S5. DLS and zeta potential measurements summary of CS, CMS and CRS. S11
B.4. Metal ions competition S12
Figure S6. UV/Vis metal ions competition. S12

A. Experimental

A.1. General. ^{1}H NMR and ^{13}C NMR spectra were recorded on a Jeol ECX 400 apparatus (400 MHz for ^{1}H and 100 MHz for ^{13}C). Calibration was performed using the chloroform peak at 7.26 ppm for ^{1}H and 77.0 ppm for ^{13}C. IR spectra of neat samples were recorded on a Nicolet Avatar 320 FT-IR spectrometer (Thermo Fisher Scientific, Dreieich, Germany). Dialysis was performed with Dialysis tubing benzoylated 10 FT from Sigma-aldrich (molecular weight cut-off 2000 g mol^{-1}). Ultrafiltration was performed with a 300 mL solvent-resistant stirred cell with regenerated cellulose membranes (molecular weight cut-off 5000 or 10000 g mol^{-1}), both from Millipore. TLC was performed on Merck aluminium sheets with silica (corn size 60) and fluorescence marker (F254). Flash column chromatography was performed on Merck silica (corn size 60). $CuSO_4$ was purchased from Acros Organics Co. Ltd. and $ZnSO_4$, $MgSO_4$, $MnSO_4$, $CaSO_4$, $CoSO_4$, $NiSO_4$, Zincon monosodium salt (*2-Carboxy-2'-hydroxy-5'-sulfoformazyl-benzene monosodium salt*) were purchased from Sigma Aldrich Co. Ltd. at highest purity available (≥99%) and used as received. All reagents and solvents were purchased from Acros, Fluka or Aldrich and used as received. Hyperbranched PG was synthesized according to literature.[1]
Water was purified through a filter and ion exchange resin using a Purite device (resistivity 18.2 MΩ·cm).

A.2. Synthesis

hPG_{10k}-$(DMEDA)_{0.7}$

The synthesis of *boc*-DMEDA was described elsewhere.[2] In a sealed tube, PG_{10k}-OMs (1.8 g, 13.5 mmol/g, 24.3 mmol OMs groups) was dissolved in 5 ml DMF and 3.46 g *boc*-N,N'-dimethylethylene diamine (18.23 mmol, 0.75 equiv.) was added and heated to 120°C for 3 days. After removal of the solvent the crude product was dialyzed in methanol. hPG_{10k}-(*boc*-DMEDA)$_{0.7}$ was dissolved in DMF:TFA (4:1) and stirred for 3 h. The solvent was evaporated yielding 0.96 g of the slightly yellow product, which was used without further purification.

^{1}H-NMR ($CDCl_3$, 400 MHz): δ = 4.18-3.21 (PG-groups), 3.20-3.14 (-N-CH_2-), 3.10-2.87 (-N-CH_2-), 2.67-2.37 (-N-CH_3) ppm.

CMS: hPG_{10k}-$(DMEDA\text{-}PEG_{1000})_{0.7}$

hPG_{10k}-$(DMEDA)_{0.7}$ (0.96 g, 1 equiv.) was dissolved in DMF. NEt_3 (2.1 equiv.) was added and stirred for 1 h. $mPEG_{1000}$-OMs (1.1 equiv.) was added and stirred at room temperature for 5 days. Dialysis of the crude product in methanol yielded 2.3 g hPG_{10k}-$(DMEDA\text{-}PEG_{1000})_{0.7}$. For the physical-chemical characterization, a mean molar mass of 83 kDa was used (deduced from ^{1}H-NMR).

^{1}H-NMR ($CDCl_3$, 400 MHz): δ = 3.67-3.51 (m, PEG and PG), 3.48-3.42 (m, -N-CH_2-) ppm.

IR: ϑ̃ = 3424, 3015, 2873, 2490, 2337, 2320, 1682, 1558, 1540, 1465, 1419, 1342, 1279, 1199, 1172, 1107, 962, 839, 799, 775, 719 cm^{-1}.

hPG_{10k}-$(TMEDA)_{0.7}$

In a sealed tube, PG_{10k}-OMs (0.5 g, 6.75 mmol OMs groups) was dissolved in 5 ml DMF and *N,N,N'*-trimethylethylene diamine (517 mg, 5.06 mmol, 0.75 equiv.) was added and heated to 120°C for 3 days. After removal of the solvent the crude product was dialyzed in methanol to yield 320 mg of the brown hard paste-like product.

^{1}H-NMR ($CDCl_3$, 400 MHz): δ = 4.41-3.41 (PG groups), 3.40-2.98 (-CH(OH)-C*H*$_2$-NMe-CH_2-) 2.87-2.57 (m, PG groups), 2.63-2.48 (m, -N-CH_2-), 2.42-2.10 (-N-C*H*$_3$) ppm.

hPG_{10k}-$(TMEDA)_{0.7}(N_3)_{0.3}$

$hPG\text{-}(TMEDA)_{0.7}$ (320 mg, 4.05 mmol OMs groups) was dissolved in DMF. After addition of NaN_3 (1.32 g, 20.25 mmol, 5 equiv. regarding OMs groups), the suspension is heated for 3 days to 60°C. After cooling, the precipitate is filtered off and the filtrate was concentrated. The residue was dialyzed in methanol to yield 235 mg product.

^{1}H-NMR ($CDCl_3$, 400 MHz): δ = 4.41-3.41 (PG groups), 3.40-2.98 (-CH(OH)-C*H*$_2$-NMe-CH_2-) 3.87-2.57 (m, PG groups), 2.63-2.48 (m, -N-CH_2-), 2.42-2.10 (-N-C*H*$_3$) ppm.

CRS: hPG_{10k}-$(TMEDA)_{0.7}$(Triazol-$mPEG_{5000}$)$_{0.3}$

DIPEA (30 mol% per triple bond) was added to 1.0 equiv. of $mPEG_{5000}$-acetylene and 1.1 equiv. of $PG\text{-}(TMEDA)_{0.7}\text{-}(N_3)_{0.3}$ per triple bond dissolved in THF (PEG_{5000} was used to compensate that only 30% of the hPG surface can be modified, instead of 70% in case of CMS) . After the mixture had been stirred for 5 min, 30 mol% per triple bond of sodium ascorbate was added, followed by 10 mol% of $CuSO_4 \cdot 5H_2O$ per triple bond. (A stock solution of sodium ascorbate and $CuSO_4 \cdot 5H_2O$ in water was prepared in concentration 100 mg/mL). THF/H_2O ratio was 1/1 (v/v). The heterogeneous mixture was stirred vigorously for 5.5 days. The precipitate was removed by centrifugation for 2 h at 11,000 rpm. The product was ultrafiltrated in H_2O/MeOH = 1:1 + TFA at pH 3 (MWCO = 10000 g mol^{-1}). Afterwards, the product was ultrafiltrated in H_2O/MeOH with NaOH (pH 10, MWCO 5000 g mol^{-1}). For the physical-chemical characterization, a mean molar mass of 224 kDa was used (deduced from ^{1}H-NMR).

^{1}H-NMR ($CDCl_3$, 400 MHz): δ = 4.20-3.35 (PG groups), 3.01-2.95 (-CH(OH)-C*H*$_2$-NMe-CH_2-) 2.89-2.77 (m, PG groups), 2.75-2.41 (m, -N-CH_2-), 2.22-2.08 (-N-C*H*$_3$) ppm.

IR: ῡ = 2946, 2880, 2740, 2694, 1960, 1466, 1455, 1360, 1340, 1279, 1240, 1145, 1097, 958, 948, 840 cm^{-1}.

Table 1. Summary of physico-chemical properties of CS, CMS, CRS.

	CS	CMS	CRS
M_w (g/mol)	22,000	83,000	224,000
Grafting ratio	70%	49%	49%
No. of theoretical complexation sites	47	33	33

A.3. Cu-loading by UV/Vis spectroscopy. UV/Vis spectra were recorded with Scinco S-3150 (range: 190-1100 nm, resolution 1024 points) in fast mode. Calibration was performed at 360.85 and 453.55 nm with holmium oxide glass. The spectra were recorded at room temperature. To assess the maximum metal cargo capacity of the polymers, a solution of the nanocarriers (80 µM) in water were prepared in 2 mL. Successive micro-additions (0.5 - 2 µL) of concentrated $CuSO_4$ solutions (0.4 M and 2 M) were added every 6 min to yield a distinct Cu/nanocarriers molar ratio within the range of 0-125. Absorbance versus the molar Cu/nanocarriers molar ratio was then fitted by a simple model based on the hypothesis that each polymer contains N complexing sites and that the binding constant of Cu(II) is the same for each site, whatever the number of loaded sites may be.

A.4. Cu-loading kinetics by UV/Vis spectroscopy. Cu-loading kinetic was monitored by UV/Vis spectroscopy by adding 4 µL of $CuSO_4$ (2 M) into a 2 mL solution of nanocarriers (80 µM) (Cu/nanocarriers ratio = 50:1). Measurements were performed at room temperature. The variation of DO with time was adjusted to an exponential function (see below) leading to the characteristic time □ (given in Table 1).

A.5. Zincon titration procedure. Solutions of nanocarriers (6.2 µM) with increasing amount of Zn(II) or Cu(II) were prepared (M(II)/nanocarriers ratio from 0 to 150 :1) into 2mL. These samples were then filtrated with centrifugal filters (molecular weight cut-off 3000 g mol^{-1}) (Ultracel®-3K - Millipore Ireland Ltd). 160 µL of filtrate were mixed with 30 µL Zincon (2.8 mM) and completed at 2 mL with B.R. buffer

pH 9. The analyzis was performed by UV-Vis spectroscopy to assess free metal ions concentrations. (Calibration curves perform with Zincon (42 µM) and concentrations of Cu(II) and Zn(II) from 0 to 40 µM).

A.6. pH-triggered release study. Solutions of Cu-loaded nanocarriers were prepared with Cu/nanocarriers ratio = 50:1 by adding an appropriate amount of a $CuSO_4$ stock solution (2 M) to a solution of nanocarriers (80 µM) dissolved in water. Then supplemental non-loaded Cu was removed through dialysis (molecular weight cut-off 2000 g mol^{-1}) in water. The dialyzed product was then dried under vacuum conditions and redissolved into 7 aliquots of 80 µM (pH 2 to 8) in Britton-Robinson Buffer (40 mM H_3BO_4, 40 mM H_3PO_4, 40 mM CH_3COOH) with 100 mM NaCl. The solutions were incubated for 2 h at 37°C and UV/Vis spectroscopy measurements were also performed at 37 °C.

A.7. pH-triggered release kinetic. Cu pH-triggered release kinetic was monitored by UV/Vis spectroscopy by adding 10 µL of HCl (2 M) into a 2 mL solution of nanocarriers (80 µM) (Cu/nanocarriers ratio = 50:1). Measurements were performed at 37 °C.

A.8. DLS and Zeta potential Dynamic light scattering (DLS) measurements and Zeta potential were conducted using a Zetasizer Nano-ZS (Malvern Instruments, Ltd, UK) with integrated 4 mW He-Ne laser, λ = 633 nm. Nanocarriers were investigated with and without pre-incubation with $CuSO_4$ (Cu/nanocarriers ratio = 50:1). The polymer concentration was 80 µM and samples were all filtered with a 20 nm filter unit except for CRS, filtered at 400 nm for aggregates reasons. The correlation function was analyzed *via* the general purpose method (NNLS) to obtain the distribution of diffusion coefficients of the solutes. The apparent equivalent hydrodynamic diameter (d) was then determined using the Stokes–Einstein equation. Mean diameter values were obtained from three different runs of the number plot. Standard deviations were evaluated from diameter distribution. For Zeta potential measurements, Doppler anemometry technique was used whereby electric field was applied across the sample solution. All measurements were carried out at 25 °C using folded capillary cells (DTS 1060).

A.9. Metal ions competition

Solutions of Cu-loaded nanocarriers were prepared with Cu/CS ratio = 20:1 by adding an appropriate amount of a $CuSO_4$ stock solution (2 M) to a solution of CS (6.2µM) dissolved in water. Then competitor metal ions (Mg, Ca, Mn, Co, Ni, Zn) were added such as M(II)/CS ratio = 100:1 and let to incubate during 24 h at 37 °C. UV-Vis measurements were performed at 37 °C.

A.10. Biological studies

Cell Culture. A human neuroblastoma SH-SY5Y cell line were cultured as described previously (www.lgcpromochem-atcc.com). Cells at a density of 60,000 cells/well in 96-well plates were used at the time of the experiment. Stock solutions of nanoparticles with Cu were prepared in Milli-Q water by thorough mixing.

For toxicity assays, SH-SY5Y-cells were incubated for 24 h with different concentrations of Cu-saturated and unloaded nanoparticles ranging from 6 nM to 100 µM.

MTT Assays. MTT assays were purchased from Promega (Mannheim, Germany) and performed in 96-well plates. This assay is based on tetrazolium salt 3-(4,5-dimethylthiazol-2-yl)-2,5-diphenyltetrazolium bromide (MTT) that is taken up into cells and reduced to yield a purple formazan product, which is largely impermeable to cell membranes, thus resulting in its accumulation within healthy cells. The number of cells was normalized, and cells were cultured in 96-well plates, incubated for 48 h, and washed three times in 1x PBS (137 mM NaCl, 2.7 mM KCl, 10 mM Na_2HPO_4, and 2 mM KH_2PO_4) followed by treatment with OptiMEM medium (Invitrogen) supplemented with individual carrier in the absence (control) or presence of Cu for 24 h. The volume of tissue culture medium in each well was 100 µL, to which 20 µL of CellTiter 96 AQueous One Solution Reagent was added. Plates were incubated for 3 h at 37°C in a humidified, 5% CO_2 atmosphere. Then the absorbance was measured at 570 nm.

A.11. Fit equations

UV-Vis Cu-loading. For a system V + M $\rightleftharpoons$ VM (K), with V: vacant site in nanocarriers, M: free metal ion and VM: complex nanocarriers-Metal. We assumed the two following hypothesis: all the complexation sites are equivalents and the adsorption of a metal ion does not modify the further complexation constants.

After resolution of this system, we found $\alpha = \frac{\rho+\gamma-\sqrt{(\rho+\gamma)^2-4\rho}}{2}$

where $OD_{Cubind} = \alpha OD_{\infty}$; n the number of vacant sites in a nanocarrier; $\rho = \frac{[M]_0}{n.[CS]_0}$; $\alpha = \frac{[VM]}{[V]_0}$; $\beta = \frac{[VM]}{[M]_0}$; $\gamma = 1 + \frac{1}{K[V]_0}$; $\frac{\alpha}{\beta} = \rho$.

Back titration Cu_{free} concentration.

The back titration fit calculation is based on same hypothesizes than above and calculated as below: $[M] = n.[CS]_0(\rho - \alpha)$ with $\alpha = \frac{\rho+\gamma-\sqrt{(\rho+\gamma)^2-4\rho}}{2}$.

Intake and outtake kinetics.

Intake and Outtake kinetics are based on simple exponential fits ($A + B.(1 - e^{-C(x-x_0)})$ and $A + B.(e^{-C(x-x_0)})$, respt.) with $\tau = \frac{-\ln(0.37)}{C}$ and x_0 the delay after which Cu is injected (10sec.)

B. Results and discussion

B.1. Cu and Zn loading capacity

UV-Vis spectroscopy was used to assess the loading capacity of CS, CMS, and CRS towards Cu ions (Figure S1 a-f). For each nanocarrier (80 µM), increasing amount of Cu was added in order to reach the maximum Cu-loading observed through the absorbance of Cu binding band. Absorbance at 580 nm was then plotted as a function of Cu:nanocarrier molar ratio and Cu capacity loading was determined using a fit calculation. Binding kinetics was also investigated by observing the absorbance of Cu-binding band at 580 nm by UV/Vis time-dependently (Figure S1 g-i). All those measurements were performed in water at room temperature.

Figure S1. UV/Vis of Cu loading capacities and loading kinetics of CS, CMS, and CRS.

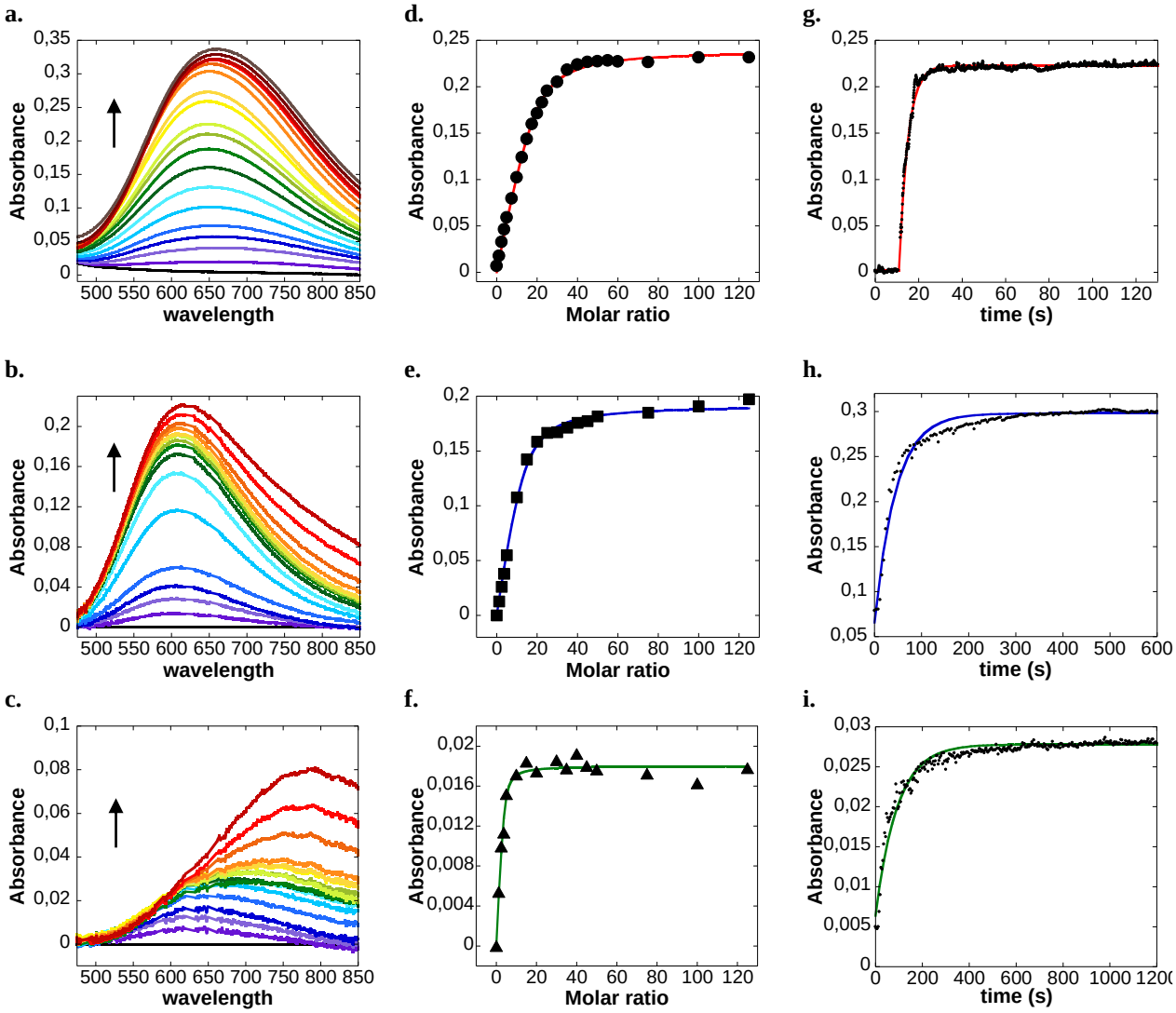

Figure S1. UV/Vis spectra of titration of a. CS, b. CMS, c. CRS with $CuSO_4$; respective absorbance at 580 nm over Cu/nanocarrier molar ratio for d. CS, e. CMS, f. CRS; Cu intake kinetic at 580nm of g. CS, h. CMS, i. CRS nanocarriers concentration 80µM at room temperature.

As a result for Cu-loading capacity, CS is able to carry 22 ± 4 Cu which correspond to 46% active sites (47 theoretical complexation sites for CS) (Figure S1 d). CMS possess a similar behavior by carrying around 14 ± 3 Cu, corresponding to 42% of active sites over 33 theoretical complexation sites (Figure S1 e). CRS appears to be less effective than the other structures by carrying 5 ± 2 Cu (15% of actives sites over the 33 theoretical complexation sites) (Figure S1 f).

Concerning the kinetics properties, absorbance was plotted over time and the resulting fitting equation offered $\tau = 4$ s for CS, $\tau = 43$ s for CMS and $\tau = 141$ s for CRS (Figure S1 g-i) representing the time after which 63% of the plateau value is reached.

In order to check those last Cu-loading capacity results, we performed a back titration based on a centrifugal filtration of the metal ion/polymer solution followed by metallic indicator analysis. As Zinc complexes are colorless (d^{10} element) and as Zincon (our metallic indicator) is well employed for Cu and Zn determination, we took benefit of this back titration to also assess Zn-loading capacity of CS nanocarriers. Thus Zincon procedure[3] was used as followed: solutions of nanocarriers incubated with increasing amount of metal ions were filtered to remove loaded nanocarriers using centrifugal filtration device (cut off 3 kDa). Then free metal ions concentration containing in the filtrate was determined through Zincon indicator.

Figure S2. Zincon procedure

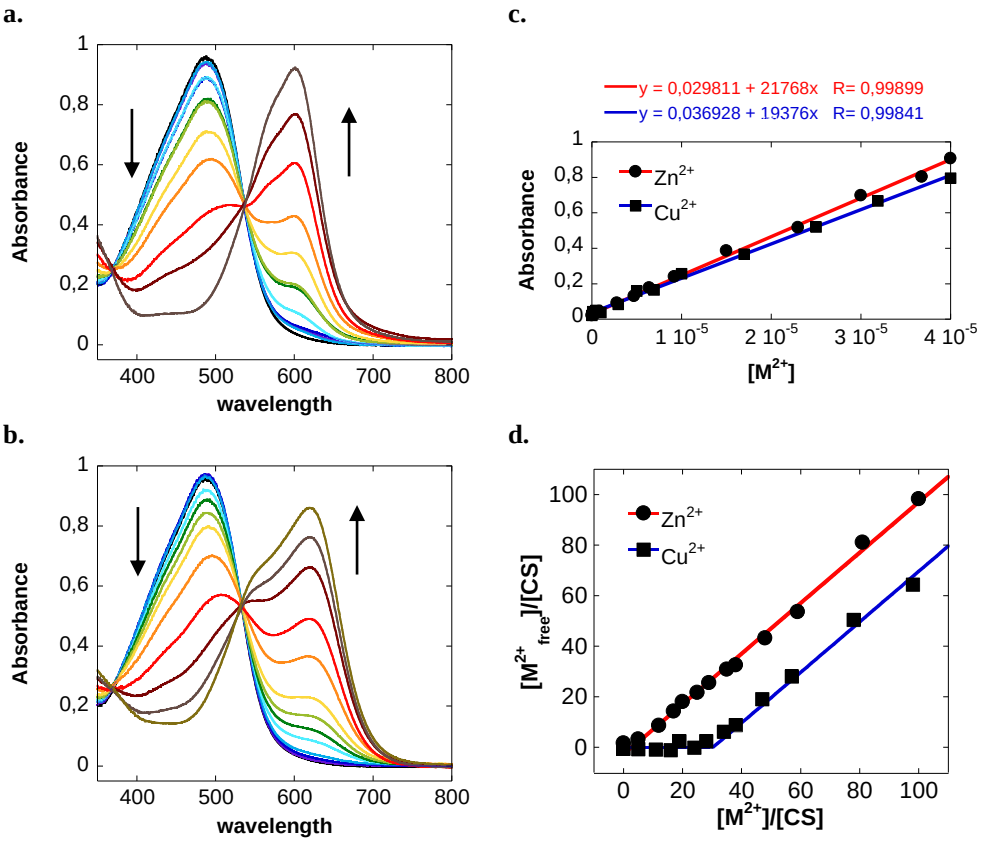

Figure S2. a. calibration spectra of Zincon-Cu, b. calibration spectra of Zincon-Zn, c. calibration curve for Zincon-Cu and Zincon-Zn, d. free Zn and Cu ions as a function of Cu/Zn:CS molar ratio (concentration determined through Zincon indicator). CS concentration 62 µM, room temperature.

Zincon-Cu and Zincon-Zn calibration curves were performed (Figure S2 a-c). Then free metal ions concentration were plotted as a function of overall metal ions:nanocarrier molar ratio. As a result, free Cu ions appeared for Cu/CS molar ratio equals 30 evidencing the saturation of CS towards Cu-loading. This result coincides with the former result received with the direct UV-Vis analysis. Moreover, free zinc ions increase linearly as a function of overall Zn ions added which indicates the inability of CS towards Zn-loading. CRS and CMS structures have shown similar behavior towards the complexation with Zn^{2+} and Cu^{2+}.

B.2. pH-triggered Cu release

pH-triggered release of Cu was also evidenced by UV-Vis spectroscopy (Figure S3 a-f). Solutions of nanocarriers with excess of Cu were dialyzed to remove free Cu ions, then dry under high vacuum and redispersed in aliquots of Britton Robinson buffers at pH 8, 7, 6, 5, 4, 3, 2. The sample was left to equilibrium for 2 hours at 37°C and then analyzed by UV-Vis at 37 °C. Release kinetics was also investigated by

observing the absorbance of Cu-binding band after addition of HCl at 580 nm by UV/Vis time-dependently (Figure S3 g-i).

Figure S3. UV/Vis and ITC analysis of Cu loading capacities and pH triggered release of CS.

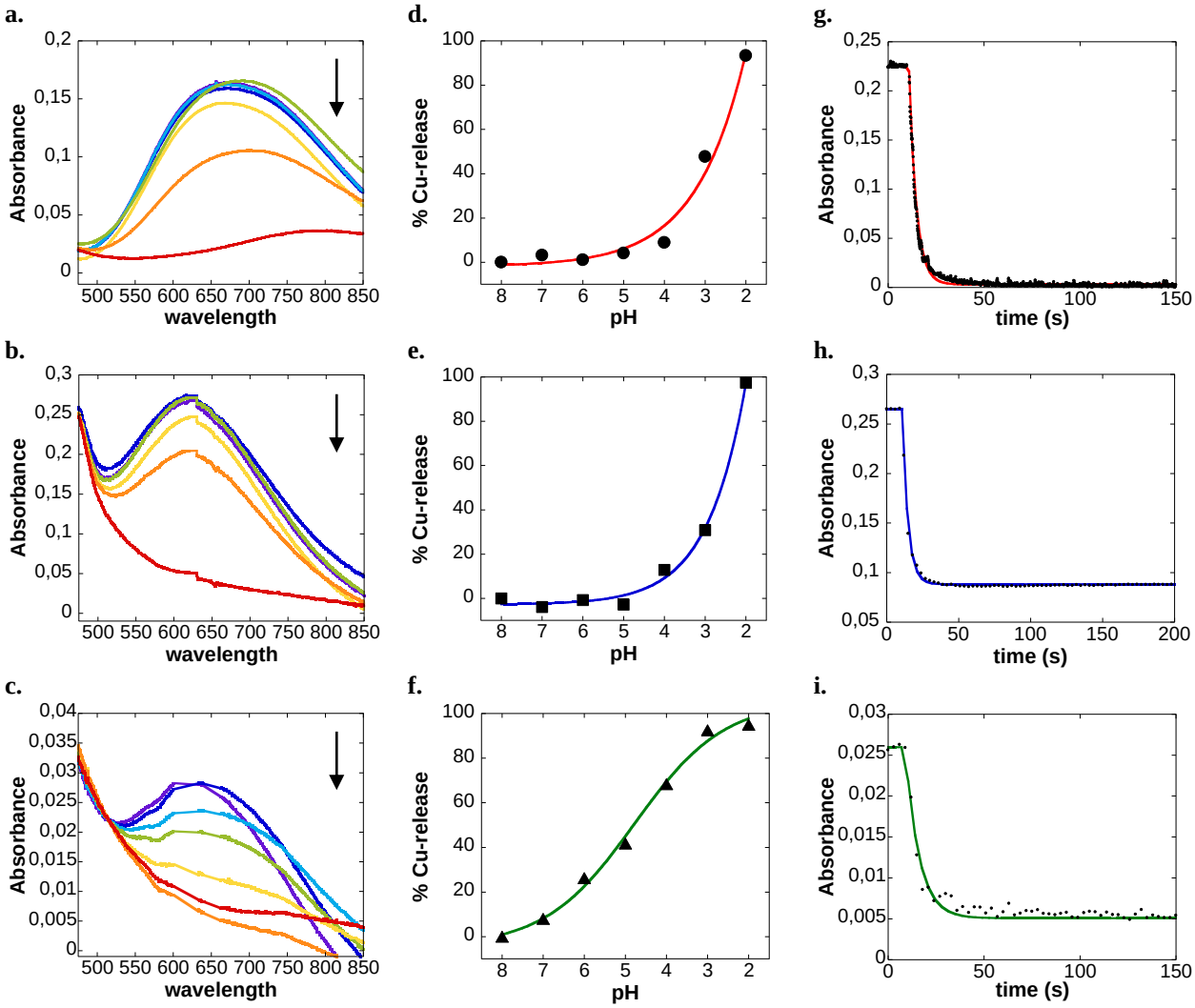

Figure S3. UV/Vis spectra of a. CS, b. CMS, c. CRS (80 µM) with $CuSO_4$, dialyzed, dried and redispersed in Britton Robinson Buffers pH 8, 7, 6, 5, 4, 3, and 2 and 0.1 M NaCl at 37°C; respective absorbance at 580 nm for d. CS, e. CMS, f. CRS; Cu outtake kinetic at 580 nm of g. CS, h. CMS, i. CRS (80 µM) in water at 37°C.

pH-triggered release evidenced a similar behavior of CS and CMS (Figure S3 a, b) with a retention of Cu until pH5 followed by a sharp release for lower pH values. CRS structure possesses a weaker release profile by starting releasing Cu from pH7 (Figure S3 c). Release kinetics equation offered τ = 4 s for CS, τ = 8 s for CMS and τ = 9 s for CRS (Figure S3 g-i) representing the time after which 63% of the plateau value is reached. The time t = 5*τ depicts the time after which the equilibrium is reached. Already after t = 19 s the Cu pH-release was finished in case of CS, t = 37 s for CMS and t= 47 s for CRS.

B.3. Colloidal behavior in water solution

DLS and zeta potential measurements were performed to assess the size and the interfacial electric potential of the empty and Cu-loaded nanocarriers.

Figure S4. DLS measurements of CS, CMS and CRS.

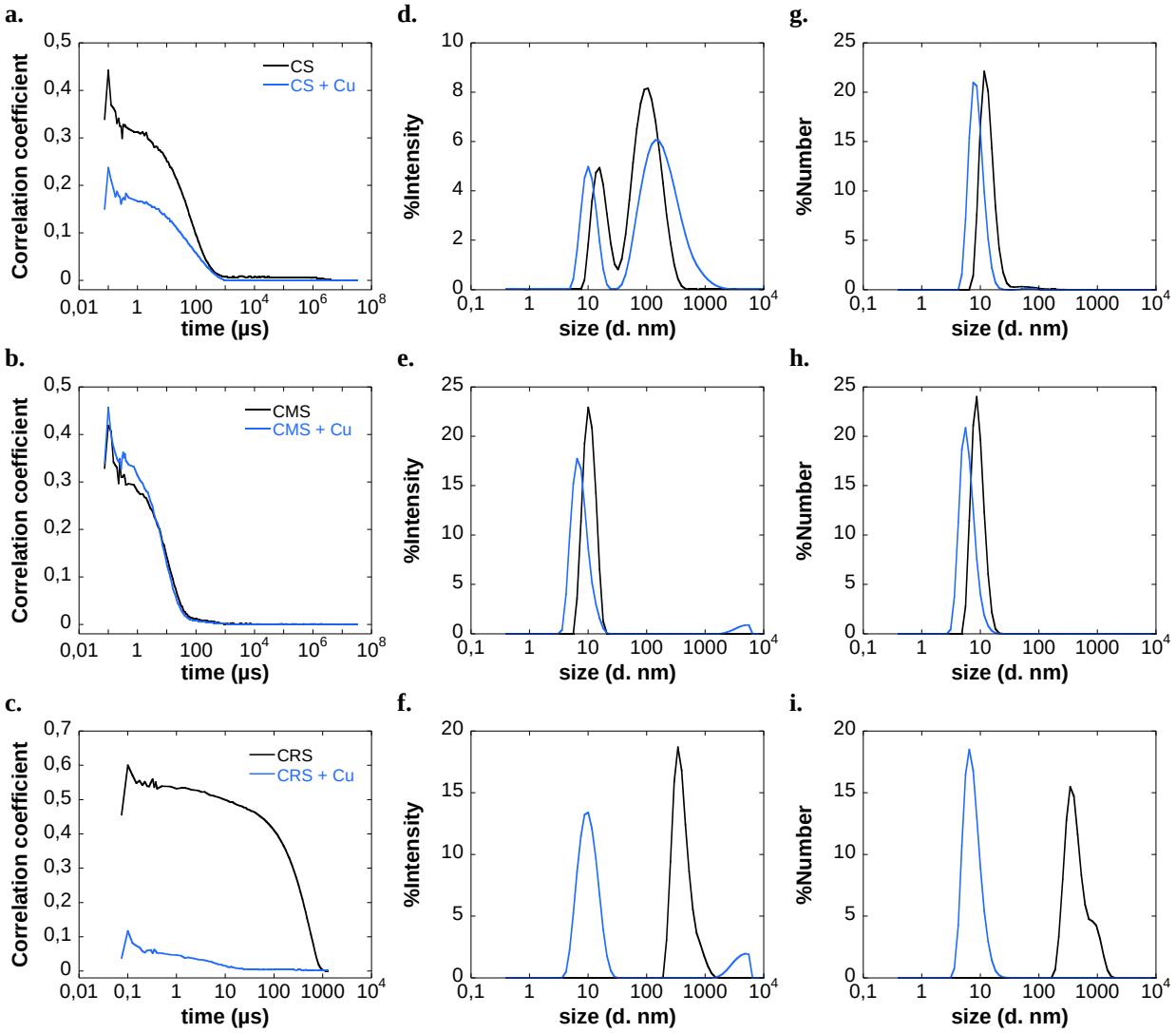

Figure S4. Correlogram of a. CS, b. CMS, c. CRS; size(%intensity) of d. CS, e. CMS, f. CRS; size(%number) of g. CS, h. CMS, i. CRS _ nanocarriers (80 µM) at room temperature, all samples filtered at 20 nm except CRS, filtered at 400 nm.

Figure S5. DLS and zeta potential measurements summary of CS, CMS and CRS.

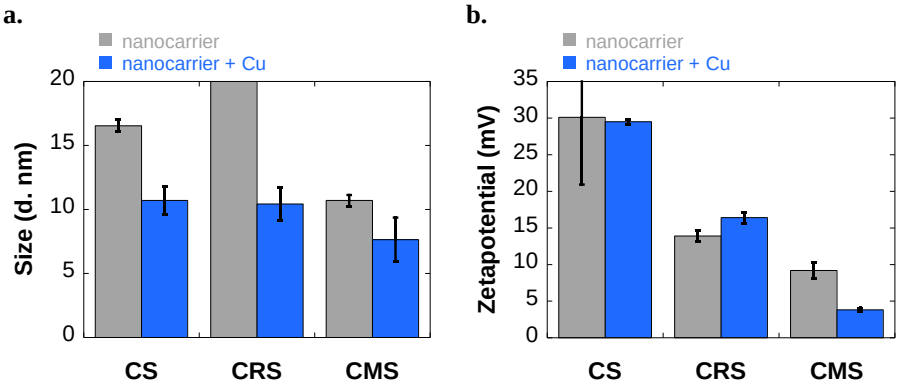

Figure S5. a. DLS and b. zeta potential measurements summary of CS, CMS, CRS at pH 7.

As a result, empty CS and CMS nanocarriers were found in solution as unimer with a hydrodynamic diameter close to 12 ± 1 nm and 8 ± 1 nm respectively (negligible amounts (<1% in number) of aggregates for CS) (Figure S4). However, CRS nanocarriers were mainly present as polydisperse aggregates in solutions (Rh above 100 nm). When Cu was stabilized inside the nanocarriers, a significant decrease of Rh was observed and Rh values were found around 6 ± 1 nm.

At pH 7, zeta potential of empty CS was found at 30 ± 9 mV. As expected, grafting of PEG chains induces a significant decrease of zeta potential that remains slightly positive for both CRS (+13.9 ± 0.8 mV) and CMS (+9.2 ± 1.0 mV). Partial protonation of amine groups may be responsible for this observation. Therefore, highest zeta potentials were measured at pH 3 due to the increase of protonation level at lower pH.

B.4. Metal ions competition

Finally, to evaluate the ability for such structures to interact with other ions, Cu-loaded CS nanocarriers were studied in the presence of competitor ions. To perform this study, excess of different metal ions (Mg, Ca, Mn, Co, Ni, Zn) were separately incubated with Cu-loaded CS nanocarriers during 1 day at 37 °C. UV-Vis measurements were monitored before and after the addition at 37 °C.

Figure S6. UV/Vis metal ions competition.

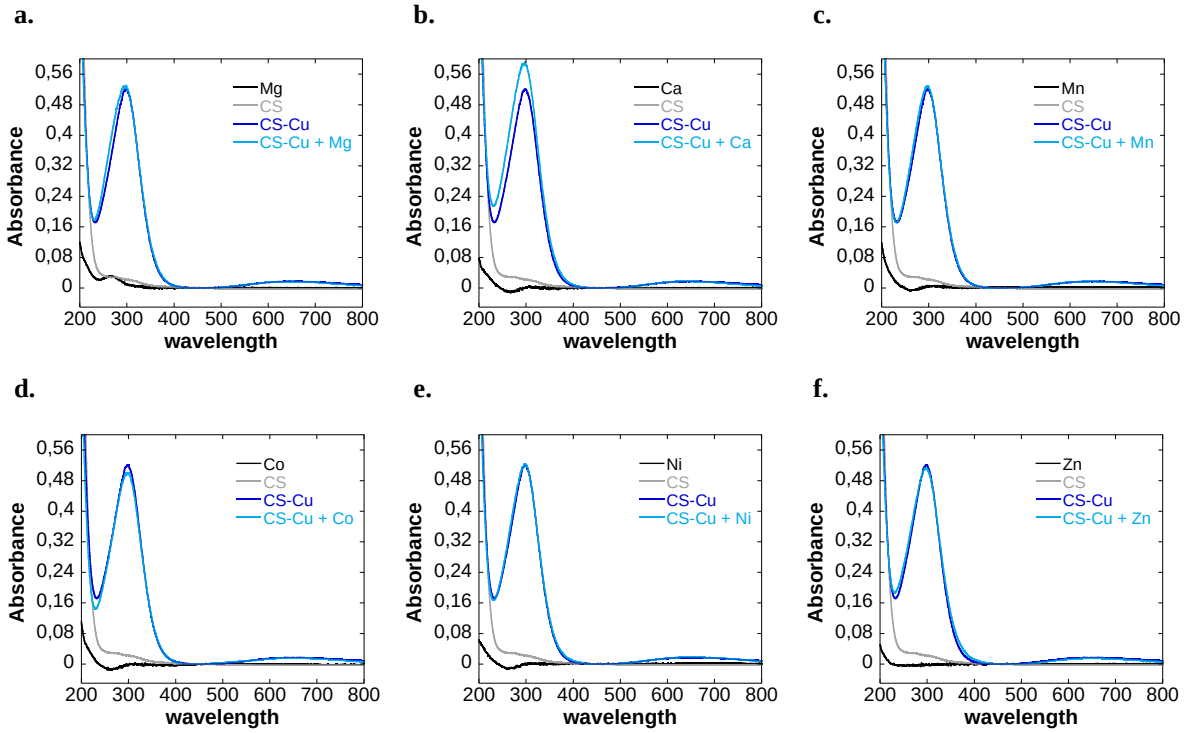

Figure S6. UV-Vis spectra of CS such as Cu:CS (20 : 1) , Metal ions:CS (100:1) Metal ions : a. Mg, b. Ca, c. Mn, d. Co, e. Ni, f. Zn. CS concentration (62 µM), incubation with competitor ions during 24 h at 37 °C.

As a result, none of the metal ions are able to displace copper ions from CS dendritic structure. Similar results were observed in the case of CMS and CRS.

References

1. A. Sunder, R. Hanselmann, H. Frey and R. Mülhaupt, *Macromolecules*, 1999, **32**, 4240-4246.
2. M. A. DeWit and E. R. Gillies, *J. Am. Chem. Soc.*, 2009, **131**, 18327-18334.
3. R. M. Rush and J. H. Yoe, *Anal. Chem.*, 1954, **26**, 1345-1347.

4 Summary

The goal of this work was to transport Cu across biological barriers as potential treatment of Cu deficiency disorders. This work investigated the biological and physicochemical properties of structurally different nanocarriers for the delivery of Cu ions to the brain. Core-shell nanoparticles (CS-NPs) based on a hyperbranched polyglycerol (hPG) core with trimethylethylene diamine (TMEDA) ligands were compared to core-multishell nanoparticles (CMS-NPs) with a hyperbranched poly(ethylene imine) (PEI) core and a doubleshell composed of alkyl- and poly(ethylene glycol) (PEG) building blocks. In the case of CS-NPs the Cu binding moieties were located in the periphery of the nanocarrier, while CMS-NPs stabilized Cu in the core. The synthesized NPs were able to encapsulate high amounts of Cu. The NPs showed low cytotoxicity and staining of the nanocarriers with proper dyes was used to follow their cellular uptake behavior. It was found that both NPs were located in the cytosol of cells, whereupon CMS-NPs entered cells via clathrine-mediated transport and CS-NPs endocytosed via another mechanism. In order to investigate whether the NPs are also able to transport Cu ions into cells, neuroblastoma cells were incubated with different concentrations of Cu-loaded NPs and the cell lysates were investigated by ICP-MS to determine the Cu content of the lysates. It was observed that both NPs were able to increase the cellular Cu level, which proves the transport of Cu by NPs by bypassing the Cu transport protein Ctr1, which is usually responsible for the Cu transport into cells. In order to release Cu from nanocarriers for potential in vivo applications, the slightly lower pH-value in the inflamed tissue of the brain in AD was chosen as a release trigger. Both NPs were able to release Cu pH-dependently, therefore, the release from CS-NP was facilitated due to the stabilization of Cu in the outermost TMEDA shell of the NPs. In contrast, the release from CMS-NPs required non-physiological pH-conditions, because the Cu ions were more shielded due to their stabilization in the PEI core of CMS-NP. Furthermore, since it was shown that Cu ions imported by NPs are accessible for biological processes, the intracellular release was proven. A cellular BBB-model was established by collaboration partners and Cu-laden NPs were tested for their permeation behavior through the BBB by ICP-MS measurements. Both types of NPs were able to transport Cu across the BBB, however, CS-NPs seem to be more suitable for in vivo application due to better cellular import behavior.

In order to further shield Cu ions from the environment and to enhance the blood circulation time, diamino functionalized hPG nanocarriers were equipped with PEG units

via two kinds of attachment. In one nanocarrier, the PEG units were attached onto the diamino ligand shell to yield a CMS architecture. In the other case, PEG moieties were directly linked to the hPG core to yield a core-random shell (CRS) architecture. The physicochemical characterization of CMS and CRS nanocarriers demonstrate the influence of the architecture on the Cu loading capacity, the binding strength, and pH-dependent release. Investigations by UV/Vis showed that, although both nanocarriers contained the same amount of theoretically existing complexation sites, the CMS architectures were able to stabilize 14 Cu ions per macromolecule, while the CRS system only encapsulated 5 Cu ions, probably due to the structural arrangement of the amino ligands, which might have been separated or disturbed by PEG units in CRS-System. The Cu release profiles of the nanocarriers, determined by UV/Vis spectroscopy at pH-values ranging from 8 to 2, showed that the release from CRS polymers already started at pH 7. Therefore, the Cu-binding was too weak for in vivo applications. However, the CMS architecture showed a suitable pH profile releasing the Cu at pH 4, which was also observed for CS-NP. For in vivo applications, it is important to have a complex which is also stable in the presence of other, competitive metal dications present in the blood, like Zn(II), Ni(II), Co(II), Mn(II), Mg(II), and Ca(II). An excess of these ions did not replace the Cu ions in the Cu:CMS complex, which indicated the strong binding and the suitability of CMS architectures for the transport in blood. For use in in vivo applications, the size of the nanocarriers have to be in a certain range. Nanoparticles with a diameter of 6 nm to 200 nm should remain longer in the blood than particles of other sizes. Thus, DLS measurements were performed to investigate the hydrodynamic radius of the Cu-loaded and empty nanocarriers. It was observed that empty CRS particles tended to form aggregates but stayed unimolecular when Cu was complexed within the nanocarrier, while CMS systems did not aggregate as either empty particles or in the complex form and therefore should have been able to achieve a long blood circulation time. The NPs might have been too big to cross the BBB, but since NPs with a positive charge are more likely to pass the BBB, the surface charge of the nanoparticles was investigated by zeta potential measurements. It was observed that partial protonation of the amino ligands led to a permanent positive charge independent of pH. Therefore the CMS and CS architectures might be good candidates to cross the BBB. Furthermore, CRS and CMS nanocarriers were less toxic to neuroblastoma cells than CS-NPs. In conclusion, CMS-NPs are a suitable candidate for in vivo application due to their low cytotoxicity and good complexation and release profiles.

5 Outlook

Due to their versatility, nanocarriers are promising candidates for the metal ion transport across biological barriers. It was shown that PEGylated nanocarriers are more biocompatible than non-PEGylated nanocarrier and thus, PEGylated nanocarriers should as well be investigated for their permeation through the BBB in a BBB-model and be evaluated for in vivo studies. The peptides G23 and Ox26 are known to promote the transport of nanoparticles across the BBB[185-186] and could therefore be attached as targeting moieties to the shell of the nanocarriers.

Since some cases have been reported, in which immune responses occurred or the blood clearance of PEG is accelerated after multiple applications, suitable alternatives for the stealth polymer need to be found. One possibility would be to replace PEG by poly(ethyloxazoline), which has similar characteristics as PEG.[187] Also poly(glutamic acid) and other polypeptides have been discussed as potential alternatives to PEG.[188] In the last decade, many reports presented zwitterionic substances as protein resistant agents,[189-191] which turned into the gold standard of protein resistant materials and therefore became suitable candidates to replace PEG.

One could also design nanocarriers which carry stimuli-responsive ligands. This would open the way towards applications of release stimuli other than pH. In order to stabilize higher amounts of Cu within the nanocarrier, other architectures could be taken into account. For example, polymersomes may be used as efficient metal ion transporters, which encapsulate Cu in its core.

Furthermore, additional ions like zinc and iron could be encapsulated in the nanocarriers. While zinc deficiency has also been suggested to increase the risk for the development of neurological disorders, iron deficiency in the brain leads to impaired learning behavior. Nanocarriers could address these deficiencies and regulate the metal ion homeostasis in the brain.

For treatment of disorders with Cu ion excess as in the case of Wilson disease, metal ions need to be removed from cells which makes nanocarriers with appropriate strong Cu binding ligands suitable candidates for this approach. In this case, the Cu-ligand bond should be extremely strong to inhibit the release of the metal. To this end, triazacyclononanes could be suitable ligands, which can be attached to hyperbranched polymers. Furthermore, nanocarriers loaded with ^{64}Cu could also be used as a prototype to investigate the body distribution of Cu and nanocarrier by positron emission tomography (PET).

6 Zusammenfassung

Das Ziel dieser Arbeit war es, Cu-Mangelerscheinungen wie die Alzheimer Krankheit (AD) zu adressieren und die Blut-Hirn-Schranke (BHS) zu überwinden. In dieser Arbeit wurden daher biokompatible Nanoträgersysteme für Kupfer (Cu)-Ionen entwickelt und die biologischen sowie physikalisch-chemischen Eigenschaften für den Transport von Cu-Ionen über die BHS untersucht. Dazu wurden Kern-Schale Nanopartikel (CS-NP) mit Kern-Multischale Nanopartikeln (CMS-NP) verglichen. CS-NP waren auf der Basis eines hyperverzweigten Polyglycerin-Kerns (hPG), der mit Trimethylethylendiamin (TMEDA) Liganden ausgestattet war, während CMS-NP aus hyperverzweigtem Poly(ethylenimin)-Kern (PEI) und einer Doppelschale aus Alkyl- und Poly(ethylenglykol) (PEG) Bausteinen aufgebaut war. Im Fall der CS-NP befinden sich die Cu-bindenden Einheiten in der Peripherie der Nanotransporter, während CMS-NP das Cu im Kern stabilisiert. Die hergestellten NP konnten große Mengen Cu stabilisieren. Die NP zeigten geringe Zelltoxizität und durch das Anfärben mit geeigneten Farbstoffen konnte ihre zelluläre Aufnahme verfolgt werden. Dabei wurde beobachtet, dass beide NP im Zytosol der Zellen lokalisiert waren, wobei CMS-NP die Zellen durch einen Clathrin-vermittelten Transport und CS-NP über einen anderen Mechanismus endozytiert wurden. Um außerdem den Transport von Cu-Ionen durch die NP zu untersuchen, wurden Neuroblastomzellen mit verschiedenen Konzentrationen der Cu-beladenen NP inkubiert und die Zelllysate mittels ICP-MS untersucht, um den Kupfergehalt der Lysate zu bestimmen. Es wurde herausgefunden, dass beide NP eine Erhöhung des zellulären Cu-Spiegels erzielen konnten. Dies belegt, dass beide NP das Cu in die Zelle transportieren, wobei das Cu Transport Protein Ctr1, das normalerweise für den zellulären Cu Transport verantwortlich ist, umgangen wird. Um die Freisetzung des Cu vom Nanotransporter für potentielle in vivo Anwendungen zu ermöglichen, wurde der leicht niedrigere pH-Wert im entzündeten Gewebe des AD-Gehirns als Freisetzungsauslöser ausgewählt. Beide NP konnten das Cu pH-abhängig freisetzen, wobei die Freisetzung vom CS-NP durch die Stabilisierung des Cu im Äußeren der TMEDA-Schale erleichtert war. Im Gegensatz dazu, benötigte die Freisetzung vom CMS-NP nicht-physiologische pH-Bedingungen, weil die Cu-Ionen durch die Stabilisierung im PEI-Kern von CMS-NP mehr abgeschirmt waren. Außerdem wurde gezeigt, dass NP-importierte Cu-Ionen für biologische Prozesse zugänglich sind, wodurch die intrazelluläre Freisetzung bewiesen wurde. Ein zelluläres BHS-Modell wurde von Kooperationspartnern etabliert und das Permeationsverhalten der Cu-beladenen NP

durch die BHS wurde mittels ICP-MS Messungen untersucht. Beide Arten von NP konnten die BHS überqueren, allerdings scheint CS-NP durch die bessere zelluläre Aufnahme geeigneter für in vivo Anwendungen zu sein.

Um Cu noch besser von der Umgebung abzuschirmen und die Blutzirkulationszeit zu verlängern, wurden diaminofunktionalisierte hPG Nanotransporter durch zwei verschiedene Verknüpfungsarten mit PEG Einheiten ausgestattet. In einem Nanotransporter waren die PEG Einheiten an die Diaminoligandenschale angebracht, um eine CMS-Architektur zu erhalten. Im anderen Fall, wurde PEG direkt an den hPG-Kern geknüpft, um ein zufällige Kern-Schale (CRS) Struktur zu erhalten. Die Synthese und physikalisch-chemische Charakterisierung von CMS und CRS Nanotransportern demonstrieren den Einfluss der Architektur auf die Cu-Beladungskapazität, die Bindungsstärke und die pH-abhängige Freisetzung. Obwohl beide Nanotransporter mit der gleichen theoretischen Anzahl von Komplexierungsstellen ausgestattet sind, zeigten UV/Vis Untersuchungen, dass CMS-Architekturen 14 Cu-Ionen pro Makromolekül stabilisieren können, während das CRS-System lediglich 5 Cu-Ionen einschloss, was auf die strukturelle Anordnung der Aminoliganden zurückzuführen ist, die wahrscheinlich durch die angebrachten PEG-Einheiten in CRS-System getrennt oder gestört wurden. Die Cu-Freisetzungsprofile der Nanotransporter, die durch UV/Vis Spektroskopie bei verschiedenen pH-Werten im Bereich von 2 bis 8 bestimmt wurden, zeigten eine Freisetzung vom CRS Polymer bereits bei pH 7, daher ist die Kupferbindung in diesem Fall zu schwach für in vivo Anwendungen. Allerdings zeigte die CMS-Architektur ein passendes Freisetzungsprofil von Cu bei pH 4, was ebenso bei CS-NP beobachtet wurde. Für in vivo Anwendungen ist es wichtig, dass der Komplex auch in der Anwesenheit von anderen, konkurrierenden, im Blut vorkommenden Metall-Diakationen wie Zn(II), Ni(II), Co(II), Mn(II), Mg(II) und Ca(II) stabil ist. Ein Überschuss dieser Ionen ersetzte die Cu-Ionen im Cu:CMS Komplex nicht, was auf eine starke Bindung und die Eignung der CMS-Architektur für den Transport durchs Blut hindeutet. Für die Anwendbarkeit in vivo, sollte die Größe der Nanotransporter in einem bestimmten Bereich sein. Nanopartikel mit einem Durchmesser von 6 nm bis 200 nm sind geeignet, um länger im Blut zu verbleiben als Partikel anderer Größe. Daher wurden DLS-Messungen gemacht, um den hydrodynamischen Radius der Cu-beladenen und leeren Nanotransporter zu untersuchen. Es zeigte sich, dass leere CRS-Partikel gerne aggregieren, aber unimolekular bleiben, wenn Cu in ihnen komplexiert ist. Das CMS-System andererseits zeigte weder als leerer Partikel, noch als Cu-Komplex Aggregate, weshalb eine längere Blutzirkulationszeit zu erwarten ist. Um die BHS zu überwinden könnten die NPs

zu groß sein, allerdings haben NP mit positivem Charakter eine höhere Chance die BHS zu passieren, weshalb die Oberflächenladung der NP mittels Zeta-Potential-Messungen untersucht wurde. Eine partielle Protonierung der Aminoliganden führte zu einer durchgehend positiven Ladung, die unabhängig vom pH-Wert war. Dies zeigt, dass die NP möglicherweise in der Lage sind die BHS zu überwinden. Des Weiteren waren CRS und CMS Nanotransporter gegenüber Neuroblastomzellen weniger toxisch als CS-NP. Zusammenfassend sind CMS-NPs durch ihre geringe Toxizität und ihre guten Komplexierungs- und Freisetzungseigenschaften geeignete Kandidaten für in vivo Anwendungen.

7 References

[1] J. Lee, M. J. Petris, D. J. Thiele, *J. Biol. Chem.* **2002**, *277*, 40253-40259.
[2] L. Rossi, M. Lombardo, M. Ciriolo, G. Rotilio, *Neurochem. Res.* **2004**, *29*, 493-504.
[3] S. Lutsenko, A. Bhattacharjee, A. L. Hubbard, *Metallomics* **2010**, *2*, 596-608.
[4] N. J. Abbott, L. Ronnback, E. Hansson, *Nat. Rev. Neurosci.* **2006**, *7*, 41-53.
[5] H. Kozlowski, M. Luczkowski, M. Remelli, D. Valensin, *Coord. Chem. Rev.* **2012**, *256*, 2129-2141.
[6] D. Strausak, J. F. B. Mercer, H. H. Dieter, W. Stremmel, G. Multhaup, *Brain Res. Bull.* **2001**, *55*, 175-185.
[7] R. M. Llanos, J. F. B. Mercer, *DNA Cell Biol.* **2002**, *21*, 259-270.
[8] V. Desai, S. G. Kaler, *Am. J. Clin. Nutr.* **2008**, *88*, 855S-858S.
[9] D. M. Danks, in *The Metabolic and Molecular Basis of Inherited Diseases*, 7th ed. (Ed.: B. A. L. Scriver C. R., Sly W. S., Valle D.), McGraw-Hill, New York, **1995**.
[10] K. Weiss, W. Stremmel, *Curr. Gastroenterol. Rep.* **2012**, *14*, 1-7.
[11] M. T. Lorincz, *Ann. N.Y. Acad. Sci.* **2010**, *1184*, 173-187.
[12] G. M. Hill, G. J. Brewer, A. S. Prasad, C. R. Hydrick, D. E. Hartmann, *Hepatology* **1987**, *7*, 522-528.
[13] H. Saito, K. Watanabe, M. Sahara, R. Mochizuki, K. Edo, Y. Ohyama, *Tohoku J. Exp. Med.* **1991**, *164*, 29-35.
[14] J. M. Walshe, *Q. J. Med.* **1973**, *42*, 441-452.
[15] G. J. Brewer, C. A. Terry, A. M. Aisen, G. M. Hill, *Arch. Neurol.* **1987**, *44*, 490-493.
[16] G. J. Brewer, F. Askari, R. B. Dick, J. Sitterly, J. K. Fink, M. Carlson, K. J. Kluin, M. T. Lorincz, *Transl. Res.* **2009**, *154*, 70-77.
[17] F. H. H. Linn, R. H. J. Houwen, J. van Hattum, S. van der Kleij, K. J. van Erpecum, *Hepatology* **2009**, *50*, 1442-1452.
[18] A. Czlonkowska, J. Gajda, M. Rodo, *J. Neurol.* **1996**, *243*, 269-273.
[19] C. J. Lang, P. Rabas-Kolominsky, A. Engelhardt, G. Kobras, H. J. Konig, *Arch. Neurol.* **1993**, *50*, 1007-1008.
[20] J. Telianidis, Y. H. Hung, S. Materia, S. La Fontaine, *Front. Aging Neurosci.* **2013**, *5*, 1-17.
[21] H. A. Hartmann, M. A. Evenson, *Med. Hypotheses* **1992**, *38*, 75-85.
[22] J. H. Menkes, *Brain Dev.* **1988**, *10*, 77-79.
[23] M. Sparaco, A. Hirano, M. Hirano, S. Dimauro, E. Bonilla, *Brain Pathol.* **1993**, *3*, 349-354.
[24] D. J. Waggoner, T. B. Bartnikas, J. D. Gitlin, *Neurobiol. Dis.* **1999**, *6*, 221-230.
[25] C. Sander, H. Niederhoff, N. Horn, *Clin. Genet.* **1988**, *33*, 228-233.
[26] A. M. Gerdes, T. Tonnesen, E. Pergament, C. Sander, K. E. Baerlocher, R. Wartha, F. Guttler, N. Horn, *Eur. J. Pediatr.* **1988**, *148*, 132-135.
[27] A. Barnea, B. M. Katz, *J. Inorg. Biochem.* **1990**, *40*, 81-93.
[28] J. Christodoulou, D. M. Danks, B. Sarkar, K. E. Baerlocher, R. Casey, N. Horn, Z. Tumer, J. T. R. Clarke, *Am. J. Med. Genet.* **1998**, *76*, 154-164.
[29] B. Sarkar, K. Lingertatwalsh, J. T. R. Clarke, *J. Pediatr.* **1993**, *123*, 828-830.
[30] S. G. Kaler, *Ann. Neurol.* **1997**, *41*, 134-136.
[31] P. M. Royce, J. Camakaris, J. R. Mann, D. M. Danks, *Biochem. J.* **1982**, *202*, 369-371.
[32] J. M. Gorell, E. L. Peterson, B. A. Rybicki, C. C. Johnson, *J. Neurol. Sci.* **2004**, *217*, 169-174.
[33] B. K. Barlow, D. A. Cory-Slechta, E. K. Richfield, M. Thiruchelvam, *Reprod. Toxicol.* **2007**, *23*, 457-470.
[34] D. R. Brown, *FEBS J.* **2007**, *274*, 3766-3774.
[35] J. Burre, M. Sharma, T. Tsetsenis, V. Buchman, M. R. Etherton, T. C. Suedhof, *Science* **2010**, *329*, 1663-1667.
[36] N. B. Cole, D. D. Murphy, J. Lebowitz, L. Di Noto, R. L. Levine, R. L. Nussbaum, *J. Biol. Chem.* **2005**, *280*, 9678-9690.

[37] J. Sian-Huelsmann, S. Mandel, M. B. H. Youdim, P. Riederer, *J. Neurochem.* **2011**, *118*, 939-957.

[38] F. Tribl, E. Asan, T. Arzberger, T. Tatschner, E. Langenfeld, H. E. Meyer, G. Bringmann, P. Riederer, M. Gerlach, K. Marcus, *Mol. Cell. Proteomics* **2009**, *8*, 1832-1838.

[39] H. S. Pall, D. R. Blake, J. M. Gutteridge, A. C. Williams, J. Lunec, M. Hall, A. Taylor, *Lancet* **1987**, *2*, 238-241.

[40] J. M. Gorell, C. C. Johnson, B. A. Rybicki, E. L. Peterson, G. X. Kortsha, G. G. Brown, R. J. Richardson, *Neurotoxicology* **1999**, *20*, 239-247.

[41] S. Rivera-Mancía, I. Pérez-Neri, C. Ríos, L. Tristán-López, L. Rivera-Espinosa, S. Montes, *Chem. Biol. Interact.* **2010**, *186*, 184-199.

[42] U. Bickel, Y.-S. Kang, J. Huwyler, in *Drug Targeting*, Wiley-VCH Verlag GmbH, **2001**, pp. 23-52.

[43] A. N. Silchenko, I. Adamchic, N. Pawelczyk, C. Hauptmann, M. Maarou, V. Sturm, P. A. Tass, *J. Neurosci. Meth.* **2010**, *191*, 32-44.

[44] S. B. Prusiner, *Proc. Natl. Acad. Sci. USA* **1998**, *95*, 13363-13383.

[45] R. H. Kimberli, G. C. Millson, L. Bountiff, S. C. Collis, *J. Comp. Pathol.* **1974**, *84*, 263-270.

[46] I. H. Pattison, J. N. Jebbett, *Res. Vet. Sci.* **1971**, *12*, 378-380.

[47] S. B. Prusiner, *Science* **1982**, *216*, 136-144.

[48] S. B. Prusiner, *Science* **1997**, *278*, 245-251.

[49] D. R. Brown, *Neurobiol. Dis.* **2004**, *15*, 534-543.

[50] S. J. Collins, V. A. Lawson, C. L. Masters, *Lancet* **2004**, *363*, 51-61.

[51] M. A. Telpoukhovskaia, C. Orvig, *Chem. Soc. Rev.* **2013**, *42*, 1836-1846.

[52] C. J. Johnson, J. P. Bennett, S. M. Biro, J. C. Duque-Velasquez, C. M. Rodriguez, R. A. Bessen, T. E. Rocke, *PLOS ONE* **2011**, *6*, e19836.

[53] K. Kuwata, N. Nishida, T. Matsumoto, Y. O. Kamatari, J. Hosokawa-Muto, K. Kodama, H. K. Nakamura, K. Kimura, M. Kawasaki, Y. Takakura, S. Shirabe, J. Takata, Y. Kataoka, S. Katamine, *Proc. Natl. Acad. Sci. USA* **2007**, *104*, 11921-11926.

[54] P. Brown, R. Meyer, F. Cardone, M. Pocchiari, *Proc. Natl. Acad. Sci. USA* **2003**, *100*, 6093-6097.

[55] E. Paramithiotis, M. Pinard, T. Lawton, S. LaBoissiere, V. L. Leathers, W.-Q. Zou, L. A. Estey, J. Lamontagne, M. T. Lehto, L. H. Kondejewski, G. P. Francoeur, M. Papadopoulos, A. Haghighat, S. J. Spatz, M. Head, R. Will, J. Ironside, K. O'Rourke, Q. Tonelli, H. C. Ledebur, A. Chakrabartty, N. R. Cashman, *Nat. Med.* **2003**, *9*, 893-899.

[56] D. R. Jones, W. A. Taylor, C. Bate, M. David, M. Tayebi, *PLOS ONE* **2010**, *5*, e9804.

[57] S. Supattapone, H. Wille, L. Uyechi, J. Safar, P. Tremblay, F. C. Szoka, F. E. Cohen, S. B. Prusiner, M. R. Scott, *Journal of Virology* **2001**, *75*, 3453-3461.

[58] S. Supattapone, H.-O. B. Nguyen, F. E. Cohen, S. B. Prusiner, M. R. Scott, *Proceedings of the National Academy of Sciences* **1999**, *96*, 14529-14534.

[59] E. J. Wild, S. J. Tabrizi, *Curr. Opin. Neurol.* **2007**, *20*, 681-687.

[60] J. H. Fox, J. A. Kama, G. Lieberman, R. Chopra, K. Dorsey, V. Chopra, I. Volitakis, R. A. Cherny, A. I. Bush, S. Hersch, *PLOS ONE* **2007**, *2*, e334.

[61] M. E. MacDonald, C. M. Ambrose, M. P. Duyao, R. H. Myers, C. Lin, L. Srinidhi, G. Barnes, S. A. Taylor, M. James, N. Groot, H. MacFarlane, B. Jenkins, M. A. Anderson, N. S. Wexler, J. F. Gusella, *Cell* **1993**, *72*, 971-983.

[62] J. G. Hodgson, N. Agopyan, C. A. Gutekunst, B. R. Leavitt, F. LePiane, R. Singaraja, D. J. Smith, N. Bissada, K. McCutcheon, J. Nasir, L. Jamot, X. J. Li, M. E. Stevens, E. Rosemond, J. C. Roder, A. G. Phillips, E. M. Rubin, S. M. Hersch, M. R. Hayden, *Neuron* **1999**, *23*, 181-192.

[63] G. Bartzokis, P. H. Lu, T. A. Tishler, S. M. Fong, B. Oluwadara, J. P. Finn, D. Huang, Y. Bordelon, J. Mintz, S. Perlman, *Neurochem. Res.* **2007**, *32*, 1655-1664.

[64] S. Krobitsch, A. G. Kazantsev, *Int. J. Biochem. Cell Biol.* **2011**, *43*, 20-24.

[65] L. H. Poon, G. A. Kang, A. J. Lee, *Ann. Pharmacother.* **2010**, *44*, 1080-1089.

[66] S. M. Hersch, H. D. Rosas, *Neurotherapeutics* **2008**, *5*, 226-236.

[67] C. L. Masters, G. Multhaup, G. Simms, J. Pottgiesser, R. N. Martins, K. Beyreuther, *Embo J.* **1985**, *4*, 2757-2763.
[68] M. P. Mattson, *Nature* **2004**, *430*, 631-639.
[69] C. B. Eckman, E. A. Eckman, *Neurol. Clin.* **2007**, *25*, 669-682.
[70] D. J. Selkoe, *Physiol. Rev.* **2001**, *81*, 741-766.
[71] R. E. Tanzi, J. F. Gusella, P. C. Watkins, G. A. P. Bruns, P. H. St. George-Hyslop, M. L. Vankeuren, D. Patterson, S. Pagan, D. M. Kurnit, R. L. Neve, *Science* **1987**, *235*, 880-884.
[72] R. Jakob-Roetne, H. Jacobsen, *Angew. Chem. Int. Ed.* **2009**, *48*, 3030-3059.
[73] S. F. Lichtenthaler, C. Haass, *J. Clin. Invest.* **2004**, *113*, 1384-1387.
[74] E. Kojro, F. Fahrenholz, *Subcell. Biochem.* **2005**, *38*, 105-127.
[75] D. M. Walsh, D. J. Selkoe, *Neuron* **2004**, *44*, 181-193.
[76] G. Bitan, M. D. Kirkitadze, A. Lomakin, S. S. Vollers, G. B. Benedek, D. B. Teplow, *Proc. Natl. Acad. Sci. USA* **2003**, *100*, 330-335.
[77] S. Lesne, M. T. Koh, L. Kotilinek, R. Kayed, C. G. Glabe, A. Yang, M. Gallagher, K. H. Ashe, *Nature* **2006**, *440*, 352-357.
[78] M. A. Lovell, J. D. Robertson, W. J. Teesdale, J. L. Campbell, W. R. Markesbery, *J. Neurol. Sci.* **1998**, *158*, 47-52.
[79] M. Kitazawa, D. Cheng, F. M. LaFerla, *J. Neurochem.* **2009**, *108*, 1550-1560.
[80] T. A. Bayer, O. Wirths, *Nervenarzt* **2008**, *79*, 117-128.
[81] L. M. Munter, H. Sieg, T. Bethge, F. Liebsch, F. S. Bierkandt, M. Schleeger, H. J. Bittner, J. Heberle, N. Jakubowski, P. W. Hildebrand, G. Multhaup, *J. Am. Chem. Soc.* **2013**, *135*, 19354-19361.
[82] B. Winblad, N. Andreasen, L. Minthon, A. Floesser, G. Imbert, T. Dumortier, R. P. Maguire, K. Blennow, J. Lundmark, M. Staufenbiel, J.-M. Orgogozo, A. Graf, *Lancet Neurol.* **2012**, *11*, 597-604.
[83] P. J. Crouch, M. S. Savva, L. W. Hung, P. S. Donnelly, A. I. Mot, S. J. Parker, M. A. Greenough, I. Volitakis, P. A. Adlard, R. A. Cherny, C. L. Masters, A. I. Bush, K. J. Barnham, A. R. White, *J. Neurochem.* **2011**, *119*, 220-230.
[84] J. J. Braymer, A. S. DeToma, J.-S. Choi, K. S. Ko, M. H. Lim, *Int. J. Alzheimers Dis.* **2011**, *2011*.
[85] P. A. Adlard, R. A. Cherny, D. I. Finkelstein, E. Gautier, E. Robb, M. Cortes, I. Volitakis, X. Liu, J. P. Smith, K. Perez, K. Laughton, Q.-X. Li, S. A. Charman, J. A. Nicolazzo, S. Wilkins, K. Deleva, T. Lynch, G. Kok, C. W. Ritchie, R. E. Tanzi, R. Cappai, C. L. Masters, K. J. Barnham, A. I. Bush, *Neuron* **2008**, *59*, 43-55.
[86] L. Lannfelt, K. Blennow, H. Zetterberg, S. Batsman, D. Ames, J. Hrrison, C. L. Masters, S. Targum, A. I. Bush, R. Murdoch, J. Wilson, C. W. Ritchie, P. E. S. Grp, *Lancet Neurol.* **2008**, *7*, 779-786.
[87] T. Borchardt, J. Camakaris, R. Cappai, C. L. Masters, K. Beyreuther, G. Multhaup, *Biochem. J.* **1999**, *344*, 461-467.
[88] P. J. Crouch, L. W. Hung, P. A. Adlard, M. Cortes, V. Lal, G. Filiz, K. A. Perez, M. Nurjono, A. Caragounis, T. Du, K. Laughton, I. Volitakis, A. I. Bush, Q. X. Li, C. L. Masters, R. Cappai, R. A. Cherny, P. S. Donnelly, A. R. White, K. J. Barnham, *Proc. Natl. Acad. Sci. USA* **2009**, *106*, 381-386.
[89] T. Nguyen, A. Hamby, S. M. Massa, *Proc. Natl. Acad. Sci. USA* **2005**, *102*, 11840-11845.
[90] R. A. Cherny, C. S. Atwood, M. E. Xilinas, D. N. Gray, W. D. Jones, C. A. McLean, K. J. Barnham, I. Volitakis, F. W. Fraser, Y.-S. Kim, X. Huang, L. E. Goldstein, R. D. Moir, J. T. Lim, K. Beyreuther, H. Zheng, R. E. Tanzi, C. L. Masters, A. I. Bush, *Neuron* **2001**, *30*, 665-676.
[91] T. A. Bayer, S. Schafer, A. Simons, A. Kemmling, T. Kamer, R. Tepest, A. Eckert, K. Schussel, O. Eikenberg, C. Sturchler-Pierrat, D. Abramowski, M. Staufenbiel, G. Multhaup, *Proc. Natl. Acad. Sci. USA* **2003**, *100*, 14187-14192.
[92] A. L. Phinney, B. Drisaldi, S. D. Schmidt, S. Lugowski, V. Coronado, Y. Liang, P. Horne, J. Yang, J. Sekoulidis, J. Coomaraswamy, M. A. Chishti, D. W. Cox, P. M. Mathews, R. A. Nixon, G. A.

Carlson, P. S. George-Hyslop, D. Westaway, *Proc. Natl. Acad. Sci. USA* **2003**, *100*, 14193-14198.
[93] C. Treiber, M. A. Quadir, P. Voigt, M. Radowski, S. J. Xu, L. M. Munter, T. A. Bayer, M. Schaefer, R. Haag, G. Multhaup, *Biochemistry* **2009**, *48*, 4273-4284.
[94] H. Q. Zheng, L. Xing, Y. Y. Cao, S. A. Che, *Coord. Chem. Rev.* **2013**, *257*, 1933-1944.
[95] K. Riehemann, Stefan W. Schneider, Thomas A. Luger, B. Godin, M. Ferrari, H. Fuchs, *Angew. Chem. Int. Ed.* **2009**, *48*, 872-897.
[96] P. Rajpoot, V. Bali, K. Pathak, *Int. J. Pharm.* **2012**, *426*, 219-230.
[97] E. Soussan, S. Cassel, M. Blanzat, I. Rico-Lattes, *Angew. Chem. Int. Ed.* **2009**, *48*, 274-288.
[98] S. A. Kulkarni, S.-S. Feng, *Pharm. Res.* **2013**, *30*, 2512-2522.
[99] H. Soo Choi, W. Liu, P. Misra, E. Tanaka, J. P. Zimmer, B. Itty Ipe, M. G. Bawendi, J. V. Frangioni, *Nat. Biotechnol.* **2007**, *25*, 1165-1170.
[100] G. M. Soliman, A. Sharma, D. Maysinger, A. Kakkar, *Chem. Commun.* **2011**, *47*, 9572-9587.
[101] D. A. Tomalia, H. Baker, J. Dewald, M. Hall, G. Kallos, S. Martin, J. Roeck, J. Ryder, P. Smith, *Polym. J.* **1985**, *17*, 117-132.
[102] D. A. Tomalia, H. Baker, J. Dewald, M. Hall, G. Kallos, S. Martin, J. Roeck, J. Ryder, P. Smith, *Macromolecules* **1986**, *19*, 2466-2468.
[103] C. J. Hawker, J. M. J. Frechet, *J. Am. Chem. Soc.* **1990**, *112*, 7638-7647.
[104] G. R. Newkome, Z. Q. Yao, G. R. Baker, V. K. Gupta, *J. Org. Chem.* **1985**, *50*, 2003-2004.
[105] M. Mammen, S. K. Choi, G. M. Whitesides, *Angew. Chem. Int. Ed.* **1998**, *37*, 2755-2794.
[106] U. Boas, P. M. H. Heegaard, *Chem. Soc. Rev.* **2004**, *33*, 43-63.
[107] C. J. Hawker, K. L. Wooley, J. M. J. Frechet, *J. Chem. Soc. Perkin Trans. 1* **1993**, 1287-1297.
[108] K. L. Wooley, J. M. J. Fréchet, C. J. Hawker, *Polymer* **1994**, *35*, 4489-4495.
[109] C. J. Hawker, E. E. Malmström, C. W. Frank, J. P. Kampf, *J. Am. Chem. Soc.* **1997**, *119*, 9903-9904.
[110] C. J. Hawker, P. J. Farrington, M. E. Mackay, K. L. Wooley, J. M. J. Frechet, *J. Am. Chem. Soc.* **1995**, *117*, 4409-4410.
[111] T. H. Mourey, S. R. Turner, M. Rubinstein, J. M. Fréchet, C. J. Hawker, K. L. Wooley, *Macromolecules* **1992**, *25*, 2401-2406.
[112] E. Buhleier, W. Wehner, F. Vögtle, *Synthesis* **1978**, 155-158.
[113] *Dendrimer Chemistry*, Wiley-VCH Verlag GmbH & Co. KGaA, Weinheim, **2009**.
[114] R. M. Crooks, M. Q. Zhao, L. Sun, V. Chechik, L. K. Yeung, *Acc. Chem. Res.* **2001**, *34*, 181-190.
[115] S. Gurdag, J. Khandare, S. Stapels, L. H. Matherly, R. M. Kannan, *Bioconjug. Chem.* **2006**, *17*, 275-283.
[116] J. J. Khandare, S. Jayant, A. Singh, P. Chandna, Y. Wang, N. Vorsa, T. Minko, *Bioconjug. Chem.* **2006**, *17*, 1464-1472.
[117] A. Papagiannaros, K. Dimas, G. T. Papaioannou, C. Demetzos, *Int. J. Pharm.* **2005**, *302*, 29-38.
[118] M. T. Morgan, M. A. Carnahan, C. E. Immoos, A. A. Ribeiro, S. Finkelstein, S. J. Lee, M. W. Grinstaff, *J. Am. Chem. Soc.* **2003**, *125*, 15485-15489.
[119] T. Ooya, J. Lee, K. Park, *Bioconjug. Chem.* **2004**, *15*, 1221-1229.
[120] J. B. Wolinsky, M. W. Grinstaff, *Adv. Drug Delivery Rev.* **2008**, *60*, 1037-1055.
[121] M. F. Neerman, H.-T. Chen, A. R. Parrish, E. E. Simanek, *Mol. Pharm.* **2004**, *1*, 390-393.
[122] J. Haensler, F. C. Szoka, *Bioconjug. Chem.* **1993**, *4*, 372-379.
[123] M. X. Tang, C. T. Redemann, F. C. Szoka, *Bioconjug. Chem.* **1996**, *7*, 703-714.
[124] R. Esfand, D. A. Tomalia, *Drug Discov. Today* **2001**, *6*, 427-436.
[125] M. Liu, K. Kono, J. M. J. Fréchet, *J. Control. Release* **2000**, *65*, 121-131.
[126] J. F. G. A. Jansen, E. W. Meijer, E. M. M. de Brabander-van den Berg, *J. Am. Chem. Soc.* **1995**, *117*, 4417-4418.
[127] P. Antoni, D. Nystrom, C. J. Hawker, A. Hult, M. Malkoch, *Chem. Commun.* **2007**, 2249-2251.
[128] R. Geddes, in *The Polysaccharides, Vol. 3* (Ed.: G. O. Aspinall), Academic Press, London, New York, **1985**.

[129] Y. H. Kim, O. W. Webster, *J. Am. Chem. Soc.* **1990**, *112*, 4592-4593.
[130] Y. H. Kim, O. W. Webster, *Macromolecules* **1992**, *25*, 5561-5572.
[131] W. H. Stockmayer, *J. Chem. Phys.* **1943**, *11*, 45-55.
[132] W. H. Stockmayer, *J. Chem. Phys.* **1944**, *12*, 125-131.
[133] P. J. Flory, *Principles of Polymer Chemistry, Vol. 1*, Cornell University Press, Ithaca, New York, **1953**.
[134] J. M. J. Frechet, M. Henmi, I. Gitsov, S. Aoshima, M. R. Leduc, R. B. Grubbs, *Science* **1995**, *269*, 1080-1083.
[135] A. Sunder, R. Hanselmann, H. Frey, R. Mülhaupt, *Macromolecules* **1999**, *32*, 4240-4246.
[136] Y. H. Kim, *J. Polym. Sci. Pol. Chem.* **1998**, *36*, 1685-1698.
[137] *Hyperbranched Polymers: Synthesis, Properties, and Applications*, Wiley-VCH Verlag GmbH & Co. KGaA, Weinheim, **2011**.
[138] J. Khandare, A. Mohr, M. Calderón, P. Welker, K. Licha, R. Haag, *Biomaterials* **2010**, *31*, 4268-4277.
[139] R. K. Kainthan, J. Janzen, E. Levin, D. V. Devine, D. E. Brooks, *Biomacromolecules* **2006**, *7*, 703-709.
[140] R. K. Kainthan, S. R. Hester, E. Levin, D. V. Devine, D. E. Brooks, *Biomaterials* **2007**, *28*, 4581-4590.
[141] R. K. Kainthan, D. E. Brooks, *Biomaterials* **2007**, *28*, 4779-4787.
[142] M. Calderón, M. A. Quadir, S. K. Sharma, R. Haag, *Adv. Mater.* **2010**, *22*, 190-218.
[143] J. Dernedde, A. Rausch, M. Weinhart, S. Enders, R. Tauber, K. Licha, M. Schirner, U. Zuegel, A. von Bonin, R. Haag, *Proc. Natl. Acad. Sci. USA* **2010**, *107*, 19679-19684.
[144] D. Gröger, F. Paulus, K. Licha, P. Welker, M. Weinhart, C. Holzhausen, L. Mundhenk, A. D. Gruber, U. Abram, R. Haag, *Bioconjug. Chem.* **2013**, *24*, 1507-1514.
[145] K. Licha, P. Welker, M. Weinhart, N. Wegner, S. Kern, S. Reichert, I. Gemeinhardt, C. Weissbach, B. Ebert, R. Haag, M. Schirner, *Bioconjug. Chem.* **2011**, *22*, 2453-2460.
[146] Z. Sideratou, D. Tsiourvas, T. Theodossiou, M. Fardis, C. M. Paleos, *Bioorg. Med. Chem. Lett.* **2010**, *20*, 4177-4181.
[147] R. Reul, T. Renette, N. Bege, T. Kissel, *Int. J. Pharm.* **2011**, *407*, 190-196.
[148] M. Krämer, M. Kopaczynska, S. Krause, R. Haag, *J. Polym. Sci. Pol. Chem.* **2007**, *45*, 2287-2303.
[149] M. Adeli, R. Haag, *J. Polym. Sci. Pol. Chem.* **2006**, *44*, 5740-5749.
[150] M. Adeli, R. Haag, Z. Zarnegar, *J. Nanopart. Res.* **2007**, *9*, 1057-1065.
[151] P. Alexandridis, J. F. Holzwarth, T. A. Hatton, *Macromolecules* **1994**, *27*, 2414-2425.
[152] C. S. Popeney, M. C. Lukowiak, C. Böttcher, B. Schade, P. Welker, D. Mangoldt, G. Gunkel, Z. Guan, R. Haag, *ACS Macro Lett.* **2012**, *1*, 564-567.
[153] M. R. Radowski, A. Shukla, H. von Berlepsch, C. Böttcher, G. Pickaert, H. Rehage, R. Haag, *Angew. Chem. Int. Ed.* **2007**, *46*, 1265-1269.
[154] J. Keilitz, M. R. Radowski, J. D. Marty, R. Haag, F. Gauffre, C. Mingotaud, *Chem. Mater.* **2008**, *20*, 2423-2425.
[155] M. A. Quadir, M. R. Radowski, F. Kratz, K. Licha, P. Hauff, R. Haag, *J. Control. Release* **2008**, *132*, 289-294.
[156] S. Nowag, X. S. Wang, J. Keilitz, A. Thomas, R. Haag, *ChemCatChem* **2010**, *2*, 807-811.
[157] J. Keilitz, M. Schwarze, S. Nowag, R. Schomäcker, R. Haag, *ChemCatChem* **2010**, *2*, 863-870.
[158] E. Fleige, B. Ziem, M. Grabolle, R. Haag, U. Resch-Genger, *Macromolecules* **2012**, *45*, 9452-9459.
[159] I. N. Kurniasih, H. Liang, V. D. Moschwitzer, M. A. Quadir, M. Radowski, J. P. Rabe, R. Haag, *New. J. Chem.* **2012**, *36*, 371-379.
[160] I. N. Kurniasih, H. Liang, S. Kumar, A. Mohr, S. K. Sharma, J. P. Rabe, R. Haag, *J. Mat. Chem. B* **2013**, *1*, 3569-3577.
[161] E. Fleige, M. A. Quadir, R. Haag, *Adv. Drug Delivery Rev.* **2012**, *64*, 866-884.
[162] J. R. Casey, S. Grinstein, J. Orlowski, *Nat. Rev. Mol. Cell Bio.* **2010**, *11*, 50-61.

[163] H. Maeda, Y. Matsumura, *Crit. Rev. Ther. Drug Carrier Syst.* **1989**, *6*, 193-210.
[164] J. Su, F. Chen, V. L. Cryns, P. B. Messersmith, *J. Am. Chem. Soc.* **2011**, *133*, 11850-11853.
[165] S. Xu, Y. Luo, R. Graeser, A. Warnecke, F. Kratz, P. Hauff, K. Licha, R. Haag, *Bioorg. Med. Chem. Lett.* **2009**, *19*, 1030-1034.
[166] M. Calderon, P. Welker, K. Licha, I. Fichtner, R. Graeser, R. Haag, F. Kratz, *J. Control. Release* **2011**, *151*, 295-301.
[167] Y. Wu, W. Chen, F. Meng, Z. Wang, R. Cheng, C. Deng, H. Liu, Z. Zhong, *J. Control. Release* **2012**, *164*, 338-345.
[168] D. Steinhilber, M. Witting, X. J. Zhang, M. Staegemann, F. Paulus, W. Friess, S. Küchler, R. Haag, *J. Control. Release* **2013**, *169*, 289-295.
[169] T. Zhou, C. Xiao, J. Fan, S. Chen, J. Shen, W. Wu, S. Zhou, *Acta Biomater.* **2013**, *9*, 4546-4557.
[170] P. J. Halbrooks, A. M. Giannetti, J. S. Klein, P. J. Björkman, J. R. Larouche, V. C. Smith, R. T. A. MacGillivray, S. J. Everse, A. B. Mason, *Biochemistry* **2005**, *44*, 15451-15460.
[171] A. Dautry-Varsat, A. Ciechanover, H. F. Lodish, *Proc. Natl. Acad. Sci. USA* **1983**, *80*, 2258-2262.
[172] K. Temming, D. L. Meyer, R. Zabinski, P. D. Senter, K. Poelstra, G. Molema, R. J. Kok, *Mol. Pharm.* **2007**, *4*, 686-694.
[173] C. Li, L. Xing, S. Che, *Dalton Trans.* **2012**, *41*, 3714-3719.
[174] L. Xing, H. Zheng, S. Che, *Chem. Eur. J.* **2011**, *17*, 7271-7275.
[175] L. Xing, Y. Cao, S. Che, *Chem. Commun.* **2012**, *48*, 5995-5997.
[176] A. W. Bosman, A. P. H. J. Schenning, R. A. J. Janssen, E. W. Meijer, *Chem. Ber.* **1997**, *130*, 725-728.
[177] H. Ejima, J. J. Richardson, K. Liang, J. P. Best, M. P. van Koeverden, G. K. Such, J. W. Cui, F. Caruso, *Science* **2013**, *341*, 154-157.
[178] C. Santini, M. Pellei, V. Gandin, M. Porchia, F. Tisato, C. Marzano, *Chem. Rev.* **2013**.
[179] W. Lu, J. Wan, Z. She, X. Jiang, *J. Control. Release* **2007**, *118*, 38-53.
[180] L. H. Reddy, R. K. Sharma, K. Chuttani, A. K. Mishra, R. R. Murthy, *AAPS J.* **2004**, *6*, e23.
[181] L. Kozlovskaya, D. Stepensky, *J. Control. Release* **2013**, *171*, 17-23.
[182] T. T. Chen, X. Y. Wang, Y. F. He, C. L. Zhang, Z. Y. Wu, K. Liao, J. J. Wang, Z. J. Guo, *Inorg. Chem.* **2009**, *48*, 5801-5809.
[183] G. Gasser, L. Tjioe, B. Graham, M. J. Belousoff, S. Juran, M. Walther, J.-U. Kunstler, R. Bergmann, H. Stephan, L. Spiccia, *Bioconjug. Chem.* **2008**, *19*, 719-730.
[184] A. F. Hollemann, N. Wiberg, E. Wiberg, *Lehrbuch der anorganischen Chemie*, 102. ed., Walter de Gruyter & Co., Berlin, **2007**.
[185] J. V. Georgieva, R. P. Brinkhuis, K. Stojanov, C. A. G. M. Weijers, H. Zuilhof, F. P. J. T. Rutjes, D. Hoekstra, J. C. M. van Hest, I. S. Zuhorn, *Angew. Chem. Int. Ed.* **2012**, *51*, 8339-8342.
[186] H. J. Lee, B. Engelhardt, J. Lesley, U. Bickel, W. M. Pardridge, *J. Pharmacol. Exp. Ther.* **2000**, *292*, 1048-1052.
[187] M. Bauer, C. Lautenschlaeger, K. Kempe, L. Tauhardt, U. S. Schubert, D. Fischer, *Macromol. Biosci.* **2012**, n/a-n/a.
[188] K. Knop, R. Hoogenboom, D. Fischer, U. Schubert, *Angew. Chem. Int. Ed.* **2010**, *49*, 6288-6308.
[189] J. Ladd, Z. Zhang, S. Chen, J. C. Hower, S. Jiang, *Biomacromolecules* **2008**, *9*, 1357-1361.
[190] R. E. Holmlin, X. Chen, R. G. Chapman, S. Takayama, G. M. Whitesides, *Langmuir* **2001**, *17*, 2841-2850.
[191] S. Chen, J. Zheng, L. Li, S. Jiang, *J. Am. Chem. Soc.* **2005**, *127*, 14473-14478.

8 Curriculum Vitae

Der Lebenslauf ist in der Online-Version aus Gründen des Datenschutzes nicht enthalten.

Der Lebenslauf ist in der Online-Version aus Gründen des Datenschutzes nicht enthalten.